The role of the cytoplasmic tail of the influenza virus M2 protein in viral morphology and replication

Matthew D Badham

A thesis submitted to the University of Kent at Canterbury for the degree of PhD in Microbiology in the Faculty of Sciences

Department of Biosciences

2018

Declaration

No part of the thesis has been submitted in the support of an application for any degree or other qualification of the University of Kent, or any other University or Institution of learning.

Matthew D Badham

19th of December 2018

ACKNOWLEDGEMENTS

Without the guidance of Dr Jeremy Rossman, my interest in this area of research would never have begun. I not only thank Jeremy for the practical and personal support, but for allowing me to work with him for almost six years. Studying from Master's to PhD level in his lab for this amount of time has allowed me to focus in developing my skills as a researcher, and my knowledge of more than just 'how to do the experiments'. Not only this, but I have been able to teach and mentor others – something which I am incredibly grateful to have been given the time and chance to do, and that has enabled me to develop as a person.

Thanks also to Mr. Ian Brown, the microscopy facilities manager, without whom I would never have gained the level of exposure to and confidence in confocal microscopy. Tight ships need a good captain. I learnt to drive a car, but never knew you could drive a microscope.

To my colleagues in the lab, past and present – Aga, Basma, Diego, Nafisa, Nikki and Max – support both professionally and personally never wavered, thanks for the laughs.

Dr. Oliver Dibben and Dr. Helen Bright and their colleagues at MedImmune in Liverpool, UK for the LAIV strains, discussions and feedback, and support for the project overall.

To my family and friends for the time, space and understanding during this long road.

Finally, special and considerable gratitude to Mr. Frederic Jackson for the help and work with a myriad of investigations, some contained within here, a lot which are not. His dedication and attention to detail were unrivalled. Thanks, Fred. I am proud to have worked with you.

ABSTRACT

The influenza A virus is the causative agent of influenza virus disease – commonly known as ‘the flu’. Considerable numbers of people are infected seasonally, with most illness resolving quickly. The social and economic impact can be severe, and presents a significant burden for healthcare systems.

Influenza A is a negative sense, single stranded RNA virus with a host-derived lipid envelope that can form both filamentous and spherical virions. The genome encodes for at least 14 genes from eight RNA segments, the main focus of this report being on the ion channel matrix protein 2 (M2). M2 is primarily responsible for allowing the flow of protons down the concentration gradient in early infection, when the virus is within an acidified endosome. The lowering of the pH within the viral core triggers viral membrane fusion with the endosomal membrane, and facilitates release of the viral RNPs in to the cell cytoplasm.

M2 is also known to interact with many of the other viral and cellular proteins during all stages of viral infection. It binds to both the matrix protein 1, M1, and possibly interacts with the nucleoprotein, NP, as well as interacting with cellular factors such as Annexin A6, and cholesterol. Biophysically, M2 is crucial during viral budding in that it provides the force necessary to induce negative gaussian membrane curvature which enables ‘pinching off’ of new virions.

Here we show that the cytoplasmic tail (CT) of M2 is able to interact with many cellular proteins and processes, such as autophagy through LC3 binding, the cellular SUMO system through a SUMO interacting motif, SIM, and the cellular intermediate filament Vimentin. We have used a myriad of techniques in an attempt to elucidate and characterise these interactions of the M2 CT, and how mutations in the M2 CT may ultimately affect viral morphology. Further understanding of viral morphology being affected by other viral proteins and has been investigated through the study of live attenuated influenza viruses (LAIVs) used in seasonal vaccinations. Through this, a medically applicable outcome of influenza morphology is also presented for future investigation.

TABLE OF CONTENTS

ABBREVIATIONS

(co-)IP – (co-)Immunoprecipitation

(v)RNP – (viral) Ribonucleoprotein

A549 - Adenocarcinomic human alveolar basal epithelial cells

ATG – Autophagy related

BCA – Bicinchoninic acid

BP – Band pass

BSA – Bovine serum albumin

CPE – Cytopathic effect

CRISPR - Clustered Regularly Interspaced Short Palindromic Repeats

DAPI – 4′,6-diamidino-2-phenylindole

DMEM – Dulbecco's modified Eagle's medium

DNA – Deoxyribonucleic acid

FITC – Fluorescein isothiocyanate

GFP – Green fluorescent protein

HA – Haemagglutinin

HDAC6 – Histone deacetylase 6

HEK-293T – Human embryonic kidney 293T (large T antigen)

HeLa – Henrietta-Lacks cells

HEX – HeLa CRISPR ATG knockout cells

HRP – Horseradish peroxidase

IAV – Influenza A Virus

Kd – Dissociation constant

LAIV – Live Attenuated Influenza Virus

LAMP1 – Lysosomal-associated membrane protein 1

LB – Lysogeny broth

LC3(b) - Microtubule-associated proteins 1A/1B light chain 3B

LIR – LC3 interacting region

LP – Long pass

M1 – Matrix Protein 1

M2 – Matrix Protein 2

M2 CT – M2 Cytoplasmic Tail

M42 – Matrix protein 42

MDCK – Madine-Darby canine kidney

MOI – Multiplicity of infection

mRNA – Messenger Ribonucleic Acid

NA – Neuraminidase

NP – Nucleoprotein

NS1 – Non-structural protein 1

NS2 / NEP – Non-structural protein 2 / Nuclear Export Protein

PA – Polymerase Acidic protein

PB1 – Polymerase Basic subunit 1

PB2 – Polymerase Basic subunit 2

PBS – Phosphate-buffered saline

PLA – Proximity ligation assay

RNA – Ribonucleic Acid

SDS – Sodium dodecyl sulphate

SDS PAGE - Sodium dodecyl sulphate polyacrylamide gel electrophoresis

SUMO – Small Ubiquitin-like Modifier

TBS – Tris-buffered saline

UBD – Ubiquitin binding domain

VLP – Virus-like particle

WHO – World Health Organisation

WT – Wild Type

1 INTRODUCTION

1.0 INFLUENZA VIRUS BACKGROUND

Influenza A virus (IAV) is a pleomorphic virus of the Orthomyxoviridae family consisting of a segmented, single stranded, negative sense RNA genome (McGeoch, Fellner and Newton, 1976; Lamb and Choppin, 1983). Responsible for seasonal outbreaks and occasional pandemics IAV is a major burden on health systems globally and is estimated to cost the US economy $87.1bn annually (Molinari *et al.*, 2007). Five to 15% of the Northern hemisphere's population is estimated to be affected per annum (WHO) with 250,000–500,000 deaths globally per year (WHO, 2014). The most severe illness occurs in immuno-compromised, elderly and very young individuals and is often followed by secondary bacterial pneumonia, resulting in significant morbidity and mortality.

1.01 Influenza virus disease – 'the Flu'

Infection with influenza A virus, the most clinically relevant of the three influenza virus types known to infect humans (Influenza B and C viruses being the others), causes disease in humans through infection of cells of the upper respiratory tract which leads to a myriad of symptoms. These symptoms can present mildly (coughing, sneezing, 'runny nose' and headaches), and do in the majority of individuals infected with seasonal flu. More serious symptoms such as high grade fever, severe muscle aches and pneumonia can occur in susceptible individuals, or during a highly infectious pandemic, and it is these instances of disease which cause concern for governments and healthcare systems across the globe. Initial infection is through contact with an infected individual shedding virus, and transmission may occur through coughs and sneezes aerosolising droplets of fluid from the upper airways which can encapsulate and carry virus to a new host. Good hygiene should be practiced in order to prevent viral introduction through the mouth, nose or eyes, by washing of hands before touching the face. If the virus does enter the airway, viral attachment to host cells is facilitated by haemagglutinin on the viral surface binding to sialic acid residues on cell surfaces, whereby entry is facilitated. Infection with IAV eventually leads to cell death through continual membrane depletion by newly forming virions, as well as activation of cellular apoptosis by viral and cellular proteins.

The potential for IAV to cause such an impact on society, both seasonally and through pandemic outbreaks, has necessitated comprehensive and vigilant drive for vaccinations, especially for 'at risk' groups such as the young, elderly and infirm. The two categories of IAV vaccines are live attenuated vaccines (LAIV) and 'killed' vaccines, with the LAIV being administered via a nasal spray, and the killed through injection. Both are produced through infection of embryonic chicken eggs, and subsequent preparation steps, be they isolation and purification of the LAIV, or formaldehyde inactivation of the killed vaccine viruses.

1.1 INFLUENZA VIRUS COMPONENTS

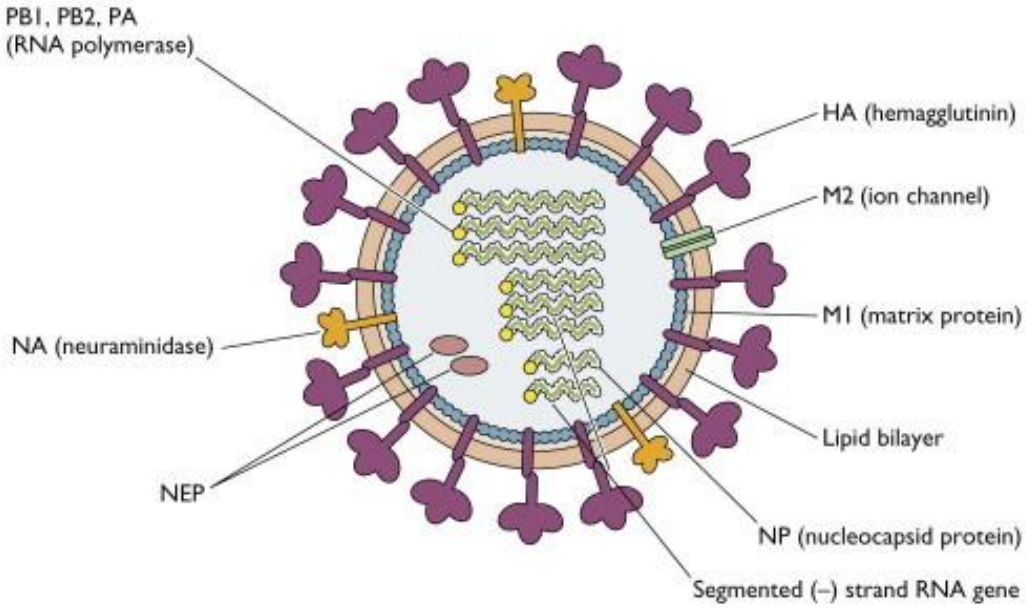

Figure 1 - (*Structure of influenza virus*, www.virology.ws/2009/04/30/structure-of-influenza-virus/. Accessed 29.10.2018)

The segmented, single strand, negative sense RNA genome of the IAV is split over eight RNA segments (McGeoch, Fellner and Newton, 1976; Lamb and Choppin, 1983), where the genetic material codes for at least 14 proteins which can be broadly generalised in to belonging in two 'families' – structural and non-structural (Figure 1). The non-structural proteins consist of the polymerase subunits – polymerase basic subunit 2 (PB2), polymerase basic subunit 1 (PB1), in some viruses polymerase basic subunit 1-F2 (PB1-F2) and the polymerase acidic protein (PA) encoded on segments one, two and three respectively, the RNA binding protein NP encoded on segment five, and the NS1 and nuclear export NEP (also known as NS2) proteins both produced from segment eight (Bouvier and Palese,

2008). IAV's has a remarkable ability to produce alternatively spliced and frame shifted copies of various proteins, each thought to have a specialised role. One example is PA-X, which is the result of a plus one frameshift in segment three. The resultant protein consists of 191 amino acids from the N terminal of PA, fused to 61 frame shifted resultant amino acids, and is termed PA-X (Jagger *et al.*, 2012). PA-X is implicated in modulating host cell gene expression, and is especially involved in attenuating disease response factors, such as the innate immune response, and thereby ism in fact, involved in attenuating the disease state in infected organisms (Gao *et al.*, 2015; Hu *et al.*, 2015). By prolonging host survival, the ability and efficiency of a virus to propagate to other live hosts is increased.

1.12 The viral polymerase (PB1, PB2, PA)

The viral polymerase is a heterotrimeric complex of each protein produced from segments one, two and three (Taubenberger *et al.*, 2005) and is a known determinant for host specificity (Subbarao, London and Murphy, 1993; Naffakh *et al.*, 2000). The PB1 subunit is involved in sequential nucleotide addition during the RNA elongation stage of viral replication (Kobayashi *et al.*, 1996), the PB2 component binds capped cellular mRNA (Guilligay *et al.*, 2008) (and the IAV protein NP (Poole *et al.*, 2004)) and the PA subunit contains the endonuclease active site responsible for cleavage (Dias *et al.*, 2009; Yuan *et al.*, 2009).

1.13 NS1 and NS2 – the 'non-structural' proteins

The NS1 protein has been implicated in the involved in nuclear export of unspliced M1 mRNA (Pereira *et al.*, 2017) and many different host interactions (Tawaratsumida *et al.*, 2014; Cheong *et al.*, 2015; Kuo *et al.*, 2016). Its partner, NEP (NS2) was originally implicated mainly in the export of vRNP complexes (O'Neill, Talon and Palese, 1998; Neumann, Hughes and Kawaoka, 2000), but has since been shown to have, in addition, very diverse functionality, including being necessary for viral budding through cellular ATPase interaction (Gorai *et al.*, 2012), and causing a push to favour vRNP production over host protein production (Robb *et al.*, 2009; Mänz *et al.*, 2012).

The structural proteins are haemagglutinin (HA) encoded on segment four, neuraminidase (NA) on segment six, and the two matrix proteins M1 and M2, both produced from segment seven (Bouvier and Palese, 2008). As well as the M1 and

M2 proteins on segment seven, certain strains of IAV have the ability through alternative splicing of this segment to produce two more, poorly characterised and understood 'M' proteins – M42 and M4 (Wise *et al.*, 2012).

1.14 Haemagglutinin and Neuraminidase

HA is the most abundant viral surface protein, present in approximately a 10:1 ratio with NA (Mitnaul *et al.*, 1996). When inserted in to the membrane of a fully formed virus, is comprised of two subunits, HA1 and HA2 (Bosch *et al.*, 1981) (*N.B. further references to HA in this body of work will refer to the active complex of both HA1 and HA2 in the viral membrane unless otherwise stated).* HA is formed as a precursor unit HA0, which undergoes homotrimerisation within the endoplasmic reticulum, before transfer to the site of budding via the Golgi apparatus (Gething *et al.*, 1986; Copeland *et al.*, 1988; Daniel N. Hebert, Brigitte Foellmer, 1995). Once at the viral surface, HA is required for viral attachment to a host cell membrane by binding to terminal sialic acid residues at the end of carbohydrate chains (Weis *et al.*, 1988), but is also essential for viral fusion mediated by the HA2 subunit once the virus is encapsulated in an acidic endosome (Durrer *et al.*, 1996). The acidic environment of the endosome causes HA to enter the 'fusion state', allowing the HA2 subunit to interact with the endosomal membrane (Garten and Klenk, 1999; Steinhauer, 1999) which plays a crucial role in the initial stages of infection, however this process is the target of some broad spectrum antiviral compounds already in clinical use in Russia and China, such as Umifenovir (Arbidol) (Kadam and Wilson, 2017). The recognition of sialic acid acid residues by HA is a key determinant of IAV tropism (Kumlin *et al.*, 2008), as different hosts display different, or differential, expression of *N*-acetyl or *N*-glycolyl linked neuraminic acids (Varki and Varki, 2007). Human airway tissue displays primarily α-2,6 linked sialic acid residues in the upper airway, and α-2,3 in the lower airway, and therefore IAVs which cause disease and replicate efficiently in humans must preferentially bind these residues (Ito *et al.*, 1997; Yamada *et al.*, 2006; Auewarakul *et al.*, 2007). As such, binding to α-2,6 residues facilitates more efficient IAV transmission, while a greater affinity to α-2,3 residues causes more severe disease. IAV is classically an avian disease with its reservoir in the bird population (Webster, 1998), which displays primarily α-2,3 linked sialic acid residues, therefore the virus must adapt its HA binding specificity to display preference to α-2,6 sialic acid residues in order to take hold in the human population. This receptor discrepancy is of vital

importance when it comes to the mixing of viruses in different host reservoirs. Pigs are a reservoir for IAV (Brown, 2000) and pose a severe threat to emergent pandemic strains owing to the expression of both avian-type (α-2,3) and human-type (α-2,6) linked sialic acid residues throughout their bodies (Nelli *et al.*, 2010). When pigs are kept in poor conditions and open farms, mixing with birds, new IAV strains with the potential for human infection can arise through antigenic shift, as will be discussed later (Wenjun Ma, 2009), and this is especially problematic in south and south east Asia (Choi *et al.*, 2005; Cyranoski, 2005).

NA, like HA is a membrane anchored, extravirally facing glycoprotein (Gamblin and Skehel, 2010) of four identical subunits which comprise the enzymatic sites, attached to a stalk region (Varghese, Laver and Colman, 1983). NA also recognises sialic acid residues as HA does (Varghese *et al.*, 1992), with NA functioning to cleave these residues in late infection, to facilitate release of newly formed virions (Palese *et al.*, 1974; Barman *et al.*, 2004). Owing to this sialic acid cleaving ability, NA is the target of small molecule pharmaceuticals used to treat influenza: Relenza® (zanamivir) and Tamiflu® (oseltamivir) (Gubareva, 2004). These are structural analogues of sialic acid, and work to inhibit the enzymatic action of NA, thus retaining newly formed virus on the host cells. Resistance to these inhibitors has been seen sporadically, but in general they remain clinically useful in both treatment and prophylaxis of IAV infection (Samson *et al.*, 2013), in contrast to the M2 inhibitor amantadine and its derivatives, to which resistance has become widespread and are no longer recommended for use (Hurt, 2014).

Aside from the enzymatic head domain of NA, the stalk is known to play a role in determining the efficiency of viral infection, through co-evolution with the changed seen in the active site, as it is needed to promote efficient folding of the NA head (Da Silva *et al.*, 2013; Nordholm *et al.*, 2013; da Silva *et al.*, 2015). Additionally, the NH_2 terminal of NA is important in NA translocation and trafficking though the endoplasmic reticulum (Bos, Davis and Nayak, 1984).

1.15 The matrix proteins

Segment seven produces the matrix proteins, M1 and M2. M1 is the most abundant viral protein (Calder *et al.*, 2010), and forms the scaffold under the lipid bilayer of the virus to provide stability (Harris *et al.*, 2001; Calder *et al.*, 2010) and anchoring points for other viral proteins (Harris *et al.*, 2006; B. J. Chen *et al.*, 2008; Rossman

and Lamb, 2011). M1 is able to multimerise upon this interaction with lipids, which is integral to the formation of new virions (Hilsch *et al.*, 2014), and this occurs at the site of budding through these lipid interactions, and interactions with other viral proteins such as HA, NA and M2 (Rossman and Lamb, 2011). M1 is also thought to play a key role in producing the force needed to drive the budding of new virions, both classically spherical (Gómez-Puertas *et al.*, 2000) and filamentous (Elleman and Barclay, 2004). In the mature virion, M1 provides the matrix necessary to allow the transmembrane HA and NA proteins to anchor (Lee, 2010) as well as binding to vRNPs (Boulo *et al.*, 2007). Binding to vRNPs is facilitated by a positively charged surface on M1 (Gagnon *et al.*, 1997), and also prevents re-importation to the nucleus after NS2/NEP binding (Boulo *et al.*, 2007). M1 also de-polymerises at low pHs, that are achieved through the action of the M2 ion channel during encapsulation in an endosome during the initial stages of viral entry to a host cell, which allows release of the genetic material of the virus necessary for infection to progress. (Batishchev *et al.*, 2016; Shtykova *et al.*, 2017). Furthermore, M2 is able to induce negative membrane curvature at the site of budding, to facilitate the release of newly formed virions (Schmidt, Mishra, Wang, DeGrado, *et al.*, 2013).

1.2 ANTIGENIC VARIATIONS – DRIFT AND SHIFT

IAV poses such a global health threat owing to its ability to emerge as antigenically novel viruses season to season, through display of genotypically novel HA and NA surface proteins (Gerhard and Webster, 1978; Both *et al.*, 1983; Schweiger, Zadow and Heckler, 2002). This phenomenon is known as antigenic drift, and an emergent antigenically novel HA, NA or double mutant appears in the global IAV circulation every two to eight years (Joshua B. Plotkin, Jonathan Dushoff, 2002; Smith *et al.*, 2004; Koelle *et al.*, 2006). The new and antigenically distinct ectodomains of HA and NA arise from point mutations in the viral genome (Sandbulte *et al.*, 2011) and become a health concern as previously immunised individuals' immune system will be naïve to this new strain of IAV. Antigenic drift in IAV is the cause of a rise and fall in severity of flu seasons, and this is especially significant when there is a mismatch between the global stock of immunisations having been produced through modelling and prediction (Grohskopf *et al.*, 2016, 2017; Grohskopf, Sokolow and Broder, 2018) versus what may be circulating. So, antigenic drift poses a seasonal threat not only as immune-competent individuals can select for point mutant viruses and become infected themselves, but as there is limited cross-

protection between antigenically drifted IAV, this can further add to the burden on public health (Epstein, 2018).

As well as antigenic drift, IAV can undergo a wider, more complex and dangerous genotypic reassortment known as antigenic shift. Antigenic shift occurs when two IAV strains mix in one host, and there is interchange between the vRNP segments. For example, one virus can exchange the entire segment four (HA) and / or segment six (NA) (Webster *et al.*, 1982). Antigenic drift is a process which produces antigenically-novel mutants slowly, enabling response from public health authorities. Comparably, antigenic shift produces a completely novel and distinct virus which poses an immediate threat (Cox and Subbarao, 2000) which may overwhelm a population on a local, national or frequently global level – a pandemic. These new 'H' and 'N' mutant viruses give rise to the well-known nomenclature, such as H1N1 and H5N1, colloquially named swine flu and bird flu respectively due to their original hosts. Current circulating seasonal strains are all descendants of past pandemics (Subbarao *et al.*, 1998), with the deadliest being the 1918 'Spanish flu' (Figure 2). This variant emerged as the result of a circulating avian influenza becoming pathogenic in the human population (Pennington, 2008) and caused the deaths of up to 50 million people, with even this figure the subject of some dispute (Johnson and Mueller, 2002).

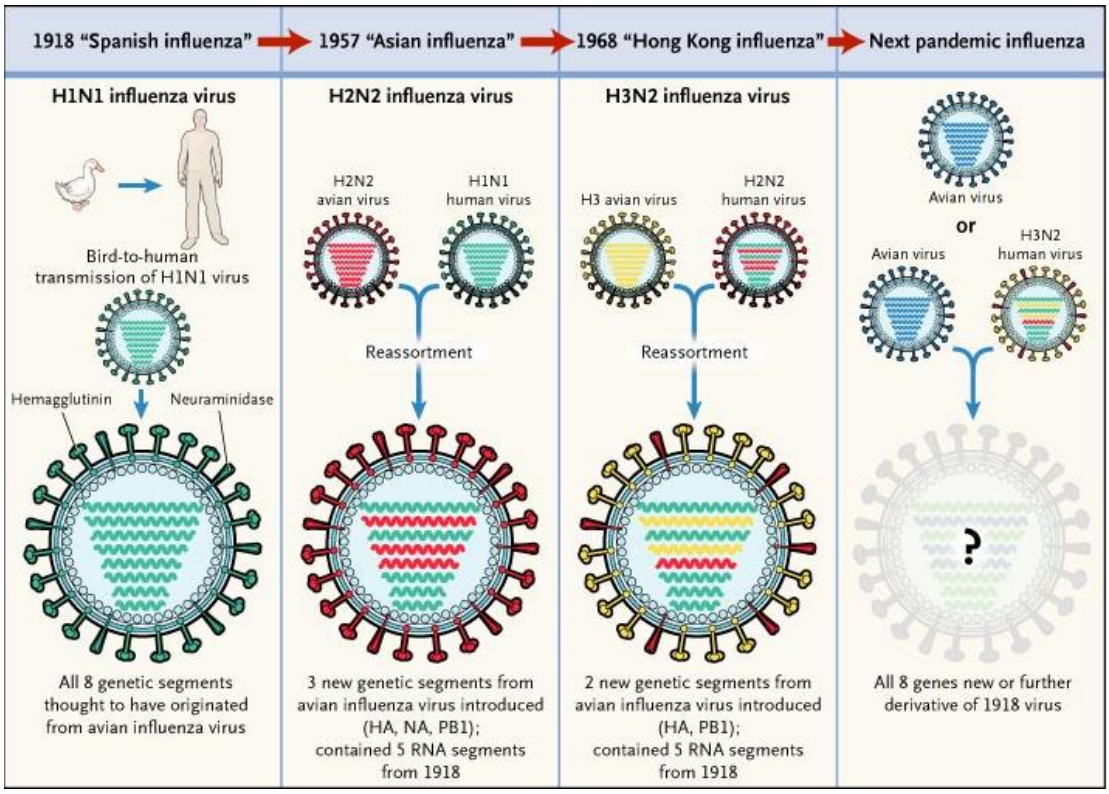

Figure 2 - Image taken from Belshe, 2005 *"The Origins of Pandemic Influenza — Lessons from the 1918 Virus"* showing the propensity for IAV to reassort in hosts – antigenic shift.

Figure 3 (taken from Kim, Webster and Webby, 2018) shows the wide array of organisms capable of acting as reservoirs for IAV strains, and the possibility of shift occurring in organisms, allowing for a virus with increased pathogenicity. Put simply, antigenic shift in IAV requires infection in an applicable animal reservoir of two different subtypes. In a single concurrently infected cell, whole gene segments can be translocated between viruses during the infection and replication processes (Burnet, 1951; Hirst and Gotlieb, 1953).

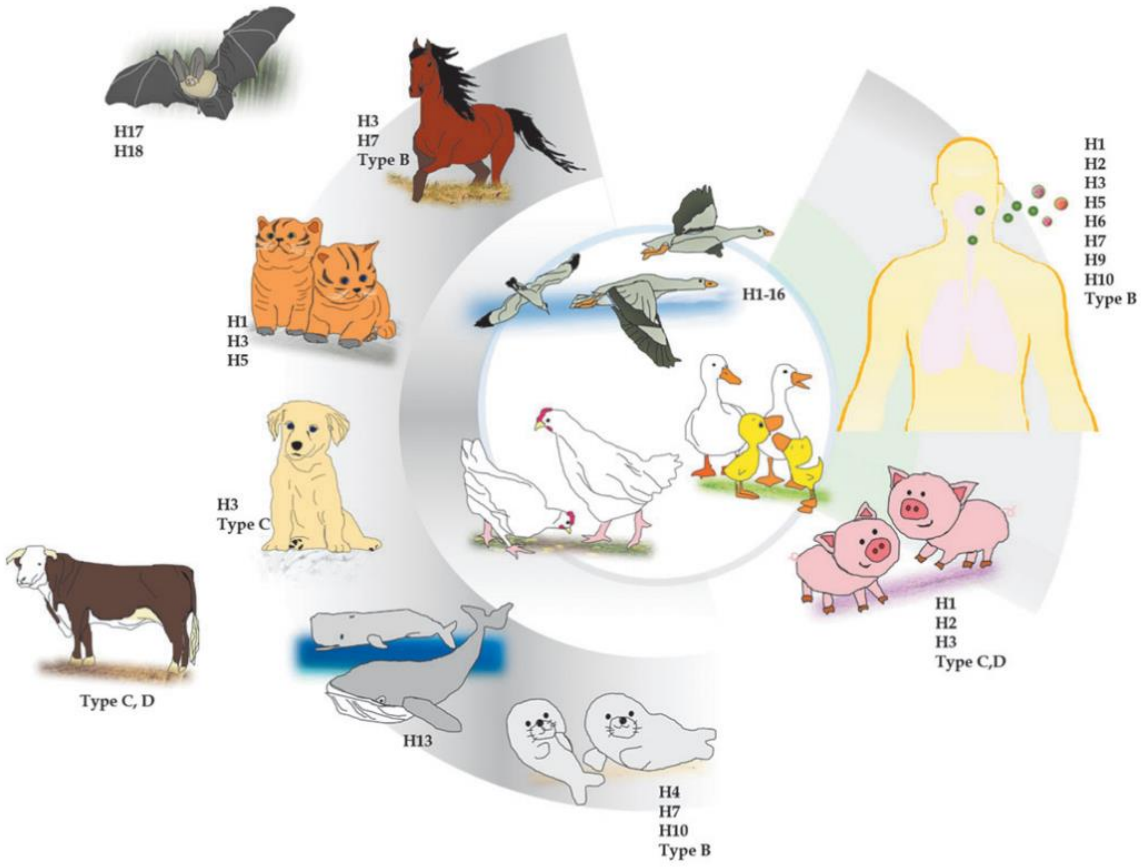

Figure 3 – Host species for IAV taken from Kim, H., Webster, R. G. and Webby, R. J. (2018) '*Influenza Virus: Dealing with a Drifting and Shifting Pathogen'*.

IAV infects the cells of the upper respiratory tract, causing illness in a wide range of hosts, including humans, pigs, horses and birds. Birds are thought to be the reservoir for IAV in the wild (Parrish, Murcia and Holmes, 2015) and are a key source for the emergence of novel IAV strains (Sharp *et al.*, 1997), such as the 1918 Spanish flu. Recent strains emerging from the wild bird population include the high

pathogenicity avian influenza virus strains H5N1 and H7N9, currently circulating in Eastern Asia where they have up to a 60% case-fatality rate in humans, though do not yet spread efficiently from person to person (Cowling *et al.*, 2013).

1.3 THE VIRAL LIFECYCLE

The IAV life cycle can be broadly categorised in to three sections: entry, replication, and budding (Figure 4). During the entry phase, viral HA attaches to sialic acid residues on the host cell surface, triggering endocytosis and the encapsulation of the virus in an acidic endosome. The low pH both triggers HA-mediated fusion of the virus and endosomal membranes and enables protons to enter the viral core, mediated by the ion channel M2. The acidificication of the viral core enables vRNP dissociation and following fusion of the viral membrane with the endosomal membrane vRNPs are released in to the cytoplasm where a nuclear localisation signal enables entry of the vRNPs in to the host cell nucleus where mRNA synthesis takes place. Nascent viral proteins are produced from mRNA and some trafficked and modified through the Golgi apparatus. vRNA is used to form progeny vRNPs which are exported from the nucleus by M1 and NS2. Assembly occurs at the plasma membrane of the host cell, where M1 polymerisation primarily provides the

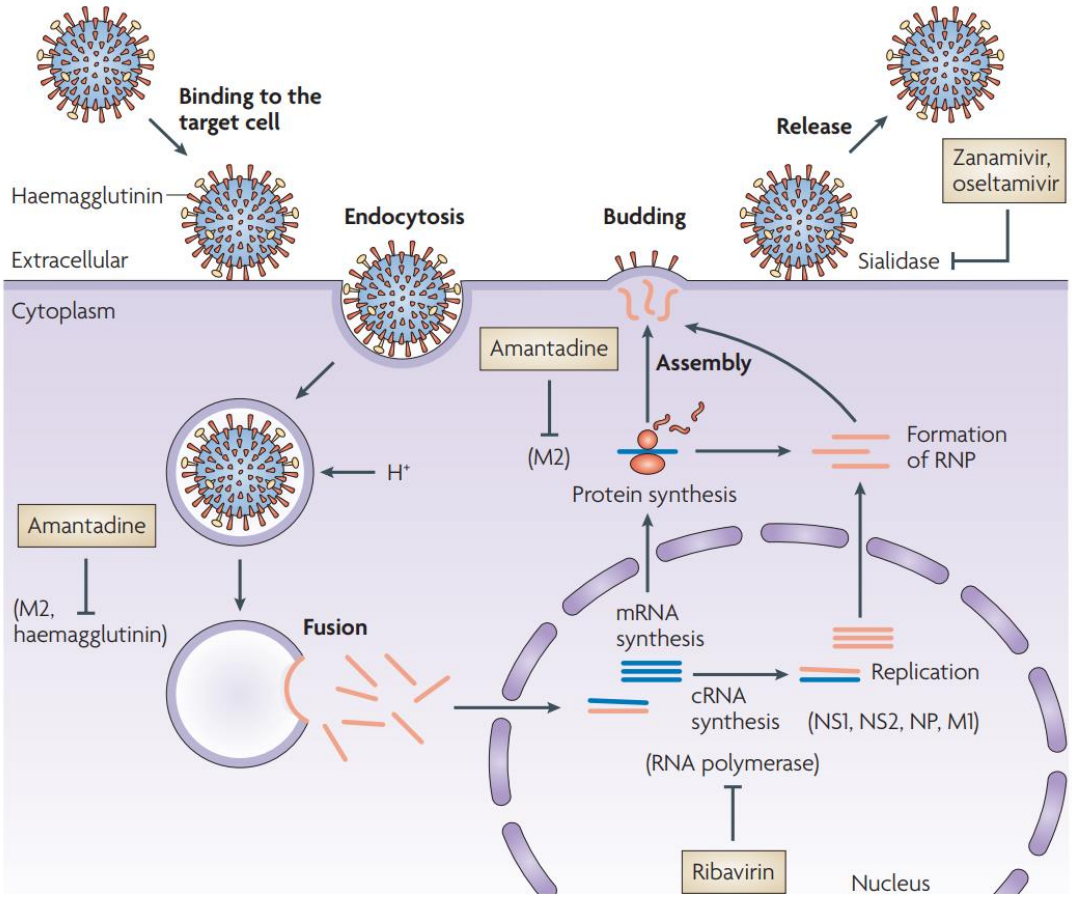

force to drive virions to bud, M2 induces negative membrane curvature to close the base of the budding virus off form the host cell plasma membrane, and NA cleaves reattached sialic acid residues, freeing the budded virus.

Figure 4 – The viral lifecycle. Image taken from von Itzstein, 2007 *"The war against influenza: Discovery and development of sialidase inhibitors"* showing a simplified schematic of the stages of the IAV lifecycle.

1.31 Viral assembly and budding

It is thought that IAV assembly and budding occurs at lipid raft domains on the apical surface of the host cell plasma membrane, where IAV proteins are brought together in high concentrations within specific membrane regions (Scheiffele *et al.*, 1999). NA and HA are both fundamentally associated with these domains, with the transmembrane domain of HA promoting the raft association (Zhang, Pekosz and Lamb, 2000). HA has the ability to induce budding of virus-like particles (VLPs) in and of itself, forming vesicles similar in appearance to viruses (Chen *et al.*, 2007). This suggests that HA may possess an intrinsic capacity to alter membrane curvature. Alternatively, the induction of membrane curvature may be driven by the crowding of HA molecules within a defined space (i.e. within a lipid raft domain). However, HA VLP budding only produces spherical particles, whereas VLPs are filamentous when M1 is also expressed (Chlanda, Schraidt, Kummer, Riches, Oberwinkler, Prinz, Kräusslich and John A G Briggs, 2015). After the formation of a viral bud, the virus remains attached to the host cell through a small membrane neck. At this point, the M2 protein alters membrane curvature, constricting the neck and causing membrane scission (Schmidt, Mishra, Wang, Degrado, *et al.*, 2013). The enzymatic action of NA can then release the fully formed virus from the host cell. Throughout this process, it is not clear when the genome is recruited to the budding virion nor the effects RNP binding has on the budding process or the formation of filamentous virions.

1.4 VIRAL MORPHOLOGY

IAV is a pleomorphic virus, known to display a range of morphological states, from filamentous to spherical, with ovoid or bacilliform intermediates often observed (Figure 4b).

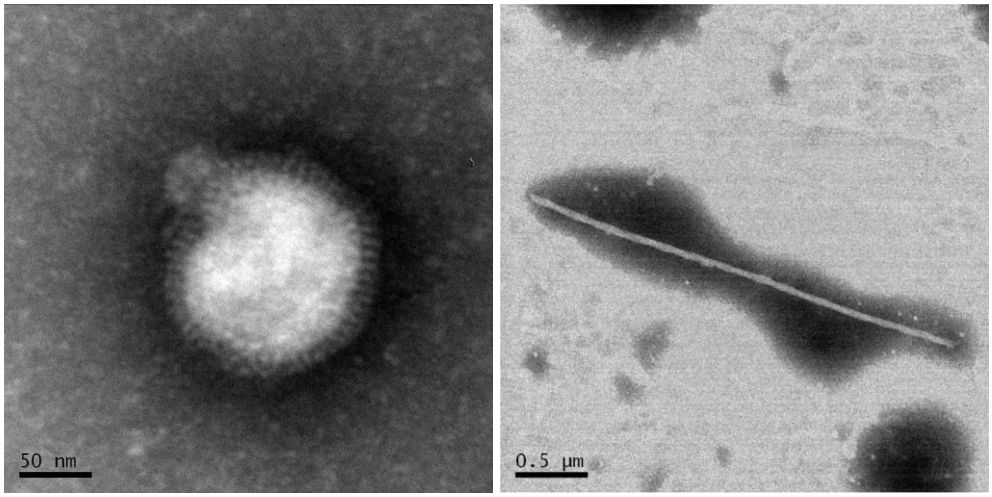

Figure 4b - TEM images of a spherically budded A/Udorn/72 virion from infected MDCK cell (left) and a viral filament from A/California/0709 (right).

In certain cases, IAV strains may produce solely spherical virions; however, filament-producing strains always produce a mixture of both filamentous and spherical virions. It is known that filamentous viruses contain only one copy of the IAV genome, thus each sphere, bacilliform or filament is thought to be a single infectious unit regardless of length (Roberts, Lamb and Compans, 1998). Structurally, viral filaments are roughly equal, or slightly smaller in diameter (80–100 nm) to spherical virus (120 nm), but extend to a significant length, sometimes upwards of 20 µm, with lengths over 50 µm not unheard of. Filamentous viruses are particularly of note as they are recurrently observed in human clinical infections (Chu, Dawson and Elford, 1949; Choppin, Murphy and Tamm, 1960; Kilbourne and Murphy, 1960; Lang *et al.*, 1968; Hayase, Y., Uno, F. & Nii, 1995; Shortridge *et al.*, 1998; Itoh *et al.*, 2009; Elton *et al.*, 2013; Seladi-Schulman, Steel and Lowen, 2013), for example, filamentous virions are seen in lung sections from fatal cases of the 2009 H1N1 pandemic (Basu *et al.*, 2011). In contrast, many laboratory strains produce solely spherical virions. The biological function of this morphology is not known nor is it understood how host adaptation can select for a specific viral morphology; however, repeated passaging of filamentous human clinical isolates in chicken eggs causes a morphological adaptation resulting in the production of only spherical virus (Kilbourne, 1959; Choppin, Murphy and Tamm, 1960) whereas adaptation to growth in guinea pigs restores filament formation (Seladi-Schulman,

Steel and Lowen, 2013). Mutations of several different viral proteins can influence filament formation during the process of adaptation. For example, the filamentous A/Udorn/72 strain becomes spherical with a single point mutation in the M1 protein (Zebedee and Lamb, 1988, 1989; Roberts, Lamb and Compans, 1998). Thus, a range of both host and viral factors governs the formation of filamentous virions during influenza virus assembly and budding.

1.41 Viral determinants of morphology

Many different studies have investigated the viral factors that determine morphology, with most focusing on the structural proteins M1 and M2 and their role in viral assembly. M1 plays a crucial role in the assembly and budding of both filamentous and spherical IAV (Scheiffele *et al.*, 1999; Zhang, Pekosz and Lamb, 2000). In 2004, Elleman and Barclay reported that M1 was also the main viral determinant of filamentous morphology (Elleman and Barclay, 2004). Swapping the 'M' RNA segment from the spherical strain, A/Puerto Rico/8/1934 (PR8), with the M segment of the filamentous strain, A/Udorn/1972 (Udorn), enabled the conversion of a spherical strain into a filamentous strain (when M-Udorn was inserted into PR8) and a filamentous strain into a spherical strain (M-PR8 into Udorn) (Zebedee and Lamb, 1989; Scheiffele *et al.*, 1999). In 2007, Chen et al. showed that M1 is required for the formation of filamentous VLPs, though it was not required to form bacilliform (<1 μm) or spherical VLPs (Gómez-Puertas *et al.*, 2000; Bourmakina and García-Sastre, 2003; Chen *et al.*, 2007).

Interestingly, in filamentous viruses, M1 appears to adopt a helical conformation (Edinger, Pohl and Stertz, 2014), which is not apparent in spherical virus, suggesting that structural variations in the M1 protein may govern viral structure (Fujiyoshi *et al.*, 1994). This has been further investigated when Burleigh *et al.* demonstrated that a number of mutations in M1 can significantly influence the morphology of budding virus, from spherical to filamentous, with aberrant 'in-between' morphologies (Burleigh *et al.*, 2005).

As the most abundant viral protein, M1 forms a layer under the viral envelope and is responsible for interacting with NA, HA and M2 to form a scaffold-like complex (Nayak, Hui and Barman, 2004). It is postulated that M2 can stabilise this complex during budding to allow for continued M1 polymerisation and the formation of a viral filament (Rossman *et al.*, 2010). In support of this hypothesis, it has been

observed that mutation of the M2 protein can dramatically affect viral morphology, with mutations in the c-terminal amphipathic helix converting a filamentous virus into a spherical one (Rossman *et al.*, 2010), whereas truncation of the c-terminus at residue 70 enables filament formation from an otherwise spherical virus (McCown and Pekosz, 2006). The effect of M2 on viral filament formation has also been studied using the monoclonal antibody 14C2, which has been shown to inhibit filamentous virus formation whilst permitting spherical virus to bud (Rossman *et al.*, 2010). 14C2 binds to the ectodomain of M2 and is thought to disrupt the binding between the M2 cytoplasmic tail and M1 (Rossman *et al.*, 2010). This is consistent with other data showing that mutation of the M2 cytoplasmic tail between residues 70–77 reduces M1-M2 interactions and subsequently the amount of M1 and RNP packaged in virions (Grantham *et al.*, 2010; Beale, Wise, Stuart, Benjamin J. Ravenhill, *et al.*, 2014). Intriguingly, a single amino acid substitution in the M2 cytoplasmic tail of the filamentous Udorn strain, Y76A, significantly reduced the number and length of filamentous viruses produced (Grantham *et al.*, 2010). However, recovery of the filamentous morphology was seen with the addition of a S71Y mutation, though it is not clear if these mutations also affect M1-M2 interactions (Grantham *et al.*, 2010). In either case, it is possible that the M2 protein affects viral filament formation by altering membrane curvature, stabilising the site of budding and therefore enabling M1 polymerisation and the elongation of a viral filament (Wharton *et al.*, 1994; Gubareva, 2004). Thus, M2 appears to modify filament formation through binding and recruitment of M1, whereas M1 itself is required for the actual structuring of the filament. This suggests that filamentous virion production is likely a multi-faceted process, affected by several different viral proteins, all occurring in the context of an array of cellular partners.

1.42 Host determinants of morphology

IAV is pleomorphic, adopting both spherical and filamentous forms (Fujiyoshi *et al.*, 1994). As described, viral morphology can be altered through adaptation to different hosts, implying that there are host-specific influences on filament formation (Seladi-Schulman, Steel and Lowen, 2013). Filamentous IAV is consistently found in human clinical isolates from laboratory confirmed cases, in the 2009 H1N1 pandemic (Basu *et al.*, 2011) and as far back as the 1957–1958 pandemic (Kilbourne, 1959), with the first identification having occurred in 1946 (Mosley and Wyckoff, 1946). It is known that filament forming strains become

spherical after repeated passage in embryonated chicken eggs, whereas the filamentous morphology is retained during passage in Madin-Darby canine kidney (MDCK) cells (Burnet and Lind, 1957; Choppin, Murphy and Tamm, 1960; Seladi-Schulman, Steel and Lowen, 2013). Thus, host cell factors play a considerable role in filament formation, and IAV morphology may represent an adaptation to a specific host cell environment. Previous research has identified several host proteins that affect viral morphology. In particular, when the Udorn virus is grown in polarised MDCK cells, filamentous virus is produced from the apical plasma membrane (Fujiyoshi *et al.*, 1994; Scheiffele *et al.*, 1999; Zhang, Pekosz and Lamb, 2000). Chemical disruption of the actin cytoskeleton causes depolarization of the cells and specifically reduces filamentous virus production whilst having no effect on the budding of spherical virus (Roberts and Compans, 1998). Considering that the upper respiratory tract consists of highly polarised epithelial cells and is the primary site of human infection, the detection of filamentous IAV in human clinical samples may be directly related to epithelial cell polarisation. However, other experiments have shown that human embryonic kidney 293T cells are capable of producing filamentous virions, despite an absence of cell polarisation and a lack of a defined apical membrane (Bruce *et al.*, 2009). Thus, the impact of cell polarisation on viral morphology may be more complicated and may be influenced by other host cell proteins or processes.

1.43 Significance of viral morphology

The biological significance of IAV morphology in human clinical infections is a subject of great interest. The production of viral filaments appears to be highly inefficient by its nature, consuming anywhere from three to thirty times the amount of plasma membrane used to bud one infectious virus (Mosley and Wyckoff, 1946; Roberts and Compans, 1998). There are several opinions on why, despite this apparent inefficiency, IAV readily produces filamentous virus in human clinical infections. As there is always a mixed population of spheres and filaments and never solely filaments, it is possible that the two morphologies are playing different roles within the host. It has been found that filament forming mutants of PR8 have higher per-molecule NA activity in vitro (Seladi-Schulman *et al.*, 2014). In addition, NA has been shown to cleave sialic acid bonds within the mucus secreted by airway epithelial cells (Cohen *et al.*, 2013; Yang *et al.*, 2014) and the greater number of NA molecules (owing to a longer viral length) may serve to more

efficiently clear this mucus layer. It is therefore plausible to think that the filamentous morphology is actually a marker of pathogenicity in vivo, whereby mucus in the airway is cleared by NA on filaments, thus allowing for a more efficient spread of the smaller spherical viruses (Vijayakrishnan *et al.*, 2013). This hypothesis is supported by a recent study that suggests that filaments are not released as efficiently as spheres from cells and may remain as cell-associated virions (Gómez-Puertas *et al.*, 2000).

In 1998, it was shown that spherical and filamentous viruses are comparably infectious in vitro and both contain a single copy of the viral genome (Roberts and Compans, 1998; Noda *et al.*, 2006; Calder *et al.*, 2010; Vijayakrishnan *et al.*, 2013). However, it has recently been reported that certain subsets of filamentous virions may lack a genome (Vijayakrishnan *et al.*, 2013). Vijayakrishnan et al. (2013) reported that longer filaments were typically devoid of a copy of the viral genome, whereas shorter filaments were not. Thus, there might not be a single type of filamentous virions, but rather a range, potentially with different functions. In the tightly packed epithelial layer of the upper respiratory tract, short, cell-anchored, infectious filaments may be able to directly deliver the viral genome to neighbouring cells without the need to release and transmit a viral particle. This process may be facilitated by the more permissive use of macropinocytosis as an alternate cell entry pathway, used by filamentous IAV (Sieczkarski and Whittaker, 2005; de Vries *et al.*, 2011; Rossman, Leser and Lamb, 2012). At the same time, longer, non-infectious filamentous virions may serve to thin and clear host respiratory mucus, facilitating the spread of spherical virions to neighbouring cells and to new hosts.

1.5 THE MATRIX PROTEIN 2, M2

Within the last decade, much focus has been on the wide and varying roles of the M2 protein. M2 is a proton channel, with this well characterised ability playing a crucial role in initial viral infection (Pinto, Holsinger and Lamb, 1992). Once endocytosed, the low pH of the endosome which encapsulates the virion is exploited by M2. Protons are allowed to flow down the concentration gradient by means of M2, entering the viral core (Figure 5). The decreased pH within the virus causes dissociation of vRNPs from M1, and subsequent release in to the cytoplasm of the host cell for nuclear import and viral protein production (Edinger, Pohl and Stertz, 2014).

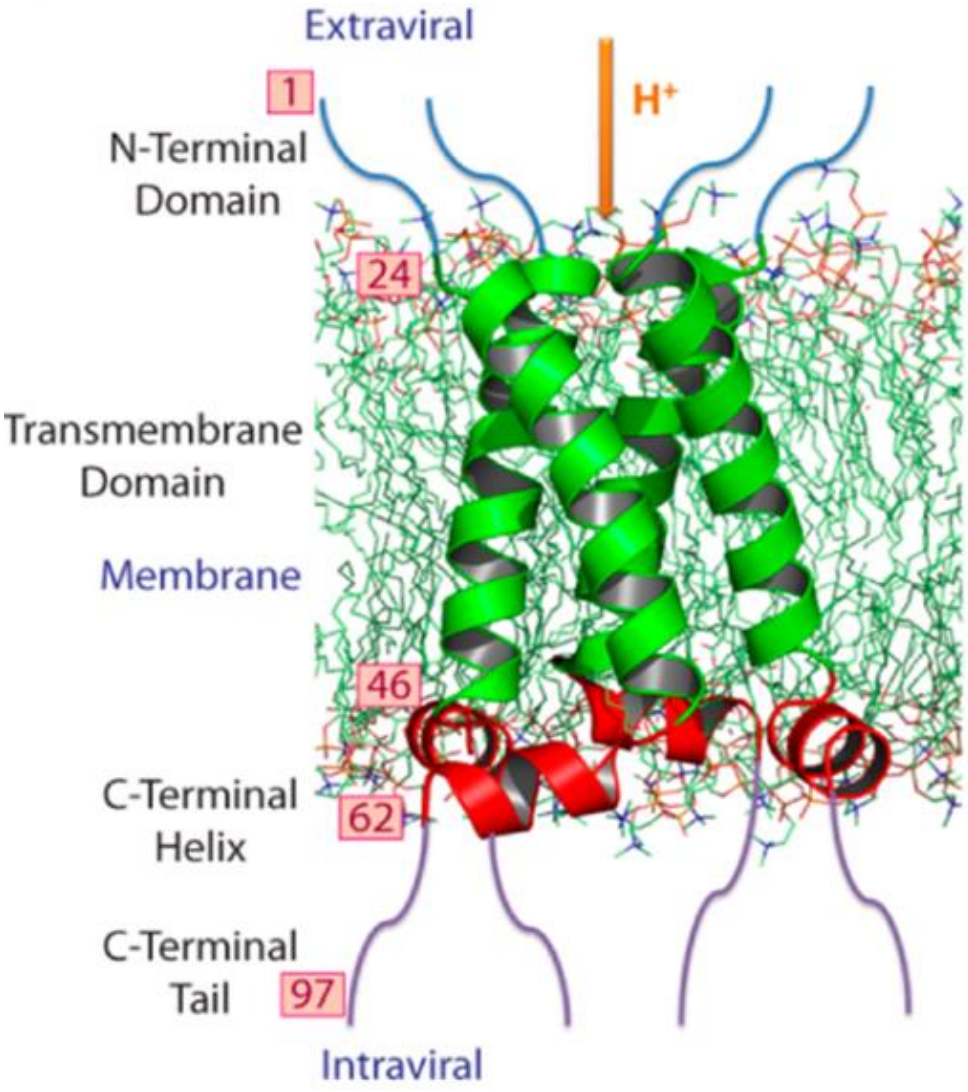

Figure 5 – The M2 ion channel. Image taken from Schmidt *et al.*, 2013 *Influenza Virus A M2 Protein Generates Negative Gaussian Membrane Curvature Necessary for Budding and Scission.*

M2 is a relatively small, 97 amino acid, ~14 kDa protein which exists as part of the virus in a homotetramer. M2 is a transmembrane protein with an externally facing, antigenic ectodomain, a transmembrane domain containing the ion channel pore, and an internal cytoplasmic tail, responsible for many viral-viral and viral-cellular interactions. The cytoplasmic tail (residues 70-77) is implicated to play an important role in the binding of M1 to M2 (McCown and Pekosz, 2006). M2 plays a role in stabilising the viral budding site by inducing negative membrane curvature at the budding site (Schmidt, Mishra, Wang, Degrado, *et al.*, 2013). Any mutation within the residues required for the interaction between M1 and M2 may inhibit IAV filament formation (Rossman *et al.*, 2010). Truncation at residue 70 of A/Udorn/72 M2 causes a loss of filament formation on the surface of cells infected with IAV and the loss of its interaction with M1 (McCown and Pekosz, 2006). Loss of filament formation has also been observed in mutations of M2 amphipathic helix (Rossman *et al.*, 2010). Residues 70-77 are also necessary for efficient production of viral particles, mutations at these residues have been shown to impair incorporation of vRNP into budding virions (Grantham *et al.*, 2010). The cytoplasmic tail of M2 can also be phosphorylated (Hughey *et al.*, 1995), ubiquitinated (Su *et al.*, 2018) and has been shown to interact with: Annexin A6 (Ma *et al.*, 2012), Hsp40 (Guan *et al.*, 2010), Calveolin-1 (Zou *et al.*, 2009), TRAPPC6AΔ (Zhu *et al.*, 2017), LC3 (Beale, Wise, Stuart, Benjamin J Ravenhill, *et al.*, 2014), Caspase (Zhirnov and Klenk, 2009) and ATPase6 (S. Mi *et al.*, 2010), though the functions of most of these modifications and interactions remain unknown.

In the budding virus, M2 is localised to the plasma membrane, but is not associated with lipid rafts as the more abundant HA and NA proteins are (Zhang, Pekosz and Lamb, 2000). M2 is thought to recruit vRNPs, which are complexed with M1, in order to package them within newly forming virions. Moreover, M2 has the ability to induce negative plasma membrane curvature. This is an essential requirement for viral budding, as without induction of this curvature, virions are unable to 'pinch off' host cells and subsequently continue infection. It is this ability of M2 to induce such curvature that has been a focus of attempting to understand why certain strains of IAV can produce infectious viral filaments. A role for M2 in filamentous virus formation has been well established but the cause remains unclear. Roberts, Lamb

and Compans reported in 1998 the ability of the monoclonal antibody 14C2 raised against the ectodomain of A/Udorn/H3N2 M2 to inhibit the formation of viral filaments (Roberts, Lamb and Compans, 1998). This phenomenon may be explained by the interference of membrane curvature by 14C2 or by M2 interacting with M1; however the discovery of cytoplasmic tail mutants by Beale et al in 2014 being able to influence morphology also add weight to the importance of M2 in this phenotype. Beale et al demonstrated the ability of the M2 cytoplasmic tail to bind to the mammalian ATG8 homolog, Microtubule-associated proteins 1A/1B light chain 3B (LC3), which enabled the virus to not only subvert cellular autophagy, but also affected the virus's ability to form filaments.

1.51 M2 and autophagy subversion

IAV can subvert autophagy by the ability of specific residues within the CT of M2 to block the fusion of autophagosome with lysosome. Autophagy is part of the cellular protein degradation and recycling machinery. In the normal pathway shown in Figure 6, proteins which have been marked for degradation through ubiquitination are engulfed by a forming double membrane phagophore, which itself is initiated by the action of ULK1 and class III PI3K complexes (Ndoye and Weeraratna, 2016). In selective autophagy, p62 is able to bind to ubiquitin tagged proteins and chaperone them to the elongating phagophore wall. p62 itself contains an LC3 interacting motif (LIR), allowing it to bind to LC3 (Pankiv *et al.*, 2007). LC3 is the main marker used to study autophagy as it is crucial for autophagosome formation and closure of the phagophore into a double membrane autophagosome vesicle (Tanida *et al.*, 2005; Mizushima and Yoshimori, 2007; Tanida, Ueno and Kominami, 2008). After the closure of the autophagosome, LC3 is contained within the lumen in complex with p62 and tagged proteins. LC3 is also present on the surface of autophagosomes (Kabeya *et al.*, 2000), where it is essential for the subsequent fusion of the autophagosome to the lysosome containing the hydrolytic enzymes required for breakdown of the autophagosome contents including LC3 and p62 (McEwan *et al.*, 2015). Several small molecule inhibitors of various stages of autophagy exist, with compounds such as chloroquine and bafilomycin A1 blocking specifically the fusion of the lysosome to the autophagosome (Mizushima, Yoshimori and Levine, 2010). In the context of IAV infection, this phenomenon is subverted by M2 (Gannagé *et al.*, 2009). The CT of M2 is known to contain a LIR, much the same as p62 (Beale, Wise, Stuart, Benjamin J. Ravenhill, *et al.*, 2014).

This may create a twofold effect in the ability of M2 to allow the subversion of autophagy by IAV, thereby preventing viral protein degradation. Firstly, M2 may compete for binding of p62 with LC3 through the highly conserved FVxI motif, which is contained in both M2 (91 – 94) and p62. This motif is found in over 99% of unique M2 sequences (Squires *et al.*, 2012). Through competitive binding disrupting the LC3-p62 interaction, and the necessity of a LC3-p62 interaction required to degrade proteins through selective autophagy, this is one way in which M2 may disrupt the pathway, though this has not yet been proven. Secondly, the binding of LC3 by the M2 LIR causes a distinct and striking relocalisation of LC3 to the plasma membrane (Beale, Wise, Stuart, Benjamin J. Ravenhill, *et al.*, 2014) (Figure 7). This sequestering of LC3 away from the site of autophagy may deplete cytoplasmic LC3 which might otherwise be available for autophagy. This may allow IAV to use autophagy machinery to enhance virion stability and budding.

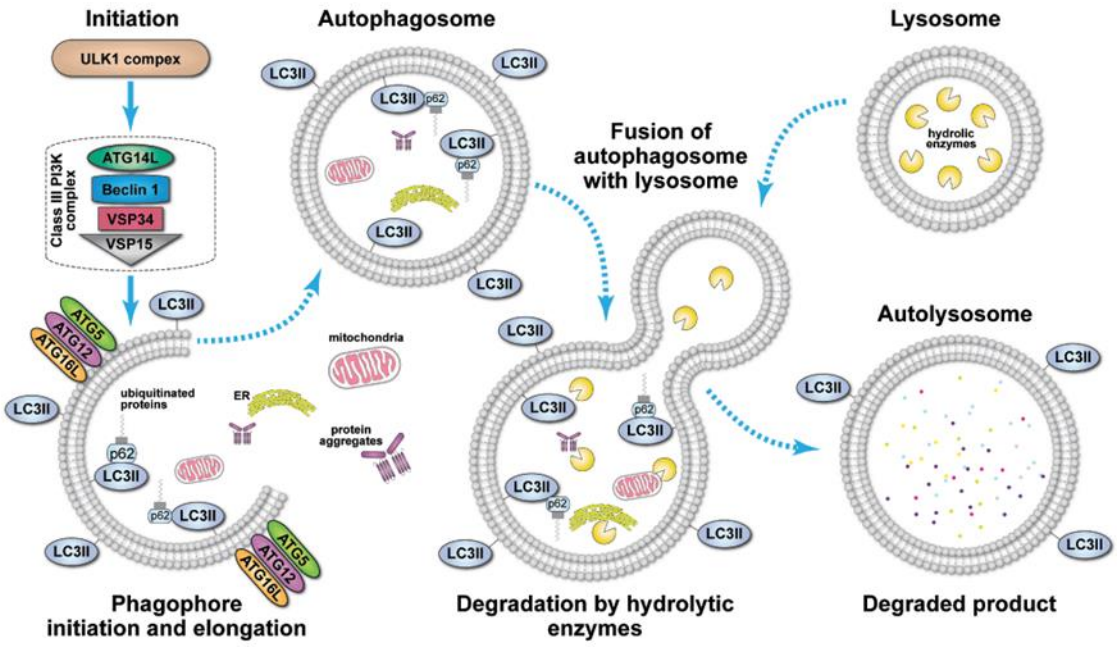

Figure 6 – Autophagy. Image taken from Ndoye and Weeraratna, 2016 *"Autophagy- An emerging target for melanoma therapy"* showing the process of autophagy initiation and progression.

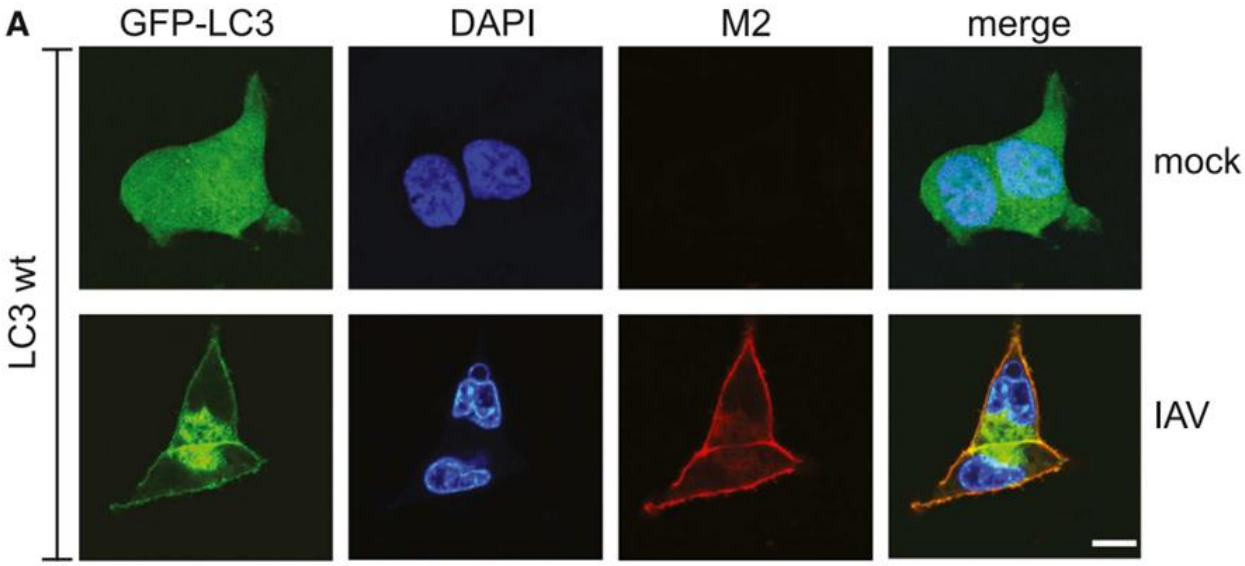

Figure 7 – LC3 relocalisation during IAV infection. Image is taken from Beale, Wise, Stuart, Benjamin J. Ravenhill, et al., 2014, and displays the distinct relocalisation of LC3 from freely cytoplasmic, to plasma membrane, upon infection with IAV.

1.52 M2 and SUMO interactions

SUMOylation is a post-translational modification (Hannoun *et al.*, 2010), which is speculated to have an important role in maturation and assembly of influenza virus. SUMO (Small Ubiquitin-like Modifiers) are predominantly located in the cell nucleus; they conjugate to many proteins and regulate cellular processes such as transcription, cell-cycle progression and DNA repair (Domingues *et al.*, 2015). SUMOylation is where SUMO is conjugated by an isopeptide linkage to a lysine residue by a small set of known enzymes.

SUMOylation of a protein via an isopeptide linkage alone, does exert physiological consequences; however, through SUMO-interacting motifs (SIM) a SUMOylated protein gains the ability to control the interactions and function of other proteins and is one of the main consequences of SUMOylation (Minty *et al.*, 2000; Yang and Sharrocks, 2010; Zhao *et al.*, 2014). SIM are less than 10 amino acids in length, they may contain phosphorylated residues and interact with SUMO via a specific surface groove (Kerscher, 2007). Properties and requirements for a SIM are conserved, however the sequence required for one SUMO paralogue does differ from another despite reasonable similarity between paralogs (Namanja *et al.*, 2012). The majority of SIMs have two main elements: a hydrophobic core consisting of three to four residues often being valine or isoleucine; and an acidic region of

glutamic acid or aspartic acid side chains, or phosphorylated serine or threonine residues. SIM hydrophobic residues bind SUMO via β2 strand which causes extension of the β-sheet of the β-grasp fold. The parallel or anti-parallel orientation of SIM to the β-strand is controlled by binding of SIM acidic residues to basic ones on SUMO, this also has the effect of strengthening the interaction of SIM-SUMO. Because of the role of acidic residues, they are only required to be within close proximity to the hydrophobic core of the SIM which leads to even wider variation in SIM motifs (Hecker *et al.*, 2006).

Multiple proteins of IAV become SUMOylated during virus replication. M1 is SUMOylated at K242 which is required for the interaction between M1 and RNP. A lack of M1 SUMOylation prevents the export of RNP (Wu, Jeng and Lai, 2011a). NS1 (Non-structural protein 1) is SUMOylated within its C-terminus at K70 and K219 which increases the stability of NS1 and promotes increased growth of IAV (Pal, Rosas and Rosas-Acosta, 2010). The N-terminal region of NP (Nucleoprotein) is SUMOylated at K4 and K7. K7 Is highly conserved amongst the many strains and subtypes of IAV however it is not required for the survival of the virus. SUMOylation of NP, however, is essential for virus growth and the intracellular trafficking of NP its self (Chen *et al.*, 2017). Preliminary data suggests that the M2 protein may also interact with SUMO, though this has not been previously examined.

1.53 M2 and caspase cleavage

The M2 CT contains multiple cellular protein interaction sites as described above. Situated at positions 87 and 88 are two aspartic acid residues, which function as the active resides of a conserved caspase cleavage site. Previous studies have determined this ability of M2 to be cleaved by cellular caspases to be necessary for pathogenicity but not necessarily for replication *in vitor* (Zhirnov and Syrtzev, 2009). Viruses with a D87 mutation, rendering M2 uncleavable, still infected and replicated in chicken hosts and retained this trait, but with reduced mortality of the host (Zhirnov and Klenk, 2009). However, the function of the caspase cleavage and the conserved D87/D88 caspase cleavage motif is not presently understood.

1.6 PREFACE

This thesis attempts to shed light on some of the more nuanced interactions of the cytoplasmic tail of M2, and how these may lead on to an influence on morphology of newly forming virions. Data is presented on the presence of a SIM within the cytoplasmic tail of M2, and its effects studied. Previously published data on the M2-LC3 interaction is expanded upon using M2 mutants which attempt to disrupt the LIR, the SIM, or both. Morphology of viruses used for LAIV vaccine production are also evaluated with well-established confocal microscopy techniques. Data and discussion presented in this body of work hopes to provide a basis for the continued study of the highly conserved cytoplasmic tail of M2, and its wide-ranging interactions with both other IAV proteins, as well as proteins of host cells.

2 MATERIALS AND METHODS

2.01 TISSUE CULTURE

HEK-293T cells (human embryonic kidney), MDCK (Madin-Darby canine kidney) cells, A549 (adenocarcinomic human alveolar basal epithelial) cells, HeLa (human epitheloid cervix carcinoma) cells and HeLa HEX ATG8 knockout cells (Nguyen, et al., 2016) were grown in Dulbecco's Modified Eagle's Medium (P04-04510, DMEM, PAN Biotech., Aidenbach, Germany). DMEM was supplemented with 10% foetal bovine serum (P30-3306, PAN Biotech) and 1% penicillin/streptomycin (15140122, Gibco Life Technologies, Thermo Scientific, Loughborough, United Kingdom). Cells were grown at 37°C in the presence of 5% CO_2 and passaged to ~80% confluency in appropriate flasks (T25, T75 or T175 – Sarstedt, Numbrecht, Germany) prior to splitting. Once desired confluency was achieved, supernatant media was discarded, and cells were washed twice with warm PBS in order to remove residual culture media containing FBS. Cells were then incubated in 0.25% Trypsin in PBS (P10-022100, PAN Biotech, Aidenbach, Germany) to facilitate detachment from the flask. Once detachment had occurred, warmed supplemented DMEM was used to wash the cells down the flask, and collect them in to a 15 ml collection tube. Cell suspension was then centrifuged at 1000 x g for five minutes at room temperature. The supernatant media was then discarded from the resultant cell pellet, and the pellet was resuspended completely in supplemented DMEM to the desired volume. To prepare a new cell culture flask for seeding, the appropriate amount of supplemented DMEM was placed in to the appropriate flask, and a volume of resuspended cell pellet was introduced.

Cell lines were obtained from the American Type Culture Collection (ATCC) or the European Collection of Cell Cultures (ECACC). Cells obtained from ATCC: HeLa (CCL-2), HEK 293-T (CRL-3216), A549 (CCL-185). Cells obtained from ECACC: MDCK (84121903). HeLa HEX cells were a kind gift from Michael Lazarou (Monash University).

2.02 CLONING OF M2 MUTANTS

pCAGGS plasmid vector containing IAV M2 from H3N2 A/Udorn/307/1972 strain was described previously (Rossman, Jing, Leser, Balannik, et al., 2010). Site directed mutagenesis was performed on this plasmid using New England BioLabs (NEB, Ipswich Massachusetts USA) Q5 Site-directed Mutagenesis Kit Protocol (product number E0554), primers were designed using NEBaseChanger v1.2.6 (http://nebasechanger.neb.com/) and manufactured by Eurofins Genomics (Wolverhampton, United Kingdom). I94M and V92S mutations were produced in pCAGGS M2 H3N2 A/Udorn/307/1972.

gBlocks Gene Fragments were designed to produce mutants F91A, I94M, and FLAG-M2 consisting of 3 repeats of IAV M2 H3N2 A/Udorn/307/1972 residues 87-97 with an N-terminal FLAG tag. gBlock Gene Fragment manufactured by Integrated DNA Technologies (Integrated DNA Technologies, Leuven, Belgium), are double-stranded, sequence-verified genomic blocks consisting of EcoRI, XhoI restriction enzyme sites surrounding the mutant IAV M2 H3N2 A/Udorn/307/1972 gene. M2 mutants produced by PCR and gBlock fragments were digested using EcoRI (FD0274), XhoI (FD0694) (FastDigest, Thermo Scientific, Loughborough, United Kingdom), separated by agarose gel electrophoresis, extracted by QIAquick Gel extraction kit (28704, Qiagen, Hilden, Germany) and ligated into pCAGGS backbone using Anza T4 DNA Ligase (IVGN2104, Invitrogen, Carlsbad, California, USA). The ligation product was transformed into NEB 5-alpha Competent E. coli (C2987I, NEB, Ipswich MA, USA) using their proprietary heat shock protocol. E. coli were grown on Lysogeny broth (LB), agar, and ampicillin plates. A single colony from each plate was grown overnight in 15ml LB with ampicillin, shaking at 200 rpm and 37°C. Plasmid was recovered by mini-prep (K0502, GeneJET Plasmid Miniprep Kit, Thermo Scientific). The concentration of plasmid stocks was measured by Implen (Munich Germany) NanoPhotometer N60 and sequenced by Source Bioscience (Nottingham, United Kingdom). Transfection quality DNA was produced by subsequent transformation and midi-prep of the plasmid (K0481, GeneJet Plasmid Midiprep Kit, Thermo Scientific), with the subsequent concentration determined by NanoPhotometer. Plasmid was subsequently aliquoted and stored at -20°C, and sequence was confirmed using the

Sanger sequenceing service provided by Source Bioscience (http://www.sourcebioscience.com/) Nottingham, UK.

2.03 VIRAL INFECTION

A/Udorn/301/1972 (H3N2) was used in most experiments as previously described by Rossman *et al.*, 2010. A/PR/8/1934, PR8ΔM2 (V7-T9 +U148A) and PR8ΔM42 (U115C) viruses were a kind gift from Professor Paul Digard at The Roslin Institute, University of Edinburgh and have been previously described (Wise *et al.*, 2012). Seasonal LIAV immunisation strains produced by MedImmune of Liverpool, UK, were a kind gift from Dr. Oliver Dibben (MedImmune).

For viral infections, cells were seeded in six well tissue culture plate at a number such to achieve ~85% confluency at point of infection. IAV H3N2 A/Udorn/301/1972 was diluted in to DMEM with no supplementation in order to provide a viral inoculum having a multiplicity of infection (MOI) of 3. The growth media was removed from the cell monolayer, cells were washed twice with warm phosphate-buffered saline (PBS, pH 7.4) as to remove infection inhibiting serum, and the viral inoculum added. Cells were then incubated for two hours at 37°C, 5% CO2, and agitated every 15 minutes. After two hours, the innoculation media was removed and new fully supplemented media was applied. Cells were incubated for 24 hours post-infection at 37°C and 5% CO2, after which they were either lysed with appropriate lysis buffer, or prepared for immunofluorescence microscopy.

VIRUS NAME	STRAIN/SUBTYPE/AREA OF FIRST DISCOVERY/YEAR OF FIRST IDENTIFICATION	ABBREVIATION
'Udorn'	A/H3N2/Udorn valley Russia/1972	A/Udorn/72 or Udorn
'PR8'	A/H1N1/Puerto Rico/1934	PR8

2.04 TRANSFECTION

Cells were seeded in six well tissue culture plate at a number such to achieve ~65% confluency at point of transfection. Typically, 1 µg of DNA was used per transfection condition, up to a maximum amount of 5 µg of DNA per well of a six well tissue culture plate. Cells were transfected using Lipofectamine 3000 reagent (L3000008, Invitrogen, Carlsbad, California, United States) for transient expression studies, and TransIT LT1 (MIR2304, Mirus Bio, Madison, Wisconsin, United States) for performing viral rescue of IAV from recombinant DNA (see sub section 'Mutant virus production'). For both products, the manufacturer's protocol was followed. For transient expression studies cells were incubated for 24 to 48 hours at 37°C and 5% CO_2, after which time they were either lysed with appropriate lysis buffer, or prepared for immunofluorescence microscopy.

2.05 LYSIS

For assays needing gentle lysis, a lysis buffer of 1% Thesit (88315, Sigma-Aldrich, St. Louis Missouri USA) in tris-buffered saline (TBS, pH 7.6) was prepared, with protease inhibitors (cOmplete Protease inhibitor cocktail, 11697498001, Roche, Sigma-Aldrich, St. Louis, Missouri, USA). For harsher and more complete lysis, a buffer of 1% NP-40 (I8896, Sigma-Aldrich) and 1% sodium deoxycholate in TBS was prepared. Incubation media (viral inoculum or transfection complex media) was removed, kept or discarded, and appropriate volume and type of lysis buffer was added to the well. Cells were incubated in lysis buffer on wet ice for 15 minutes with occasional agitation. Cells were then gently scraped down with a sterile pipette tip, and collected in to a 1.5 ml collection tube. The lysate was centrifuged at 15,000 x g at 4°C for ten minutes, after which time the supernatant was removed, aliquoted and stored appropriately. The insoluble material was discarded.

2.06 WESTERN BLOTTING AND IMMUNOPRECIPITATION

For all immunoprecipitations, the Thermo Scientific Classic IP kit (26146, Thermo Scientific, Loughborough, United Kingdom) was used, and the manufacturer's instructions were followed. This includes the instructions for preparation of the elutions for protein gel electrophoresis. Whole cell lysates were prepared for protein gel electrophoresis by the addition of 2 x Laemmli sample buffer (4% sodium dodecyl sulphate, 20% glycerol, 120 mM Tris-Cl pH 6.8, 0.02% w/v

bromophenol blue) in a 1:1 ratio with lysate. β-mercaptoethanol was added to a final concentration of 5%, and samples were boiled at 95 to 100°C for ten minutes before being allowed to cool completely. Samples were run on Biorad criterion TGX 4-12% Bis-Tris gels (3450124, Bio-Rad, Hercules, California USA) using the manufactures protocol and tank, in tris-glycine-SDS (25 mM Tris, 192 mM Glycine, 0.1% SDS, pH 8.3) running buffer. Transfer on to PVDF membranes was performed using Bio-Rad (Hercules, California, USA) Trans-Blot Turbo RTA Midi PVDF Transfer Kit (1704272), following the manufacturer's protocol. PVDF membranes were blocked in 5% milk w/v in TBS-Tween (TBS plus Tween-20 [Sigma-Aldrich] 0.1%) for 1 hour, before appropriate dilution of primary detection antibody in fresh blocking solution was applied overnight at 4°C with agitation. After which, membranes were washed three times in TBS-T before the addition of secondary horseradish peroxidase (HRP) conjugated antibody, diluted appropriately in TBS-T, incubated for 1 hour with agitation at room temperature. Membrane was then further washed three times with TBS-T and twice with TBS. Chemiluminescent development of the membrane was achieved using the Clarity Western ECL Substrate (1705060S, Bio-Rad) as per the manufacturer's protocol. Developed membranes were then visualised on a Syngene G: Box chemi-XX6 imager (Cambridge UK).

2.07 IMMUNOFLUORESCENCE MICROSCOPY

For immunofluorescense microscopy, cells were seeded in wells containing 22 x 22 mm coverslips. After appropriate assaying, cells were washed twice with PBS to remove debris, before fixing in 4% paraformaldehyde (PFA) for 20 minutes on wet ice. PFA was then safely removed, cells were further washed twice in cold PBS to arrest fixation, and if required were permeabilised with 0.1% Trition X-100 (Sigma-Aldrich, St. Louis Missouri USA) in TBS for 10 minutes. Cells were then blocked using 1% bovine serum albumin (BSA) and 0.05% Tween in TBS for 1 hour. Blocking solution was then removed, and primary antibody diluted in blocking solution was added, and incubated for two hours to overnight at 4°C. Then, primary antibody was removed, cells were washed four times with TBS, and secondary fluorescently conjugated antibody was added to the cells in blocking solution for two hours. Cells were again washed four times with TBS, before two water washes to remove residual salts. Coverslips were mounted on glass slides using ProLong

Gold Reagent containing DAPI (P36931, Invitrogen). When ready for imaging, prepared glass slides were imaged on a Zeiss LSM880 confocal microscope. Laser lines of nanometer wavelengths 405, 488, 561 and 633 were used to excite the relevant fluorophores attached to secondary antibodies (e.g. Donkey anti-Mouse AlexaFluor 488), or small molecules (e.g. DAPI to visualise dsDNA) and the resultant fluorescence was collected using an adjustable emission collection range when conducting standard confocal microscopy (range 380 nm to 750 nm). When utilising the Airyscan capability of the LSM880, emission filters had to be chosen manually to accurately collect the correct fluorescence emission. The available filter sets were: Band Pass (BP) 420 nm – 480 nm plus BP 495 nm – 550 nm; BP 420 nm – 480 nm plus BP 495 nm – 620 nm; BP 495 nm – 550 nm + Long Pass (LP) 570 nm; BP 570 nm – 620 nm plus LP 645 nm.

2.08 FLUORESCENCE POLARISATION

Fluorescence polarisation was performed using a short FITC-labelled M2 peptide FITC-Ahx-DSHFVSIELE residue 88-97 (Biomatik, Wilmington Delaware USA) from the H3N2 A/Udorn/307/1972 strain at a concentration of 50 nM. 50 µl of distilled, sterile water was placed into each well of a black flat bottomed 96 well plate. A serial dilution of the protein ligand was performed at the following staring concentrations: 4µM SUMO1/2/3 (Boston Biochem, [K-700]), 25 µM LC3A (Boston Biochem, [rhHis6-LC3/MAP1 LC3A, UL-430]), 25 µM LC3B (Enzo, Farmingdale, New York, USA [BML-UW1155-0500]) and 10µM Ubiquitin (Boston Biochem, U-530). 50 µl of 50 nM M2-FITC peptide was added and incubated for 10 minutes with the ligand. The plate was imaged using BMG Labtech CLARIOstar Plate Reader, performing a top down fluorescence polarisation scan exciting at 490 nm and collecting emission spectra at 525 nm.

2.09 MASS SPECTROSCOPY

A T75 tissue culture flask of confluent HEK-293T cells was transfected with pCAGGS FLAG-M2 consisting of three repeats of IAV M2 H3N2 A/Udorn/307/1972 residues 87-97 (IDT) using the transfection protocol described

previously. Cells were lysed and immunoprecipitated using monoclonal IgG2b anti-Flag antibody (CSB-MA000021M0m, Cusabio CusAb, College Park, Maryland, USA) as previously described, with the following alterations: Cells were lysed in 900µl of TBS plus Thesit lysis buffer. 10 ng of Flag antibody was used in the immunoprecipitation and 50 µl of sample buffer elution was used. Sample was run on Bio-Rad Mini-Protean TGX Gels in Tris-Glycine-SDS running buffer. The gel was run to ensure that all protein within the sample was within a single band 2 cm into the gel. Coomassie staining was performed on the gel, whereby the single dye front containing the proteins to be analysed was excised. After excision, the band was stored in sterile distilled water and frozen at -20°C. Subsequent preparation of the sample and mass spectroscopy was kindly performed by Kevin Howland at the University of Kent Biomolecular Science Facility.

2.10 BIOINFOMATICS

GPS-SUMO 1.0 (http://sumosp.biocuckoo.org/) SUMOylation prediction software was used to analyse the sequence of A/Udorn/1972 M2. Influenza Research Database (https://www.fludb.org/) was used to compile and align 8588 unique sequences of IAV M2. A Logo was then created using WebLogo 3.6.0 (https://pypi.org/project/weblogo/).

2.11 PROXIMITY LIGATION ASSAY

Cells were washed and fixed using 4% PFA for 10 minutes on wet ice (as per 'Immunofluorescence Microscopy', with blocking and diluent reagents taken from the Duolink PLA kit, DUO92101) and permeabilised using 0.1% Trition X-100 in TBS for 10 minutes. Incubation in appropriate primary antibodies was conducted, before utilising the Duolink Proximity Ligation Assay ('PLA', Sigma-Aldrich [product DUO92101]) reagents and protocol, within which was contained necessary secondary antibodies. Duolink protocol is available online at https://www.sigmaaldrich.com/technical-documents/protocols/biology/duolink-fluorescence-user-manual.html.

2.12 MUTANT VIRUS PRODUCTION

IDT gBlock fragments were designed for V92S, I94M, F91A, H90Y and H90S to contain the restriction sites ClaI and ApaI. gBlock fragments and pHH21 containing the A/Udorn/301/1972 M segment were digested with ClaI (FD0144), ApaI (FD1414) (FastDigest, Thermo Scientific) and then processed in the same way as pCAGGS M2 mutant cloning to produce mutant pHH21 IAV M segment H3N2 A/Udorn/301/1972 mutant plasmids. Below is ClustalOmega sequence alignment for indicated M2 mutants:

```
v92s      AGTCTATGAGGGAAGAATATCGAAAGGAACAGCAGAGTGCTGTGGATGCTGACGACAGTC  120
h90s      AGTCTATGAGGGAAGAATATCGAAAGGAACAGCAGAGTGCTGTGGATGCTGACGACAGTT  120
h90y      AGTCTATGAGGGAAGAATATCGAAAGGAACAGCAGAGTGCTGTGGATGCTGACGACAGTT  120
i94m      AGTCTATGAGGGAAGAATATCGAAAGGAACAGCAGAGTGCTGTGGATGCTGACGACAGTC  120
f91a      AGTCTATGAGGGAAGAATATCGAAAGGAACAGCAGAGTGCTGTGGATGCTGACGACAGTC  120
          ************************************************************

v92s      ATTTTTCTAGCATAGAGCTGGAGTAAAAAACTACCTTGTTTCTACTAATAACCCGGCGGC  180
h90s      CTTTTGTCAGCATAGAGCTGGAGTAAAAAACTACCTTGTTTCTACTAATAACCCGGCGGC  180
h90y      CTTTTGTCAGCATAGAGCTGGAGTAAAAAACTACCTTGTTTCTACTAATAACCCGGCGGC  180
i94m      ATTTTGTCAGCATGGAGCTGGAGTAAAAAACTACCTTGTTTCTACTAATAACCCGGCGGC  180
f91a      ATGCTGTCAGCATAGAGCTGGAGTAAAAAACTACCTTGTTTCTACTAATAACCCGGCGGC  180
           *  *   ***** ********************************************
```

Recombinant viruses were rescued using the method previously described by Fodor *et al.*, 2007 using HEK-293T cells as initial viral producers, and MDCKs as whole virus replicators in co-culture. Briefly, this process involves transfection of HEK 293T cells with all eight reverse genetics, pHH21 based vectors containing inserts coding for each viral segment, plus relevant mRNA production, using the transfection reagent TransIT-LT1 (Mirus Bio, Madison, Wisconsin, United States). HEK 293T cells are grown in a six centimetre tissue culture dish in co-culture with MDCK cells. Once confluency of the dish reaches ~80%, the transfection complexes are added to the cells. The principle being that HEK-293T cells are efficient acceptors and translators of DNA via transfection and can produce the initial virions in this way. MDCK cells are poor acceptors of DNA from transfection, but excellent acceptors of virus for infection and subsequent replication. After 48 hours, or when significant cytopathic effect (CPE) from virus is seen, supernatant is harvested, clarified by centrifugation (≥14,000 x g for 15 minutes), aliquoted and frozen at -80°C or used immediately. This clarified supernatant should contain some viable virus at a low but unknown titre. Subsequently, T75 tissue culture flasks containing MDCK cells only can be infected with this passage zero (P0) rescue supernatant, then the resultant

supernatant containing expanded viral titre can be quantified using the plaque assay method.

2.13 TRYPAN BLUE COUNTING

Cells were trypsinised, added to the supernatant and centrifuged at 100g for 5 minutes. Cells were resuspended in serum free media and diluted 1:1 with 0.4% w/v trypan blue solution and incubated for 5 minutes. Cells were counted using haemocytometer and the percentage viability calculated.

2.14 ANTIBODIES

Anti-M2 14C2 and polyclonal goat anti-Udorn antibodies were used as previously described (Rossman *et al.*, 2010). Anti-SUMO was obtained from Sigma Aldrich under the product code PRS3969 and Abcam (Cambridge, UK) under the product code antibodies ab11672. Anti-Vimentin antibody was obtained from Cell Signalling Technologies (London, UK) under product code D21H3, as was anti-CK2 (#2656), anti-VATPase (#13569), anti-Clathrin (#4796), and anti-EIF3a (#2538). Anti-HA was obtained from the influenza A antisera panel from BEI (NR-3148) Manassas, VA, USA.

Antibody	**Company/Cat No.**	**Diltion used (Western blot)**	**Diluion used (IF microscopy)**
14C2 anti-M2 ectodomain	Laboratory stocks (historic)	1:500	1:200
Anti-Udorn polyclonal	Laboratory stocks (historic)	1:1000	1:500
Anti-HA	BEI antisera panel, NR-3148	1:500	1:200
Anti-SUMO	Sigma Aldrich, PRS3969	1:1000	1:100
Anti-Vimentin	Cell Signalling Technologies, D21H3	1:1000	1:200

Anti-CK2	Cell Signalling Technologies, 2656	1:1000	N/A
Anti-vATPase	Cell Signalling Technologies, 13569	1:1000	N/A
Anti-Clathrin	Cell Signalling Technologies, 4796	1:1000	N/A
Anti-EIF3a	Cell Signalling Technologies, 2538	1:1000	N/A

3 RESULTS

3.0 M2 CT INTERACTIONS WITH SUMO DURING VIRUS ASSEMBLY AND BUDDING

The M2 protein of IAV is a 97 amino acid long, membrane spanning protein which functions mainly as an ion channel to allow the acidification of the viral core during the initial stages of IAV infection, when the virus is contained within an endosome during entry. Structurally, M2 exists natively as a homotetramer (Holsinger and Alams, 1991) and contains three main domains – the ectodomain from positions 1 – 24, the transmembrane domain containing the pore through which protons flow from positions 25 – 43, and finally the cytoplasmic tail from positions 44 – 97 (Schnell and Chou, 2008; Pielak and Chou, 2011). Modifications of proteins within the cell through either covalent SUMO binding, or interaction, is known to play a crucial role in several processes, both in the uninfected cell and in the virally infected cell. SUMO's effect on target proteins is broad, influencing gene expression and repression (Gostissa *et al.*, 1999; Müller *et al.*, 2000; Girdwood *et al.*, 2003), subcellular localisation (Sternsdorf, Jensen and Will, 1997; Chakrabarti *et al.*, 2000; Kishi *et al.*, 2003) and structural and functional stability (Bies, Markus and Wolff, 2002; Lin *et al.*, 2003; Ghioni *et al.*, 2005). SUMO is known to play an advantageous role in viral infection, such as during Epstein-Barr virus infection (Adamson and Kenney, 2001) and during Ebolavirus infection (Chang *et al.*, 2009), as well as during the host immune response (Shuai and Liu, 2003; Liu, 2004; Z. Mi *et al.*, 2010). Furthermore, SUMO modification is known to occur in the proteins of IAV, namely of the matrix protein, M1, at position K242 (Wu, Jeng and Lai, 2011a) and the polymerase subunit PB1, the nucleoprotein NP and the non-structural protein NS2 (Pal *et al.*, 2011). Additionally, IAV infection is known to increase global cellular expression of SUMO (Pal *et al.*, 2011).

The interaction of the cellular small ubiquitin-like modifier, SUMO, with IAV M2 was predicted through bioinformatic analysis of the M2 sequence using a SUMO predictor, GPS-SUMO (http://sumosp.biocuckoo.org/) and confirmed using co-immunoprecipitation, and further using an in-situ interaction assay, the proximity ligation assay (PLA). Co-immunoprecipitation is a reliable method of studying protein-protein interplay, be they covalent links or weaker interactions, but is not without its technical drawbacks, such as disruption of the interactions during lysis. PLA is a more sensitive way to study these interactions, without disturbing the cell membrane through lysis, or disrupting the interactions.

3.01 The M2 CT contains a SUMO interacting region

Early studies (data not shown) alluded to an interaction between the M2 protein of the IAV strain A/Udorn/72 H3N2 and the small ubiquitin like modifier of the host cell, SUMO. To understand what part of M2 was responsible for this interaction, the M2CT sequence of A/Udorn/72 IAV was analysed using the GPS SUMO prediction software and the results are displayed in Table 1. SUMO interaction denotes a non-covalent interaction between the sequence of interest and SUMO. SUMOylation refers to covalent linkage of SUMO to the region. Here, interaction is specifically analysed and not covalent linkage, as M2 is not predicted to be SUMOylated. Position 92-96 returns the part of M2 of most interest, with a 'score' of 50 or greater taken to be significant. This provoked interest, as this overlaps with positions 91 – 94 of the M2CT, which has been studied by Beale *et al.*, 2014 and is the viral LIR domain (Figure 8). Position 91 is of particular note, as substitution for an alanine at this position results in a loss of LIR functionality.

This region of the M2CT is highly conserved, with all strains retaining both the LIR and SIM as seen in the logo composition of Figure 9. The conservation of residues 91 – 97 points to an important role for this region of the M2CT with possible implications for the role of the LIR in SUMO interaction. It is important to note the conservation of H90 (Figure 9), which will be discussed later in this work.

Domain	Position	Sequence	Score	Type
N-terminal ectodomain	3-7	LLTEV	32.4	SUMO Interaction
Transmembrane	26-30	LVVAA	47.8	SUMO Interaction
Transmembrane	33-37	IGILH	51.2	SUMO Interaction
Transmembrane	39-43	ILWIL	57.9	SUMO Interaction
C-terminal Amphipathic helix	49	K	15.7	SUMOylation
C-terminal Amphipathic helix	60	K	29.8	SUMOylation
C-terminal	78	K	22.5	SUMOylation
C-terminal Cytoplasmic Tail	92-96	VSIEL	53.4	SUMO Interaction

Table 1 – **Full length A/Udorn/72 H3N2 M2 contains several potential SUMO binding or interaction sites.** Bioinformatic predictions using GPS SUMO 1.0 of SUMO interacting regions or SUMOylation of the A/Udorn/72 strain of influenza A.

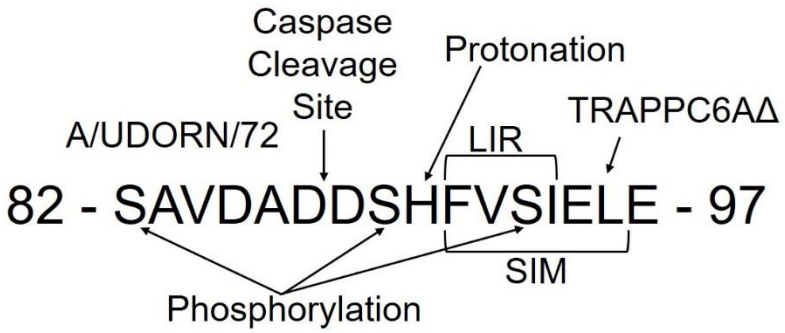

Figure 8 – **The cytoplasmic tail of A/Udorn/72 H3N2 M2 contains many cellular interacting sites.** Amino acid sequence of the cytoplasmic tail region of the M2 protein from the A/Udorn/72 H3N2 strain of IAV. Detailing of the various characteristic sites are annotated. Note the SIM overlap with the LIR.

Figure 9 - **Logo comprised of BLAST of 8,588 IAV M2CT sequences from 82-97.** Unique IAV sequences were analysed through the Influenza Research Database (https://www.fludb.org/). WebLogo (https://pypi.org/project/weblogo/) was then used to produce the logo.

Bioinformatic predictions of interactions of the M2 CT with SUMO and LC3 provided a basis for further investigation. These predictions then allowed point mutations to be designed within the M2 CT in order to specifically influence SUMO interaction and LC3 interaction and assess their impact on virus replication.

3.02 Mutations in the M2 CT are predicted to influence its interactions

Using bioinformatic predictions detailed in the previous figures, it is possible to infer changes in interactions with cellular proteins, namely LC3 and SUMO, through point mutations, deletions or double point mutations. GPS SUMO and previous literature was used to elucidate function-altering mutations (Table 2-3) which were then engineered into the pCAGGS vector for transient expression.

Mutation	Function
H90S	Deprotonated mimic
H90Y	Protonated mimic
F91A	Loss of LIR
V92S	Loss of SIM
I94M	Loss of LIR and loss of SIM

Table 2 – **Point mutations in the M2 CT and their predicted effects**

	SUMO Interaction Score	LC3 Interaction Score
Wild Type	53.4	9
F91A	51.5	0
V92S	0	6
I94M	0	0

Table 3 - **Both mutant transient expression vectors and viruses were produced (ref. M&M section once numbered).** The table shows bioinformatic predictions of SUMO and LC3 interactions of the new mutant sequences. Initially, point mutants were tested using SUMO interaction prediction software (GPS SUMO, available online at http://sumosp.biocuckoo.org/) and LIR interaction prediction software (iLIR, available online at http://repeat.biol.ucy.ac.cy/cgi-bin/iLIR/iLIR_cgi). These mutations were then engineered in to pCAGGS expression vectors using site-directed mutagenesis for transient protein expression studies in mammalian cell lines.

M2CT mutants were produced by site-directed mutagenesis, informed by the bioinformatical predictions indicated in Table 1. These plasmids encoding for point mutant M2 proteins, plus wild type M2 and a control vector (empty pCAGGS) were then transfected in to HEK-293T cells using TransIT-LT1, in combination with an LC3-GFP expression plasmid, in order to confirm an *in vitro* interaction through co-immunoprecipitation. 24 hours post transfection, the cells were lysed, and immunoprecipiatated using anti-SUMO and anti-GFP antibodies in order to elucidate the mutants' ability to affect the interaction between these two cellular proteins.

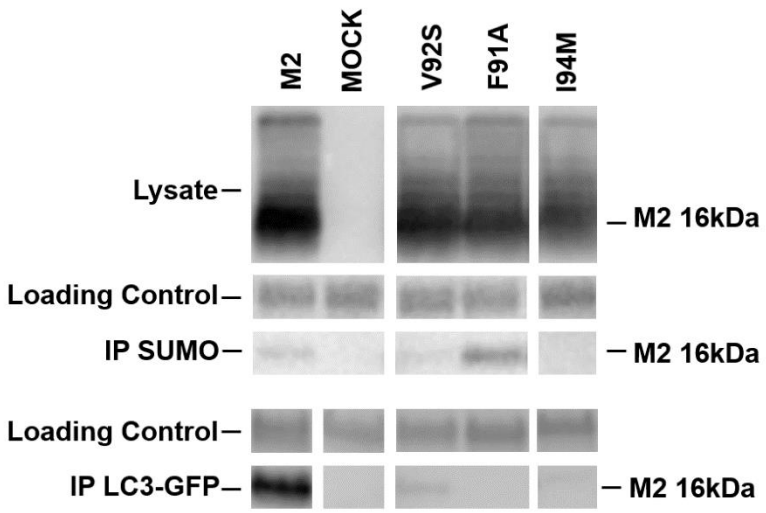

Figure 10 – **Mutations in the M2 CT affect interaction with LC3 and SUMO.** HEK-293T cells were co-transfected with pCAGGS vectors containing the genes for A/Udorn/72 H3N2 M2, or M2 mutants V92S, F91A or I94M, and LC3 fused with GFP. Cells were incubated for 24 hours, after which point they were lysed. Figure indicates one blot from a triplicate repeat.

M2 and all of the mutants are present in whole cell lysate at just under 16 kDa as shown, and lysates are loaded equally. The IP SUMO elution shows faint positive banding in the M2 and F91A lanes, with slight presence in the V92S lane. I94M shows no positive co-immunoprecipitation at all, and the mock lane is negative.

M2 co-immunoprecipitates strongly with LC3-GFP as is known from previous studies (Beale, Wise, Stuart, Benjamin J. Ravenhill, *et al.*, 2014), and there is presence too in the V92S lane, though slightly reduced, with the F91A, mock and I94M lanes being completely clear as predicted.

Additionally, it can be inferred from the above blot that M2 is in an interaction complex with SUMO, and not a covalent linkage owing to the presence of a positive 14C2 detection at just under 16 kDa. SUMO has a molecular weight of ~12 kDa, therefore, a covalent M2-SUMO complex would produce a 14C2 banding pattern of closer to 25 kDa.

Coimmunoprecipitation studies were informative in confirming bioinformatic data. To further characterise the interactions seen above, an ‘in-situ’ interaction assay was subsequently performed.

2.03 M2 co-immunoprecipitates with SUMO in transfection but not infection

Interaction of M2 with SUMO is seen in transfection studies through co-immunoprecipitation. This method can be affected by various external factors in sample preparation, including lysis conditions, which can obscure weak non-covalent interactions. Whilst co-immunoprecipitation is a reliable study, using an 'in-situ' interaction assay such as proximity ligation will show interactions using a more sensitive method of detection through nucleic acid based probes and enzymatic amplification. To further characterise M2-SUMO interactions, PLA was performed using plasmid-based expression (Figure 11), and a more relevant infection system using mutant viruses (Figure 12). Mutant viruses were produced using a reverse genetics based expression system as first described by Pleschka *et al.*, 1996. Eight plasmids encoding for the eight IAV genome segments were transfected in to a co-culture of HEK 293T cells and MDCK cells. HEK 293T cells efficiently express proteins from a plasmid system, whilst MDCK cells readily become infected, and produce virus. Co-culture supernatant was harvested and further amplified in MDCK cells, before viral titres were obtained in order for samples to be used for study. Mutant IAV produced in this way was verified genetically by Sanger DNA sequencing (Source Bioscience, Nottingham, UK).

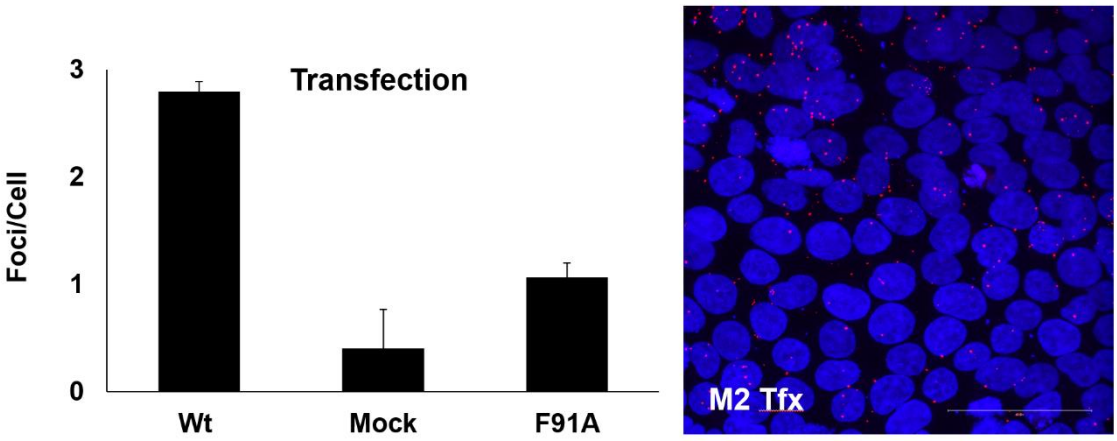

Figure 11 – **Transiently expressed wild type M2 interacts more strongly with SUMO than the F91A mutant as analysed *in-situ* using PLA.** HEK-293T cells were co-transfected with pCAGGS vectors containing the genes for A/Udorn/72 H3N2 M2, empty pCAGGS ('Mock') or F91A for 24 hours and then prepared for PLA using antibodies 14C2 and anti-SUMO. Figure indicates one image from a triplicate repeat set.

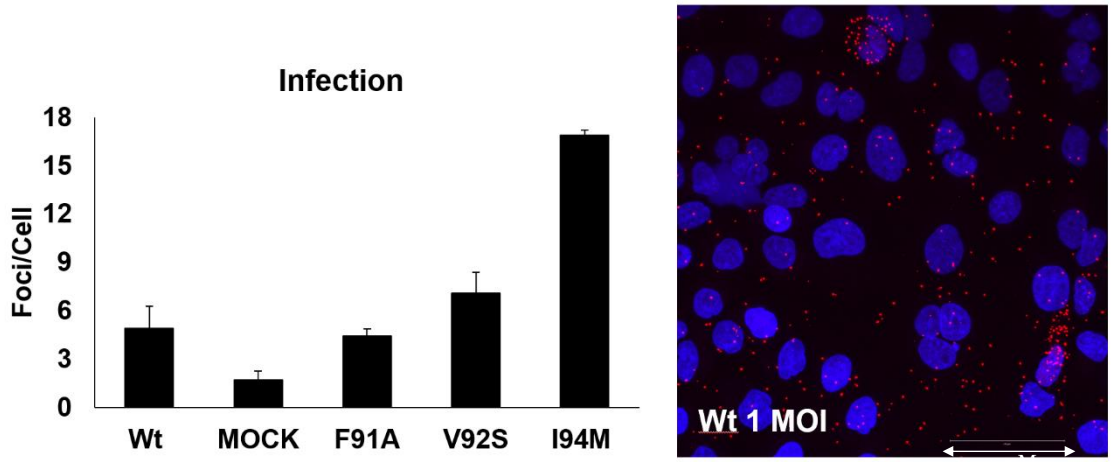

Figure 12 – **Wild type (Wt) M2 and mutants F91A and V92S interact at a similar level with SUMO, whereas the double SUMO/LC3 mutant I94M interacts more robustly.** A549 cells were infected with Wt (A/Udorn/72 H3N2), mutant (F91A, V92S or I94M) or mock infection for 18 hours and then prepared for PLA using antibodies 14C2 and anti-SUMO. Figure indicates one image from a triplicate repeat set.

Co-immunoprecipitation of M2/mutants and SUMO was unable to be performed in viral infection (data not shown). No banding patterns on Western blots were visible after co-immunoprecipitation was performed following viral infection with wild type virus or the rescued M2 CT mutants. Immunoprecipitation conditions were altered, and differential pulldown antibodies were used (14C2, SUMO or polyclonal anti-Udorn), but no reliable results were obtained, unlike when M2 or mutants are transiently expressed alone. Instead, proximity ligation assays (PLA) were used to deduce interactions *in vitro*. The PLA uses the principle of two primary antibodies bound to two ligands being in close proximity, whereby a fluorescent signal can be produced using the provided secondary antibodies and reagents. Unless the two antigens are significantly close to one another, i.e.

interacting, then no signal will be produced. Where M2 has been transfected as in Figure 11 wild type M2 is shown to have a higher number of foci per cell than F91A. However, during viral infection (Figure 12) whilst the number of foci per cell are comparable for wild type and F91A; I94M and I94S have significantly increased numbers of foci per cell in comparison to wild type and an inverse relationship is shown for M2-SUMO binding between transfection and infection. This indicates that during viral infection, there are other factors at play in relation to how M2 is modified, interacts with SUMO, and what role an M2-SUMO interaction can have on the viral lifecycle.

3.04 The binding of M2 to SUMO, but not LC3, is pH dependent

The initial stages of infection involve the encapsulation of the entering virus in an acidified endosome. This acidification has a range of effects, with the most prominent being the flow of protons through the lumen of the ion channel of M2 in order to lower the pH in the viral core, which itself causes a cascade of events leading to the uncoupling of vRNPs and the fusion of the viral membrane with the endosomal, allowing release of viral genetic material in to the cell cytoplasm. Histidine at position 90, well within the cytoplasmic tail region of interest in LC3 and SUMO interactions, is highly conserved (Figure 9) and is able to be protonated at low pHs, though no effect of this protonation has been previously demonstrated. To mimic the low pH environments which the M2 CT experiences, and examine how this may influence LC3 and SUMO interactions, purified LC3 and SUMO proteins were mixed with a C terminus peptide of M2 (88–DSHFVSIELE–97) with a FITC label, in a fluorescence polarisation assay. The output of this assay enables the calculation of binding constants of the cellular proteins with the viral peptide.

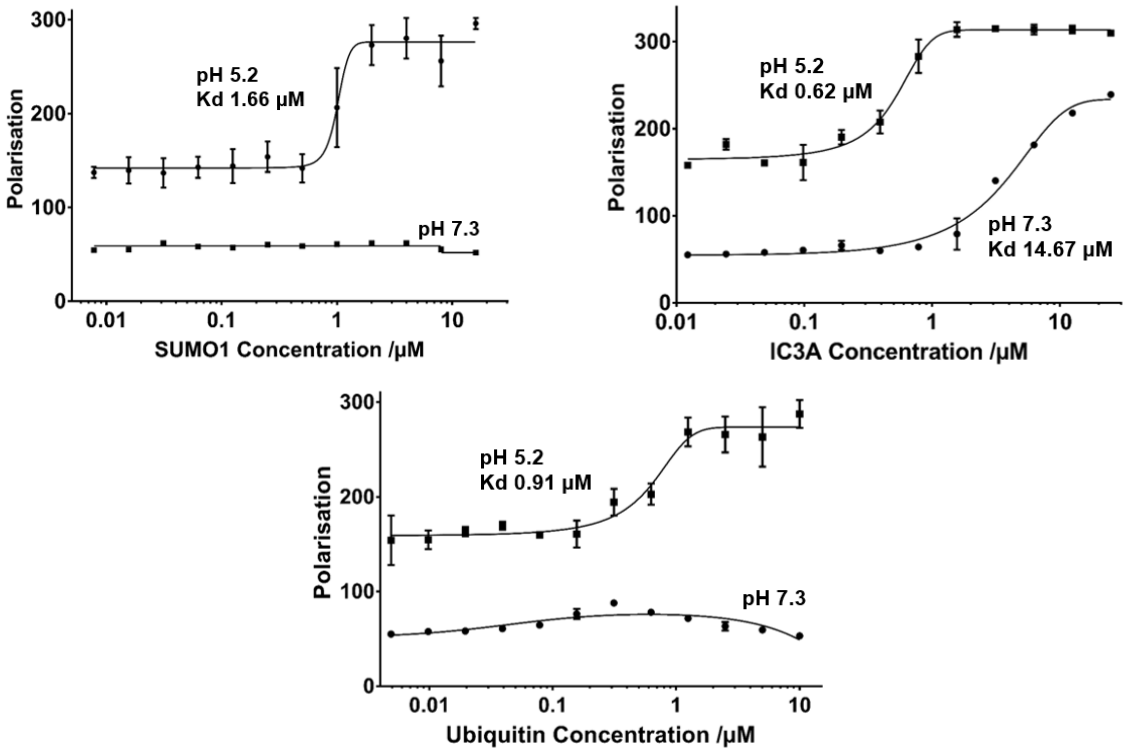

Figure 13 – **Binding of SUMO to an M2 C-terminus peptide is pH dependent, whereas binding to LC3 is not.** M2 C-terminus peptide (DSHFVSIELE) was obtained from Biomatik (Oxford, UK) labelled with FITC such to enable detection through fluorescence. Values were collected using the Clariostar software, and data points analysed and plotted in Graph Pad Prisim. Figure indicates one data set from a triplicate repeat set.

Figure 13 shows the Kd of labelled M2 C-terminus peptide with SUMO, LC3 and the control protein Ubiquitin at physiological pH versus an acidic environment, such which may be found in an acidified endosome during the initial stages of IAV infecting a host cell. Specifically, here the ability of residue H90 is studied to investigate potential protonation, which is predicted to occur at and below pH 6.4 (Huyghues-Despointes *et al.*, 2003). The Kd of M2 C-terminus with SUMO1, LC3 and Ubiquitin is of comparable magnitude at pH 5.2, however binding of M2 C-terminus with SUMO1 and Ubiquitin at pH 7.3 seemingly does not occur, where it does for LC3 albeit with a relatively high Kd in relation to LC3's binding at pH 5.2. It can be inferred that the ability of H90 to be protonated at acidic pHs plays an important role in SUMO and LC3 binding of the M2CT, considering the acidic environment of endosomes, the role of M2 as an ion channel, and the conservation of H90. The data in Figure 13 also demonstrates ubiquitin binding potential, possibly indicating a broader propensity for the M2 CT to bind ubiquitin-like molecules.

3.05 H90 protonation does not affect SUMO interaction during viral assembly

In an attempt to further characterise the protonation deficient mutant H90S, PLA was once again conducted using this mutant virus in an infection model, probing for M2 and SUMO and quantifying foci. Ammonium chloride is used to block the acidification of endosomes, and therefore prevent or attenuate protonation of H90 in the wild type virus. This would provide some insight as to whether protonation of H90, at least in the endosomal stages of assembly and budding, was required for SUMO interaction in the M2 CT. Cells were infected with either wild type virus, the unprotonatable H90S mutant, or a mock infection, and allowed to incubate for 18 hours. Proximity ligation assays were then performed, and resultant images obtained and analysed using confocal microscopy.

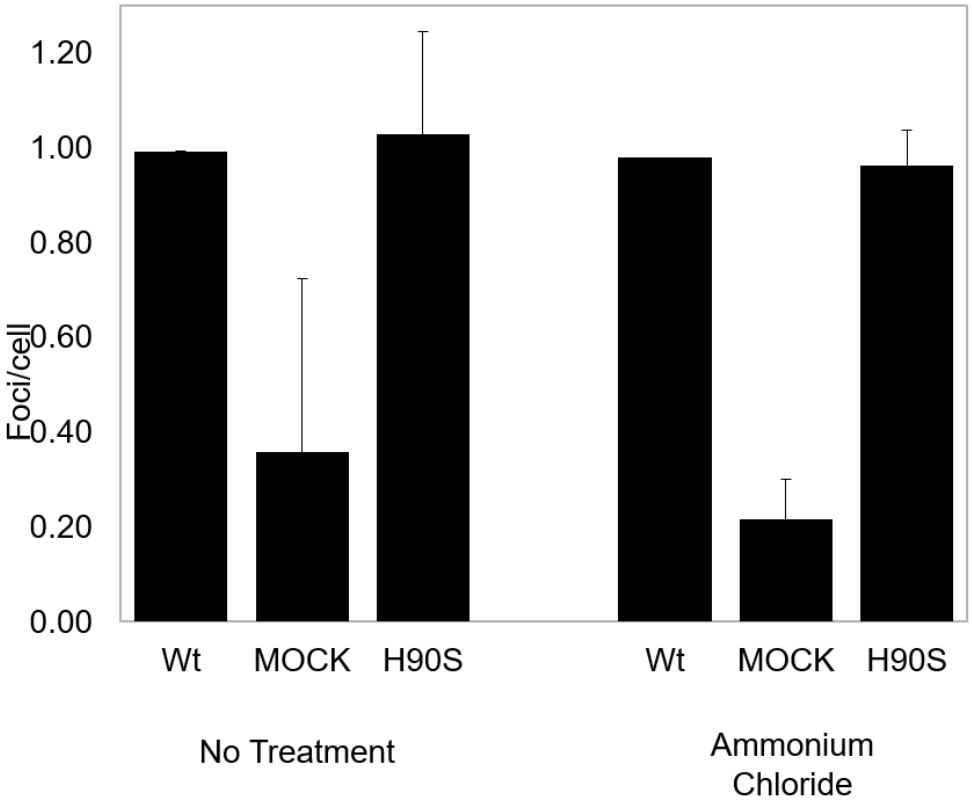

Figure 14 – **Endosomal acidification does not affect M2 interactions with SUMO.** A549 cells were infected with Wt (A/Udorn/72 H3N2), mutant H90S or mock infection for 18 hours in the presence or absence of ammonium chloride, and then prepared for PLA using antibodies 14C2 and anti-SUMO. Figure indicates one data set from a triplicate repeat set.

The lack of a protonatable histidine residue or the neutralisation of endosomal pH by the addition of ammonium chloride during infection causes no noticeable difference in the foci : cell ratio when analysing M2 / SUMO foci using PLA. This suggests that SUMO interaction with the M2 CT is not influenced by H90 protonation in endosomes during virus assembly. H90 protonation may affect SUMO interactions during virus entry; however, the low quantity of M2 in the virion prevented this measurement.

3.06 M2 can interact with the intermediate cellular filament Vimentin

After data showing convincing interaction of M2 with SUMO, and literature supporting M2 binding of LC3 in the autophagy pathway, a mass spectrometry study of potential other interacting partners of the M2 CT was undertaken in order to investigate which SUMOylated cellular proteins M2 may be interacting with. A protein expression plasmid was synthesised containing three repeats of positions 87 to 97 of M2 from A/Udorn/72 H3N2 with a FLAG tag on the N terminus. 48 hour expression of this construct in HEK 293T cells was conducted, and subsequently processed using large scale co-immunoprecipitation using anti-FLAG antibody. After SDS PAGE purification, a sample was sent to Mr. Kevin Howland at the University of Kent School of Biosciences Biomolecular Science facility for mass spectrometry analysis.

Accession	Peptide Count	Unique Peptides	Confidence Score	Max Fold Change	Description
P08670	12	12	70.2	5.18	Vimentin
Q8NEV1	12	11	81.7	3.21	Casein Kinase II Subunit α3
P38606	20	20	134.7	1.28	V-Type Proton ATPase Catalytic Subunit A
Q00610	19	17	87.1	Infinity	Clathrin Heavy Chain 1
Q14152	65	64	409.9	5.80	Eukaryotic Translation Initiation Factor 3 Subunit A (elf3a)

Table 4 - **Selected mass spectrometry results obtained after transfection of HEK-293T cells with an expression vector containing M2(87-97)-FLAG3.** HEK293T cells were transfected with vector expressing residues 87 – 97 of the A/Udorn/72 H3N2 M2 protein fused to a FLAG tag for 48 hours. Figure indicates one data set from a triplicate repeat set.

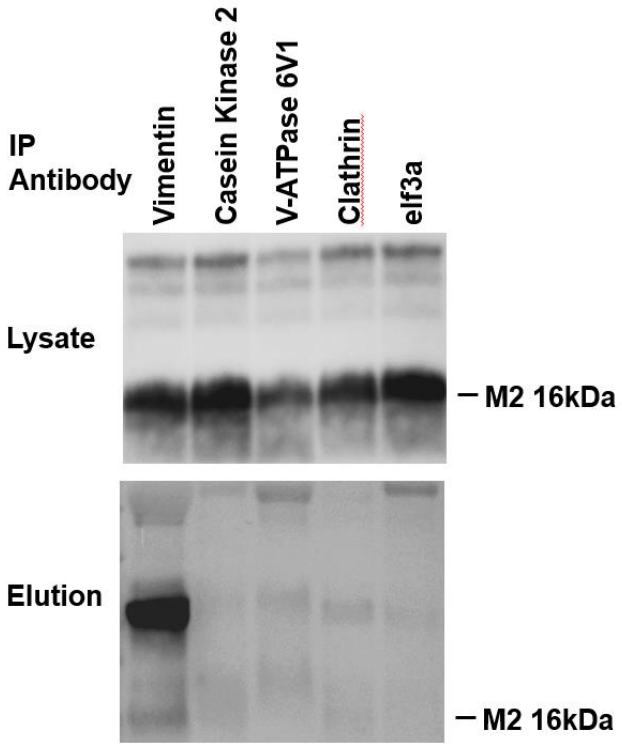

Figure 15 – **M2 co-immunoprecipitates with the intermediate cellular filament Vimentin.** Western blot showing results of a co-immunoprecipitation performed with antibodies to interacting proteins suggested by mass spectrometry. HEK293T cells were transfected with A/Udorn/72 H3N2 M2 and incubated for 48 hours, after which point they were lysed in Thesit lysis buffer, centrifuged at 12,000 x g for ten minutes at 4°C, and the insoluble pelleted material was discarded. Co-immunoprecipitation was performed with antibodies to Vimentin, Casein Kinase 2, V-ATPase 6V1, Clathrin and elf3a. Eluates run on protein gel electrophoresis, and Western blotting performed. Membranes were probed with 14C2 to determine any M2 interacting partners. *A 'mock' was not performed, as WT (M2 in this case) is the control, and we are looking for differences compare to WT, and not the ultimate phenotype.*

Mass spectrometry analysis returned over 250 potential interactions, five of which are shown in Table 4 that were selected for further investigation by studying previous literature which had suggested links between the cellular proteins and SUMO interactions, SUMOylation and IAV infection and lifecycle, one of which being Vimentin (Wu and Panté, 2016). Vimentin is an intermediate cellular filament involved in anchoring of cellular organelles, cellular structuring, and in the formation of aggresomes to mediate the degradation of aggregated proteins, often in the context of autophagy. Antibodies to the positive hits were then used to perform co-immunoprecipitation of M2 transfect HEK293T cells, and the resulting elutions analysed by western blotting (Figure 15). The resulting image shows M2 and Vimentin co-immunoprecipitation, indicating a strong interaction, but no interaction was seen for the other candidates. Interestingly, immunoprecipitated vimentin was not of the predicted molecular weight of SUMOylated vimentin,

indicating that M2 interacts not through a SUMO interaction with SUMOylated vimentin, but through another medium not investigated here.

3.07 M2CT mutant viruses do not adversely affect cell viability and all replicate with similar kinetics

Understanding the extrapolated effects of M2 mutations in whole viral infection on cellular survival, and replication capability of mutant viruses is crucial to determining if these mutations would be advantageous, either through a primary or secondary mechanism of M2 CT interaction. If mutations interfering with SUMO interactions or LC3 binding confer greater cell mortality or replicate to significantly higher titres than a wild type virus, investigations in to viral hijacking of these cellular pathways would warrant significant and meticulous study, as any impact on human disease could be severe. Cells were infected with indicated mutant viruses at 1 MOI for the viability and growth kinetics assays, and either analysed trough trypan blue exclusion for the former or plaque assay to determine time point titres for the latter.

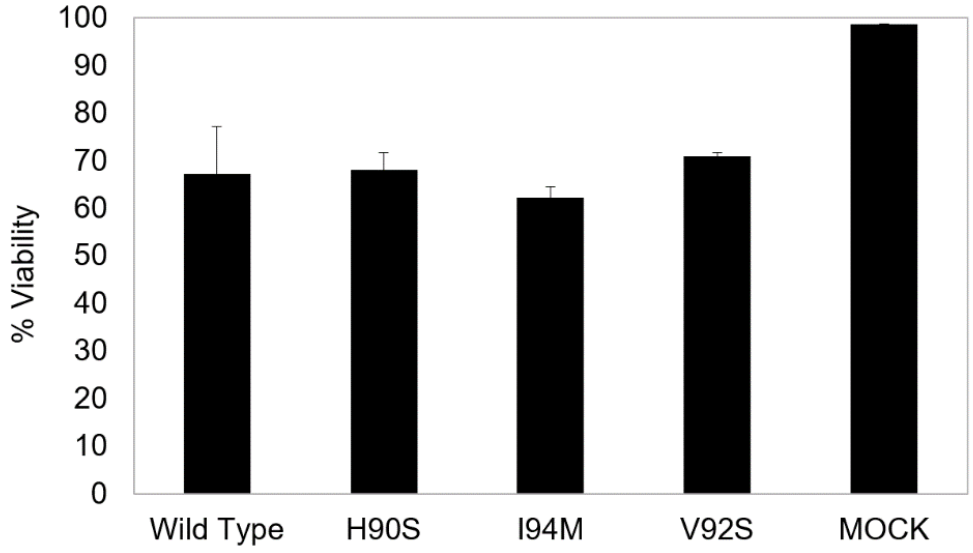

Figure 16 – **Cell viability is broadly equal between wild type and mutant M2 viruses.** Bar chart showing percentage cell viability 18 hours post infection with 1 MOI of viruses A/Udorn/72 H3N2 (wt), mutants H90s, I94M or V92S, or mock infection. After infection in a 3.5cm dish for 18 hours, cells were washed with warm PBS, trypsinised, pelleted and resuspended. Viability was determined by trypan blue exclusion counting, using a haemocytometer and handheld counter. Graph is indicative of data from a triplicate repeat set.

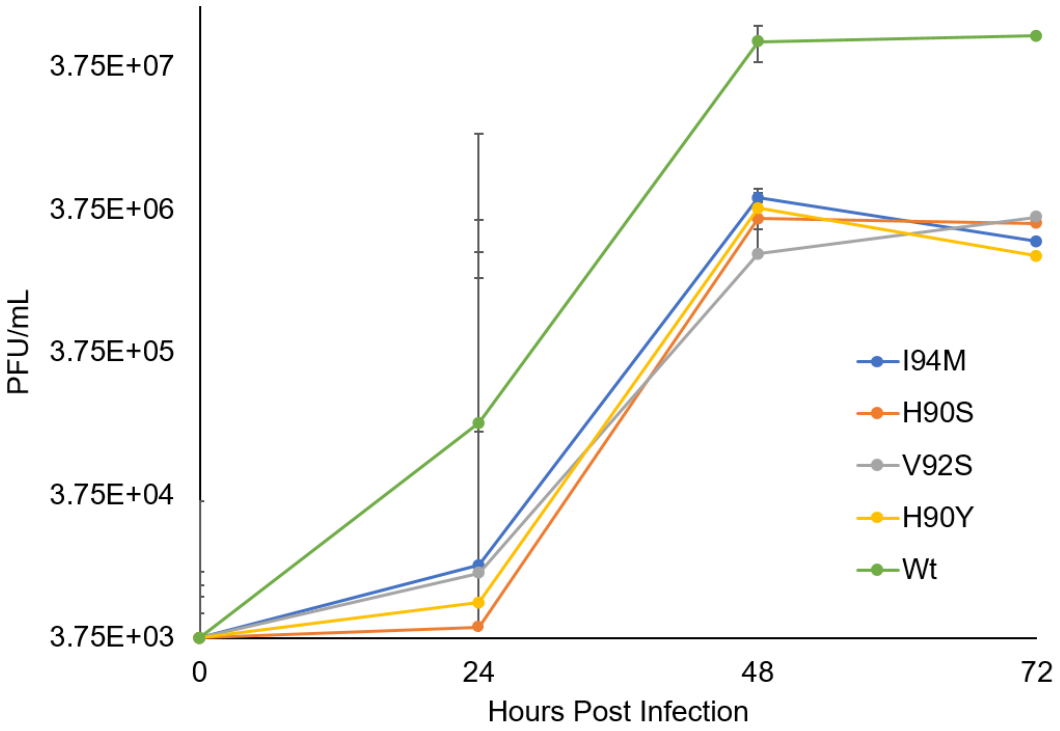

Figure 17 – **Growth kinetics of wild type A/Udorn/72 H3N2 compared with M2 CT mutant viruses.** Line chart showing the viral titre in plaque forming units per mL (PFU/mL) at 24, 48 and 72 hours post infection. Viruses A/Udorn/72 H3N2 (Wt), or mutant viruses I94M, H90S, V92S or H90Y were allowed to infect A549 cells for 24, 48 and 72 hours at 0.01 MOI. Graph is indicative of data from a triplicate repeat set. *A 'mock' was not performed, as WT virus is the control, and we are looking for differences compare to WT, and not the ultimate phenotype.*

Cell viability assays shown in figure 16 demonstrate that mutant viruses have a negligible effect on cell survivability of IAV infection compared to both the wild type virus and mock infection.

The line chart in figure 16 represents the growth kinetics of the mutant and wild type virus over the course of three days. All of the mutant viruses replicate similarly to one another, suggesting that the protonation mutants (H90S/H90Y) and the LIR/SUMO binding/interacting mutants (I94M/V92S) display a slight reduction in replication capacity. This attenuation of replication seen in the mutant viruses is recurrent and repeatable in other plaque assay investigations. The wild type virus is shown to replicate and grow to one log greater titre than the mutants. The data suggests that the intact functions of the wild type M2 CT may play a role in efficient IAV budding and replication, and that mutations which affect these functions slightly impairs the normal replication of IAV.

3.08 M2-SUMO localisation is variable when mutations in the CT are present

It is known that mutations in the M2 CT can affect viral assembly and morphology, and also from this study that M2 has the ability to interact with SUMO and LC3. To understand whether mutations specifically disrupting predicted SUMO interactions with the M2 CT cause a change in morphology of budding virus, or a change in cellular localisation of SUMO, confocal microscopy was performed using the generated mutant viruses and A549 cells.

Four colour immunofluorescent microscopy was conducted, in order to visualise the distribution of A/Udorn/72 H3N2 proteins as a whole (namely HA, NA, M1 and NP which are detected well by the polyclonal anti-Udorn antibody), M2 itself (wild type and mutants all detected by 14C2), SUMO and the nucleus.

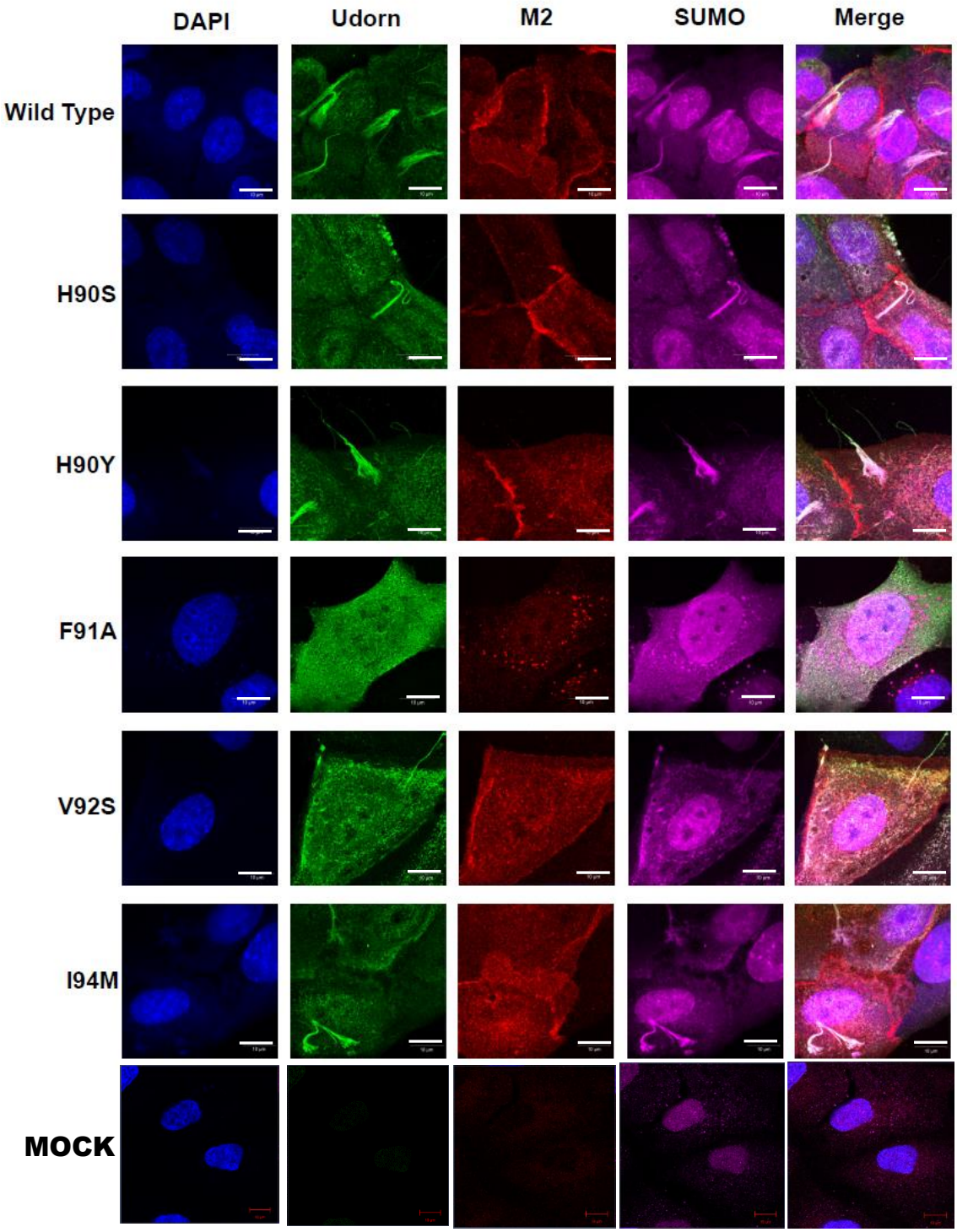

Figure 18 – **Confocal microscopy images of M2 and SUMO distribution in infected cells.** A549 cells grown on glass coverslips were infected with 1 MOI of A/Udorn/72 H3N2 (wild type) or M2 mutants H90S, H90Y, F91A, V92S or I94M and infection was allowed to proceed for 18 hours. Image data is indicative of results seen in a triplicate repeat set. **Scale bar 10 µM**.

Figure 18 demonstrates the differences in morphology of mutant viruses, and the change in distribution of M2 and SUMO across these viruses. SUMO is normally found in greatest quantity in the nucleus, and this is evident in the wild type virus infection. Long filaments in the green Udorn channel can be seen protruding from the infected cells, which is characteristic of A/Udorn/72. M2 is mostly distributed to the plasma membrane, and the viral filaments contain significant amounts of SUMO, which is likely attributable to the fact that M1 is known to be SUMOylated, and M1 is the viral protein in greatest quantities. H90Y and H90S display morphologies most similar to wild type, with arguably slightly more cytoplasmic M2 staining, which provides further indication that H90 mutations may not directly affect the ability of M2 to bind SUMO, as per previous figures. Both V92S and I94M show far more cytoplasmic M2 staining than wild type virus. F91A is noteworthy as having distinct M2/SUMO colocalised foci and completely lacking viral filaments, as has previously reported with the autophagy subversion defective mutant (Beale, Wise, Stuart, Benjamin J. Ravenhill, *et al.*, 2014) and.

3.09 M2 and CT mutants colocalise with LC3 and LAMP1 regardless of mutation in infection

Mutations affecting the LIR of the M2 CT are known to, in certain circumstances, influence localisation of both LC3 and M2 in host cells. Here we looked at if mutation of sites which affect both the LIR and the SIM can have the same effect on LC3 localisation and the subsequent progression of autophagy as a well-established LIR mutants such as F91S (Beale, Wise, Stuart, Benjamin J. Ravenhill, *et al.*, 2014). pCAGGS vectors containing genes for indicated mutants were transfected in to A549 cells alongside a pEGFP vector containing lysosomal associated membrane protein 1 (LAMP) and a pCDNA vector containing LC3-mCherry, followed by antibody staining of M2 and confocal microscopy visualisation.

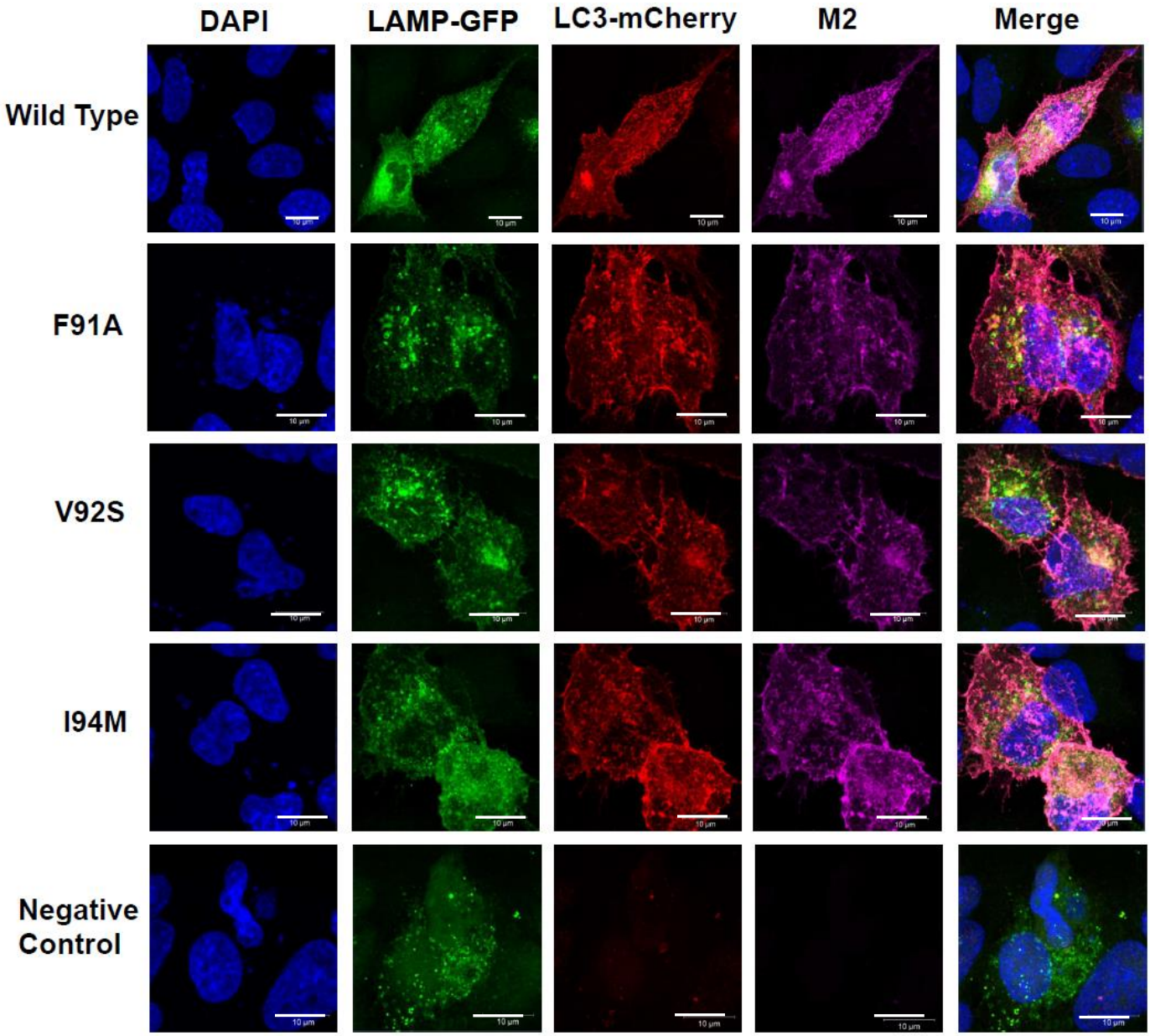

Figure 19 – **The effects of cellular LAMP1 and LC3 localisation with M2.** Using Lipofectamine 3000, A549 cells were transfected with LAMP1-GFP, LC3-mCherry and either pCAGGS vectors containing the genes for A/Udorn/72 H3N2 M2, or M2 mutants V92S, F91A or I94M, or an 'empty' pCAGGS vector. Image data is indicative of results seen in a triplicate repeat set. **Scale bar 10 µM.**

Figure 19 shows the induction and progression of autophagy by M2 and M2 mutants. M2 is seen predominantly at the plasma membrane of the cells, and with WT M2 a strong colocalisation between M2, LC3 and LAMP1 can be observed. Conversely, in the LIR mutant F91A, LAMP1 appears to colocalise strongly with LC3 but neither colocalise particularly strongly with M2. In the SIM mutants V92S and I94M, LAMP1, LC3 and M2 localise well together, though with less LAMP1 colocalization than with WT M2. I94M appears to affect lysosomal formation, as the localisation of LAMP1 is far more cytoplasmic than punctate, indicating altered lysosomal formation. I94M also appears to display more LC3 localisation to the plasma membrane than both F91A and V92S, suggesting that there be interplay between SUMO and LC3 binding and M2 localisation. To attempt to determine what role the cellular autophagy machinery may be having on the behaviour of M2, M2 localisation and viral morphology were examined using HeLa and CRISPR HeLa knockout cells deficient in autophagy.

3.10 Aberrant morphology and subcellular localisation of viral proteins is seen when autophagy pathways are not present

In the case of the M2 F91A mutant, which is unable to bind LC3, a distinct lack of filamentous virus is seen (Figure 18). This study speculates that there may be an interplay between LC3 binding, SUMO interaction and M2, coalescing in affects on morphology. Wild type HeLa cells are known to display the filamentous virus phenotype when infected with wild type A/Udorn/72 H3N2 virus, much like MDCK and A549 cells. Using a CRISPR knockout HeLa cell line (in which all six human isoforms of LC3 have been knocked out), henceforth referred to as HEX, morphology studies using confocal microscopy and mutant viruses were conducted. The HEX cell line does not express any of the mammalian ATG homologue genes, which contain ATG8 (mammalian LC3 homologue), and therefore cannot undergo the process of autophagy. This may have wide ranging effects on viral replication as a whole, but the proceeding figure focusses mainly on the localisation of M2 and SUMO within this system.

HeLa and HEX cells were infected with the wild type viruses or mutants, incubated for 18 hours and prepared for confocal microscopy using polyclonal anti-Udorn, 14C2 and anti-SUMO antibodies.

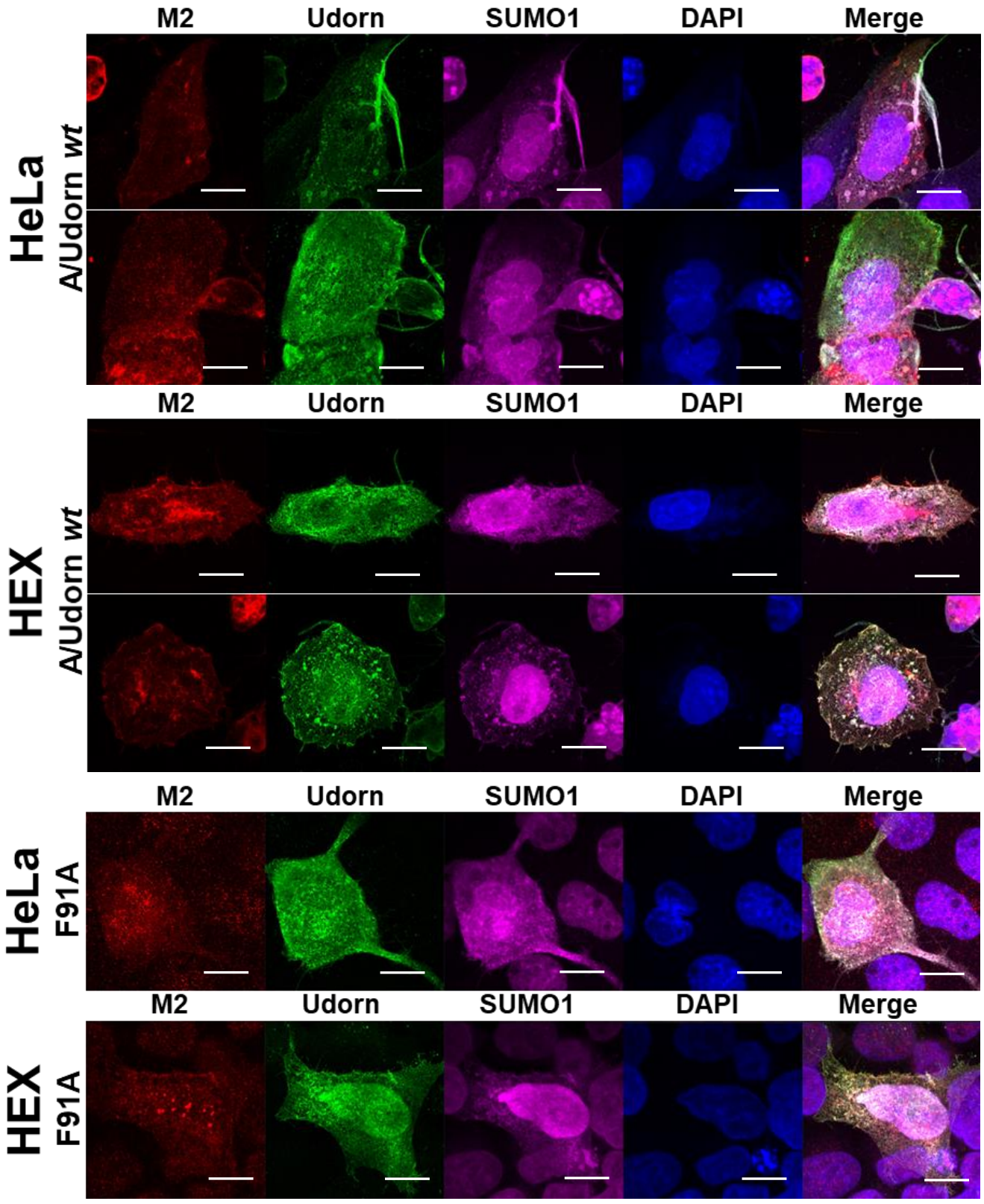
M2
Udorn
SUMO1
DAPI
Merge
HeLa
A/Udorn wt
HEX
A/Udorn wt
HeLa
F91A
HEX
F91A

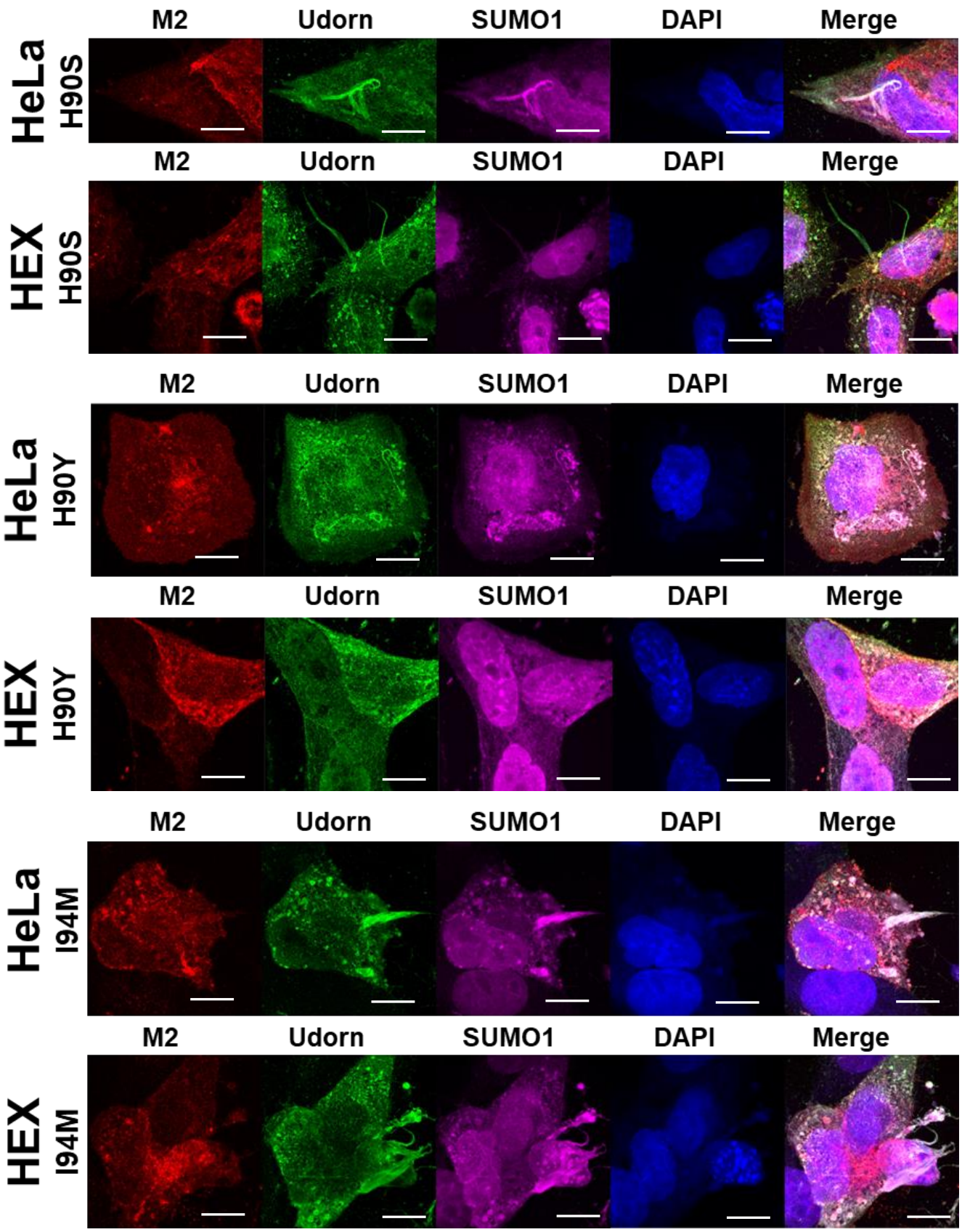
M2
Udorn
SUMO1
DAPI
Merge
HeLa H90S
HEX H90S
HeLa H90Y
HEX H90Y
HeLa I94M
HEX I94M

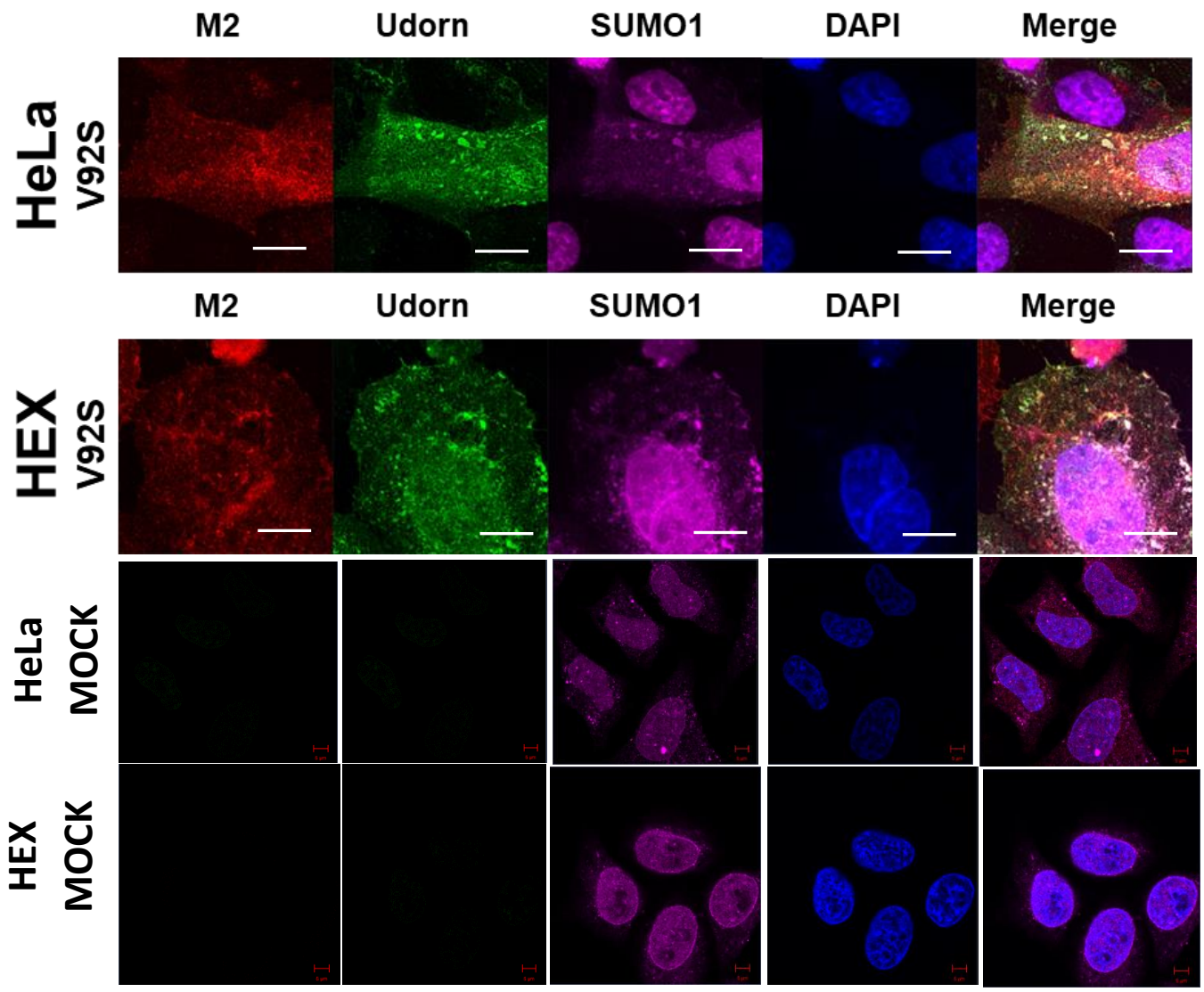

Figure 20 – **Confocal microscopy images of M2 and SUMO localisation in infected HeLa or HEX cells.** HeLa or HeLa ATG knockout cells (HEX) deficient in the ATG family of proteins (therefore unable to perform autophagy) were infected with 1MOI of either A/Udorn/72 H3N2 (wt), F91A, H90S, H90Y, I94M or V92S mutant viruses. Image data is indicative of results seen in a triplicate repeat set. **Scale bar 5 µM**

In all infection scenarios, SUMO is found in the highest concentration within the nucleus of both wild type HeLa cells and HEX cells, with localisation also seen in areas also positive for viral protein, including viral filaments (Figure 20). No significant difference was seen in SUMO colocalization with viral proteins when comparing the different mutants and cell types. Overall viral filament formation was reduced in HEX cells and the F91A mutant, consistent with the role of LC3 in filament formation; however, H90Y and V92S mutants were reduced in filament

formation in all cells whereas I94M formed robust filaments even in HEX cells. This suggests that autophagy and SUMO binding both affect viral morphology.

3.11 Morphology of budding M2 CT mutant viruses shows irregularity in quality and quantity of filaments produced as analysed by HA staining

HA is the most abundant viral surface protein, and is uniformly present over the entire surface of IAV, in both the spherical and filamentous forms of the virus. To both further confirm and qualify the ability of the mutant viruses to form filamentous virions we analysed the HA distribution specifically in mutant viruses at the later budding stages of infection. A549 cells were infected with 1 MOI of the relevant viruses for 18 hours and prepared for confocal microscopy, staining with a specific anti-H3 antibody without permiabilisation.

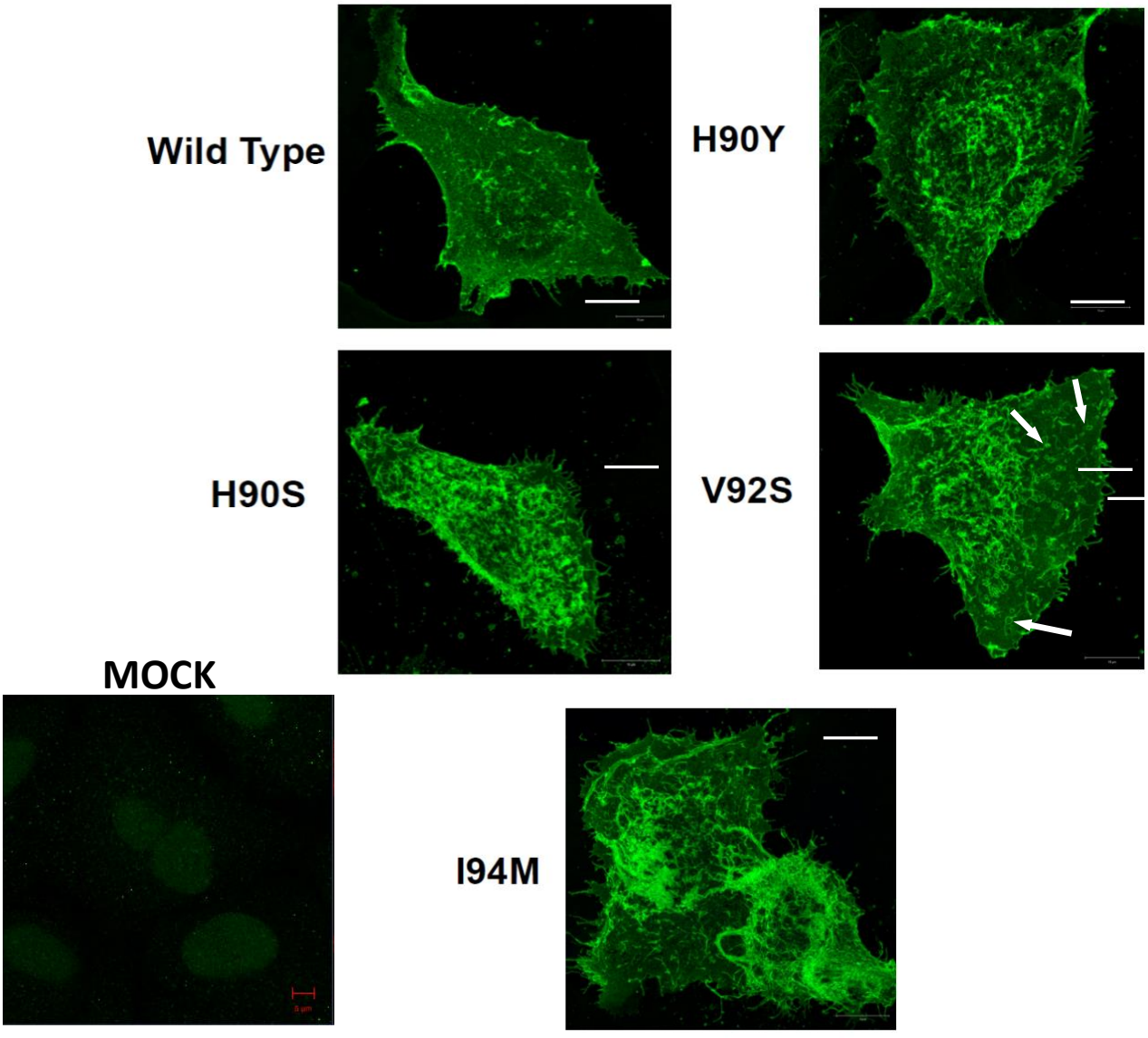

Figure 21 – **Confocal microscopy images showing surface HA distribution in infected cells**. A549 cells grown on glass coverslips were infected with 1 MOI of A/Udorn/72 H3N2 (wild type) or M2 mutants H90Y, H90S, V92S or I94M, and infection was allowed to proceed for 18 hours. Image data is indicative of results seen in a triplicate repeat set. **Scale bar 5 µM.**

All of the mutant viruses appear to show slightly stronger cell surface HA staining in comparison to wild type virus (Figure 21). In contrast to HeLa infections, all mutants displayed a somewhat filamentous phenotype (Figure 21). Of note are V92S and I94M mutant viruses. V92S shows unusual ring shaped staining patterns which are not observed in the wild type, or other mutants. Some these appear in relation to budding filaments, and may be Archetti bodies (white arrow, V92S panel). I94M appears hyper filamentous in comparison to wild type, similarly to seen in HeLa infections (Figure 20).

3.12 Mutant M2CT viruses display altered levels of viral protein incorporation

As the M2 CT mutations affected virus replication and protein localisation, but not overall viral protein expression, we investigated if any of these affects were due to altered virus assembly. This was achieved by looking at the levels of viral protein incorporation in to budded virions. After determining no change in viral replication kinetics (but a reduction in overall viral capacity), and studying effects of cellular localisation with potential interacting partners, the levels of viral proteins of interest in budded virus were quantified. This may give some insight in to whether the mutations in the CT of M2 have an effect on viral packaging and protein incorporation. Cells were infected with wild type or relevant mutant viruses, supernatant harvested after 18 hours, protein levels standardised using BCA assay and a Western blot performed.

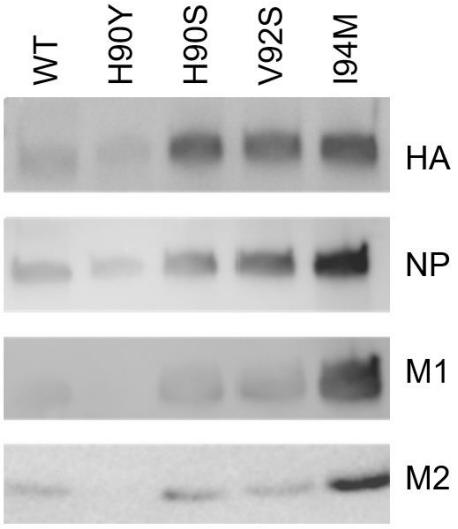

Figure 22 – **Western blot of supernatant taken from infected cell culture.** A549 cells were infected with 1 MOI of A/Udorn/72 H3N2 (WT) virus, or mutants H90Y, H90S, V92S or I94M. At 18 hours post infection, supernatant was collected from infected cells to quantify viral protein levels in budded virus. Blot is indicative of data seen in a triplicate repeat set. *A 'mock' was not performed, as WT virus is the control, and we are looking for differences compare to WT, and not the ultimate phenotype.*

HA and NP protein levels in H90Y are comparable to those of wild type, however interestingly M2 and M1 are totally undetectable (Figure 22). I94M shows a marked increase in all levels of viral protein, especially M2 and NP, possibly indicating this mutation conferring an advantage in viral packaging, but with no discernible increase in infectivity. H90S and V92S show comparable levels of viral protein incorporation. The differing levels of protein incorporation in to newly formed virions may be as a result of the altered protein localisation as seen in figure 18-19.

3.13 Some M2CT mutants alter the distribution of vRNP in late infection

M2 is known to interact with M1 through motifs in the cytoplasmic tail, and M1 is responsible for anchoring the viral surface proteins HA and NA, as well as forming an intermediary binding link between these external viral proteins and the vRNP in the viral core, though it is not known if the CT of M2 is a direct binding partner of vRNP, or if the M1-M2 interaction is indirectly responsible. It is known however, that disruptions upstream of the mutations generated in this study do affect vRNP incorporation in to newly forming virions (McCown and Pekosz, 2005, 2006; Grantham *et al.*, 2010). To evaluate whether the mutant viruses produced in this study also have an effect on vRNP localisation in late infection, cells were infected with either wild type or mutant viruses, and incubated for 18 hours. Cells were then prepared for confocal microscopy using an antibody specific to vRNP.

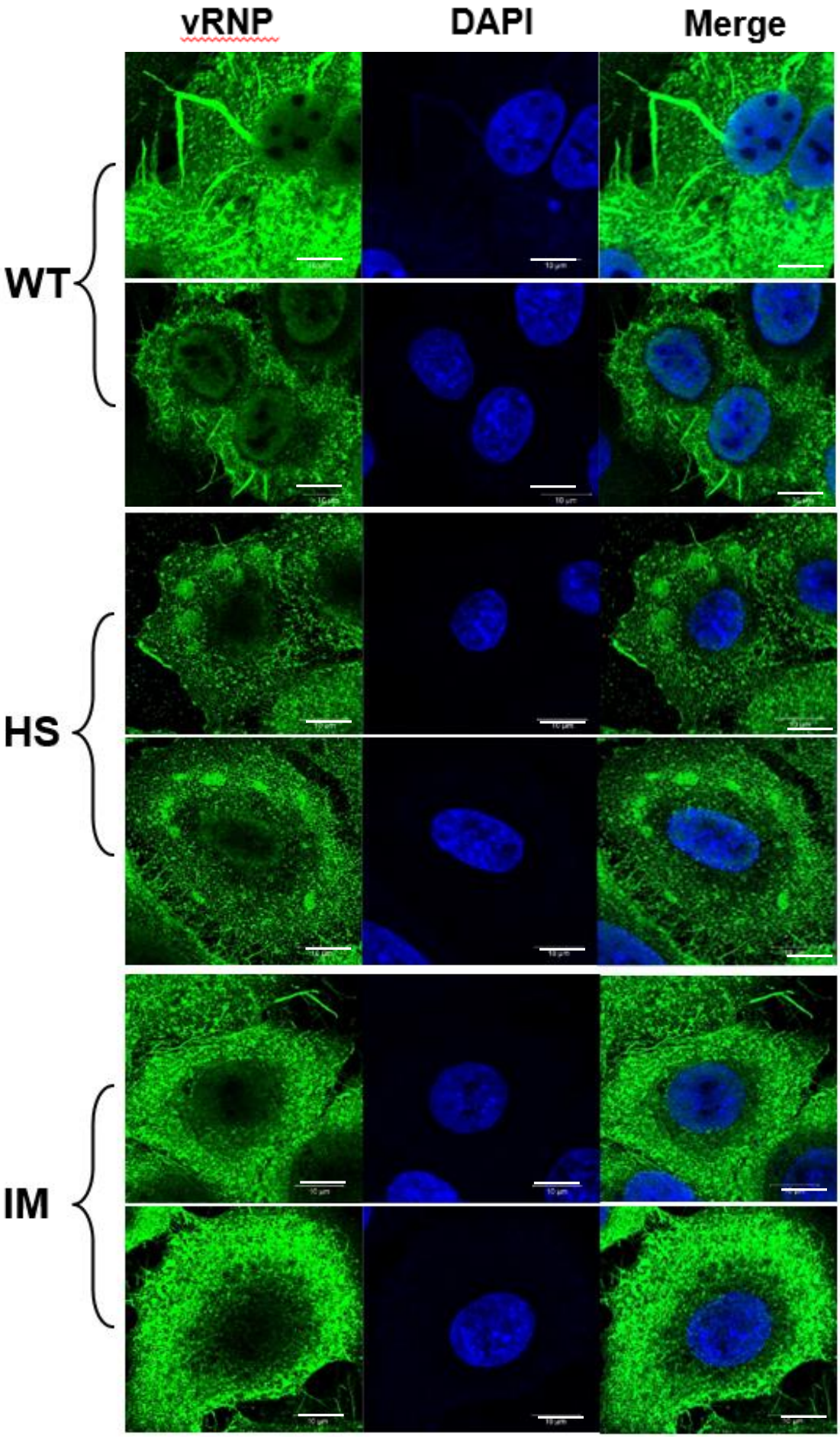
vRNP
DAPI
Merge
WT
HS
IM

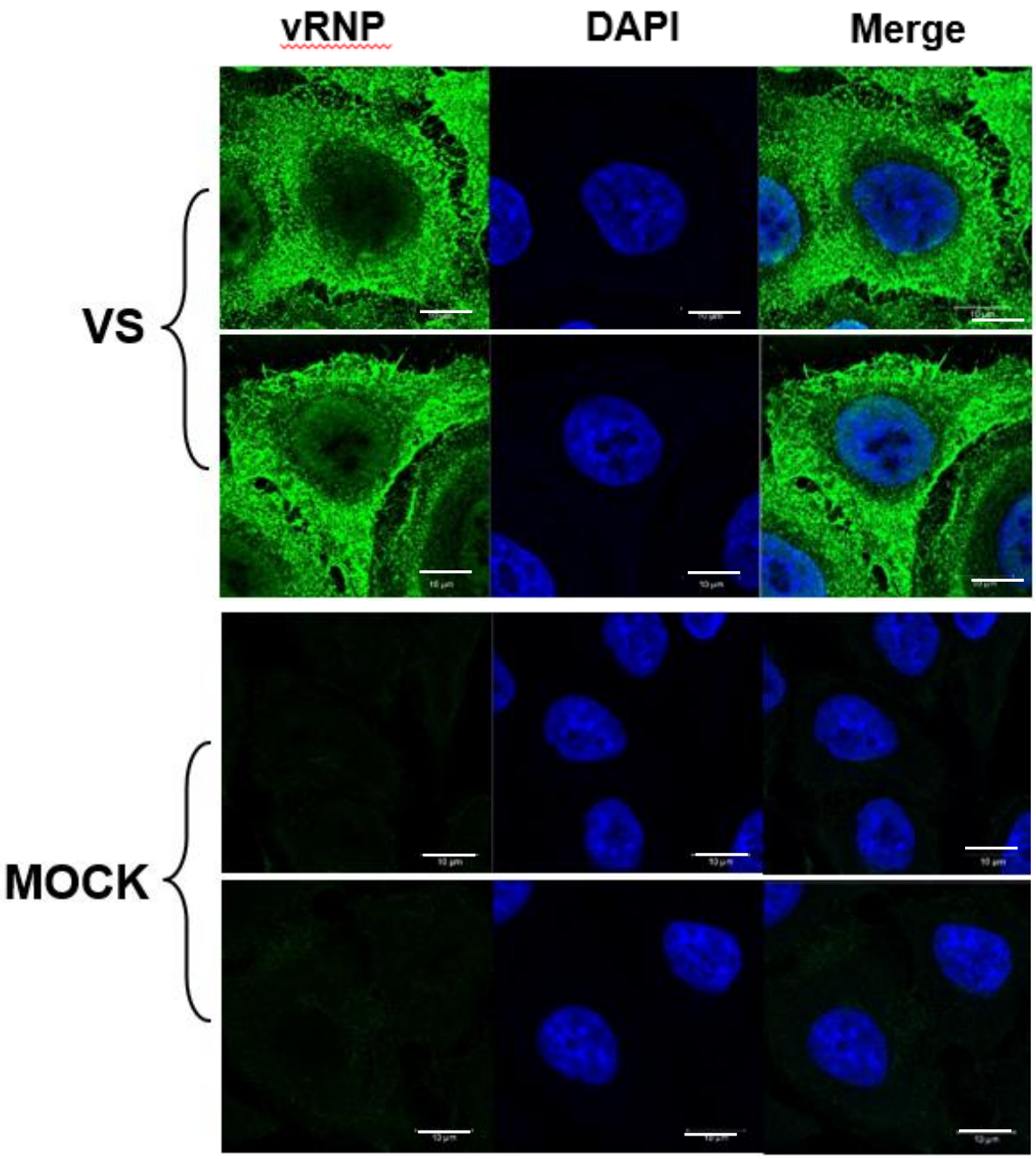

Figure 23 – A549 cells grown on glass coverslips were infected with 1 MOI of A/Udorn/72 H3N2 (wild type) or M2 mutants H90S, V92S or I94M, or a Mock infection media containing no virus, and infection was allowed to proceed for 24 hours. Image data is indicative of results seen in a triplicate repeat set. **Scale bar 10 µM.**

Figure 23 shows infected cells probed with anti-vRNP antibody to investigate cellular distribution of vRNP in the different mutant viruses. All viruses show vRNP export from the nucleus, with both I94M and V92S showing the lowest remaining levels of vRNP localisation in the nucleus. In contrast, H90S displays aberrant localisation of vRNP perinuclearly in globular like bodies of unknown function. Interestingly, the wild type virus shows some vRNP staining within the filaments, this is not seen in any of the mutant viruses.

3.14 vRNP distribution in early infection (~5 HPI) displays defects in nuclear trafficking in certain M2 CT mutants

As Figure 23 showed altered vRNP localisation late in infection, we also sought to determine if the M2 CT mutations affected early localization. vRNP localisation was studied in the wild type and mutant viruses to determine its distribution in the infected host cell. Cells were infected with relevant viruses and prepared for confocal microscopy after five hours of incubation post infection.

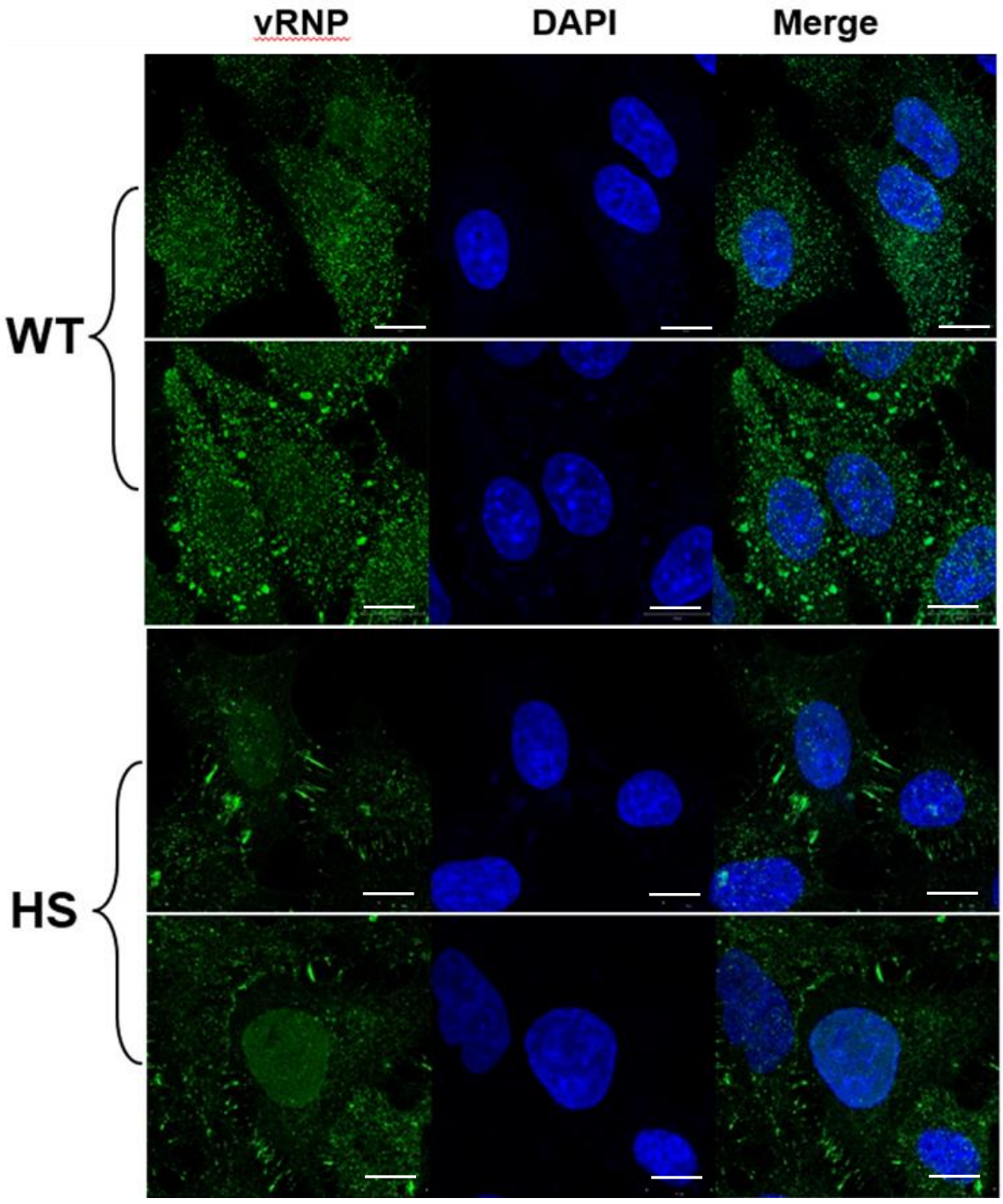

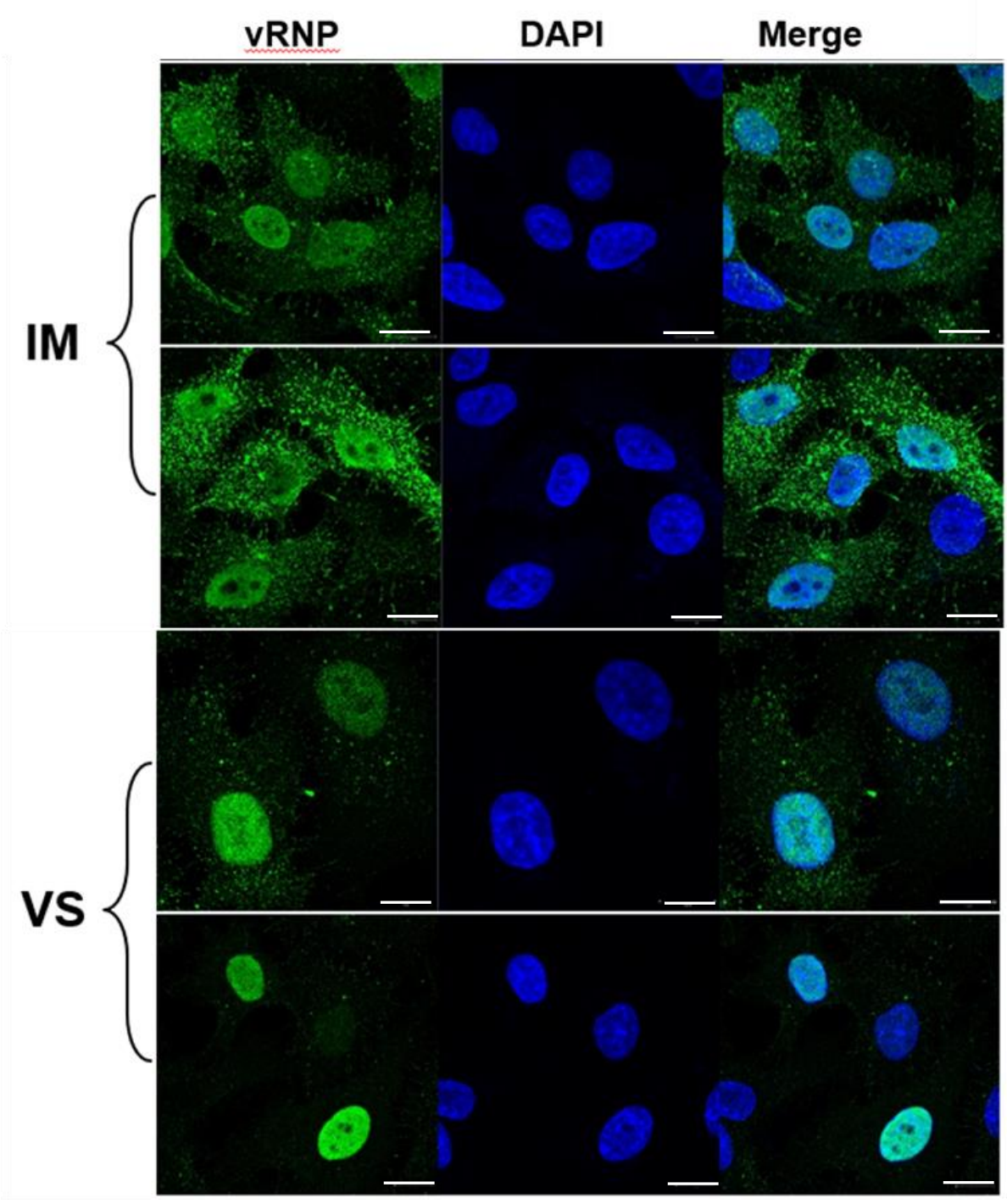
vRNP
DAPI
Merge
IM
VS

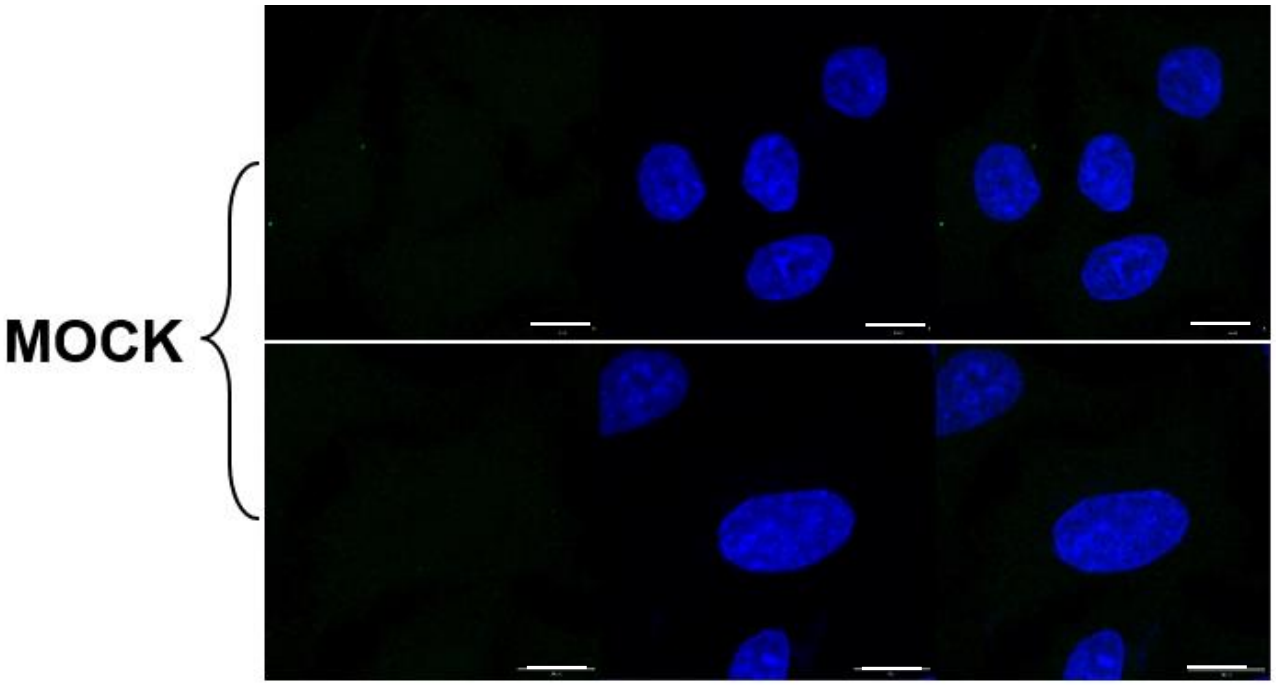

Figure 24 – **Confocal microscopy images showing vRNP distribution 5 HPI.** A549 cells grown on glass coverslips were infected with 1 MOI of A/Udorn/72 H3N2 (wild type) or M2 mutants H90S, V92S or I94M, or a Mock infection media containing no virus, and infection was allowed to proceed for five hours. Image data is indicative of results seen in a triplicate repeat set. **Scale bar 10 µM.**

Figure 24 shows A549 cells infected with indicated virus and stained at five hours post infection. Notably, most of the mutant viruses display distinct nuclear localisation of vRNPs compared to wild type virus. V92S shows this localization most clearly, with the majority of vRNP being localised to the nucleus. This suggests that the mutants may be delayed in vRNP nuclear export compared to WT virus. In contrast, the LIR/SIM mutant I94M shows near WT levels of vRNP nuclear export.

3.15 vRNP distribution in very early infection (~1HPI) is not greatly affected by mutations in the M2 CT

As the M2 CT mutations affect vRNP trafficking late in infection we investigated if the mutations also affected uncoating and early trafficking of viral proteins within the host cell. vRNP uncoating and release is essential for the propagation of IAV, as the genetic material of infecting viruses must reach the host cell nucleus for the progression of infection and the production of progeny virions. To investigate uncoating and vRNP trafficking cells were incubated with relevant virus for one hour post infection. After the incubation, cells were prepared for confocal microscopy using anti vRNP antibody.

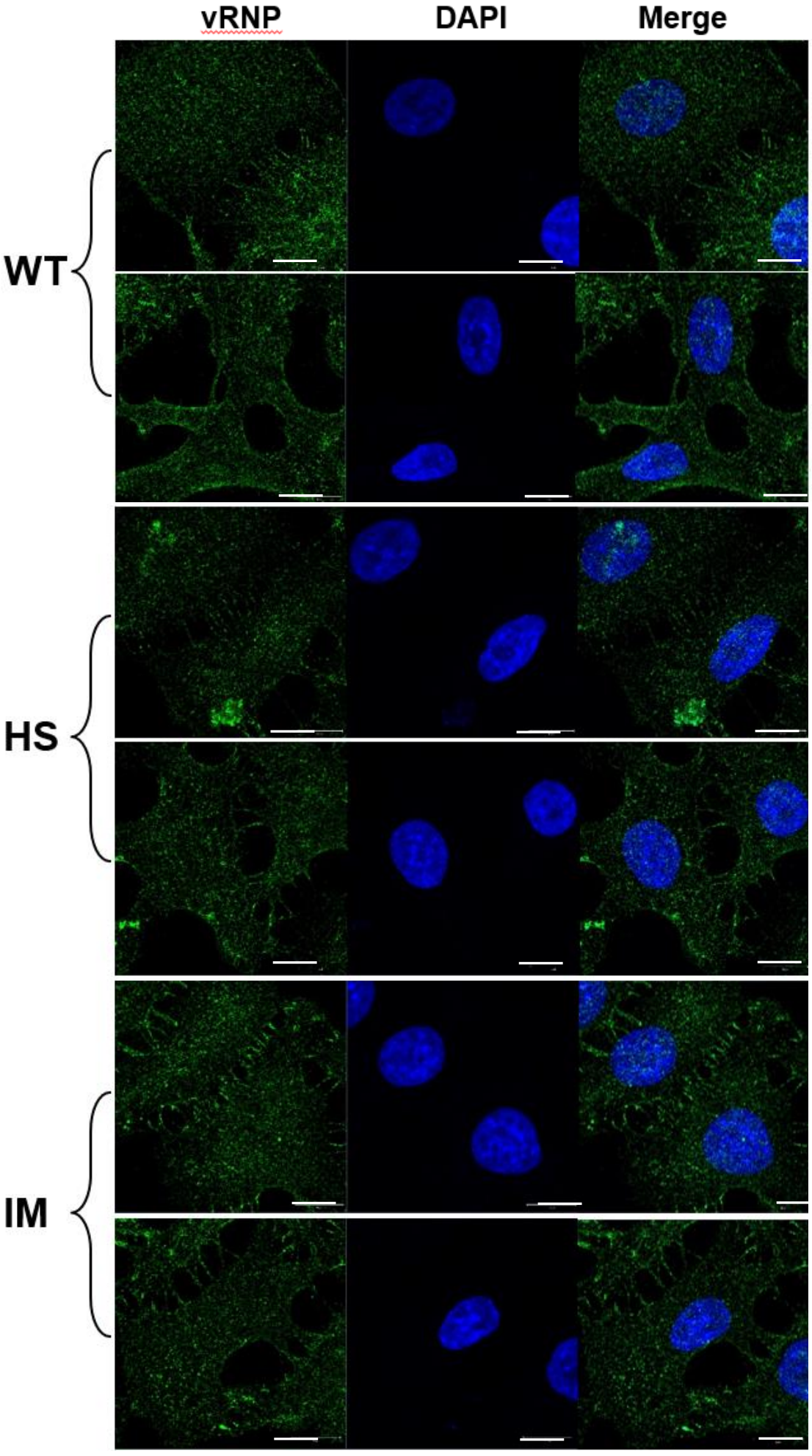
vRNP
DAPI
Merge
WT
HS
IM

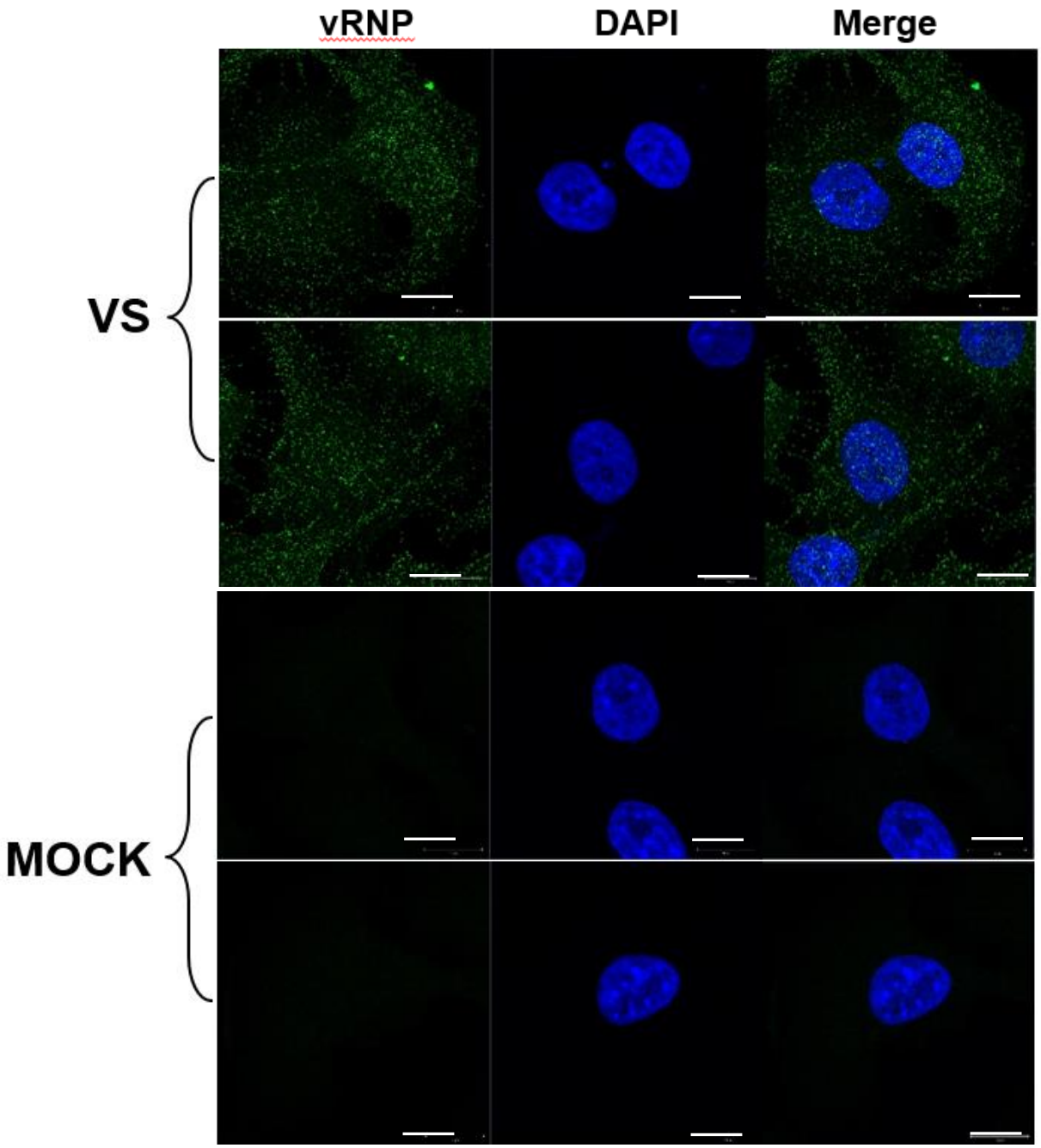

Figure 25 – **Confocal microscopy images showing vRNP distribution in early infection.** A549 cells grown on glass coverslips were infected with 1 MOI of A/Udorn/72 H3N2 (wild type) or M2 mutants H90S, V92S or I94M, or a Mock infection media containing no virus, and infection was allowed to proceed for one hour. Image data is indicative of results seen in a triplicate repeat set. **Scale bar 10 µM.**

At one hour post infection, all viruses had entered the cells, with some vRNPs localised at or near the plasma membrane and some vRNPs within the nucleus (Figure 25). The H90S mutant virus displays some vRNP clustering, whereas the V92S mutant appears to show greater cytoplasmic distribution. To further evaluate any differences in early entry and uncoating between the wild type virus and mutant viruses, a further study of M1 and HDAC6 was conducted.

3.16 Mutations in the M2 CT appear to affect uncoating as qualitatively analysed through M1 staining, but localisation of HDAC6 is unaffected

HDAC6 is an enzyme with a wide array of functions, not only its deacetylation activity, most notably of tubulin (Hao *et al.*, 2013), but also playing a key role in the formation of aggresomes. Aggresomes are defined by the formation of a vimentin 'cage' around a collection of proteins which have been marked by degradation by autophagy for example, and through ubiquitinylation (Johnston, Ward and Kopito, 1998). IAV is known to incorporate ubiquitin chains in to the budding virus, and it is speculated that this causes recruitment of HDAC6 to the uncoating virion in the late endosome, and vRNPs are released in to the cytoplasm in an HDAC6 dependent manner (Banerjee, Miyake, Nobs, *et al.*, 2014). To analyse if the M2 CT mutant viruses produced for this study had an effect on viral uncoating, A549 cells were infected either with wild type virus, or with mutant viruses as indicated. After five hours of incubation post infection, cells were prepared for confocal microscopy using anti-M1 and anti-HDAC6 antibodies.

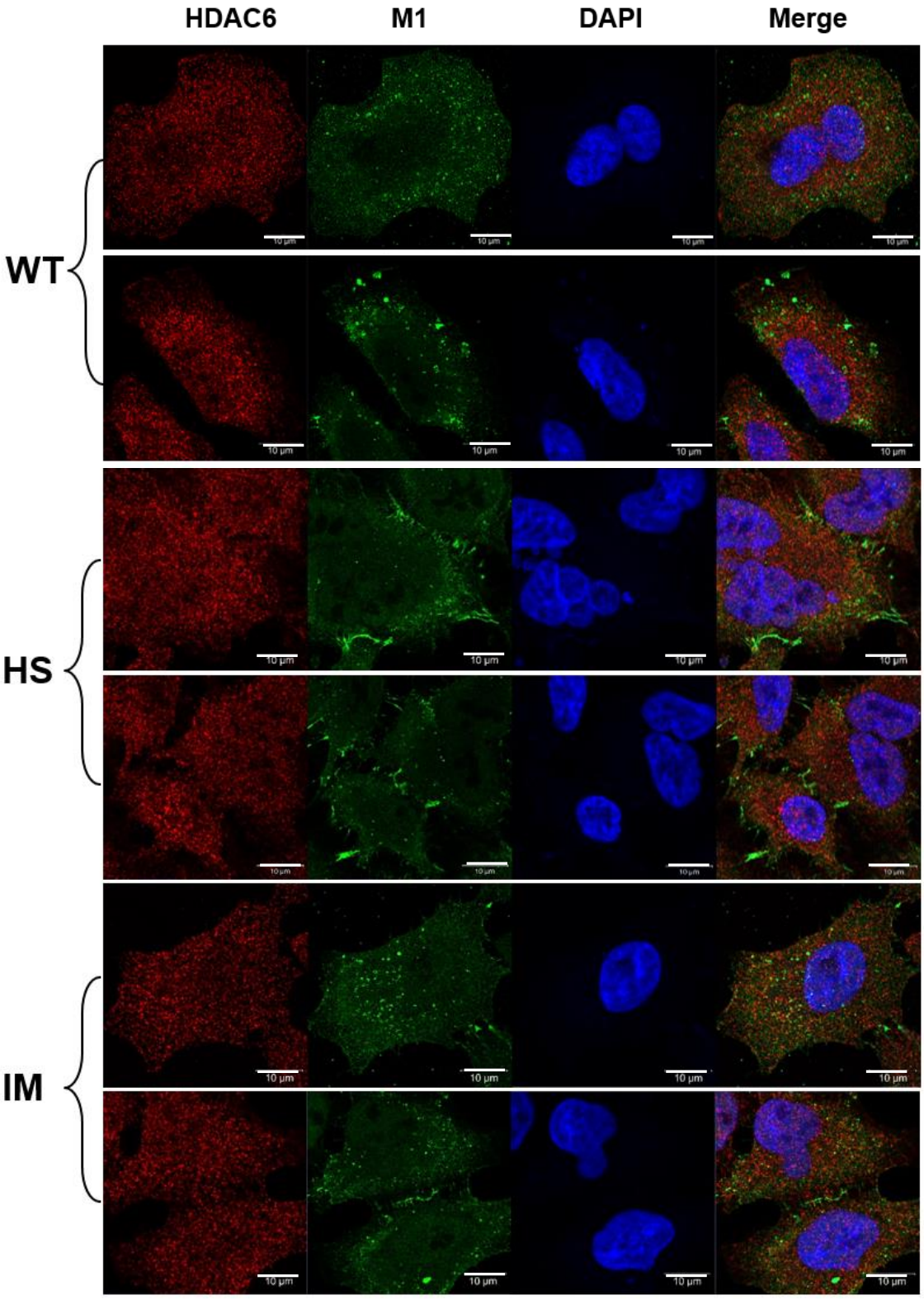
HDAC6
M1
DAPI
Merge
WT
HS
IM
10 µm

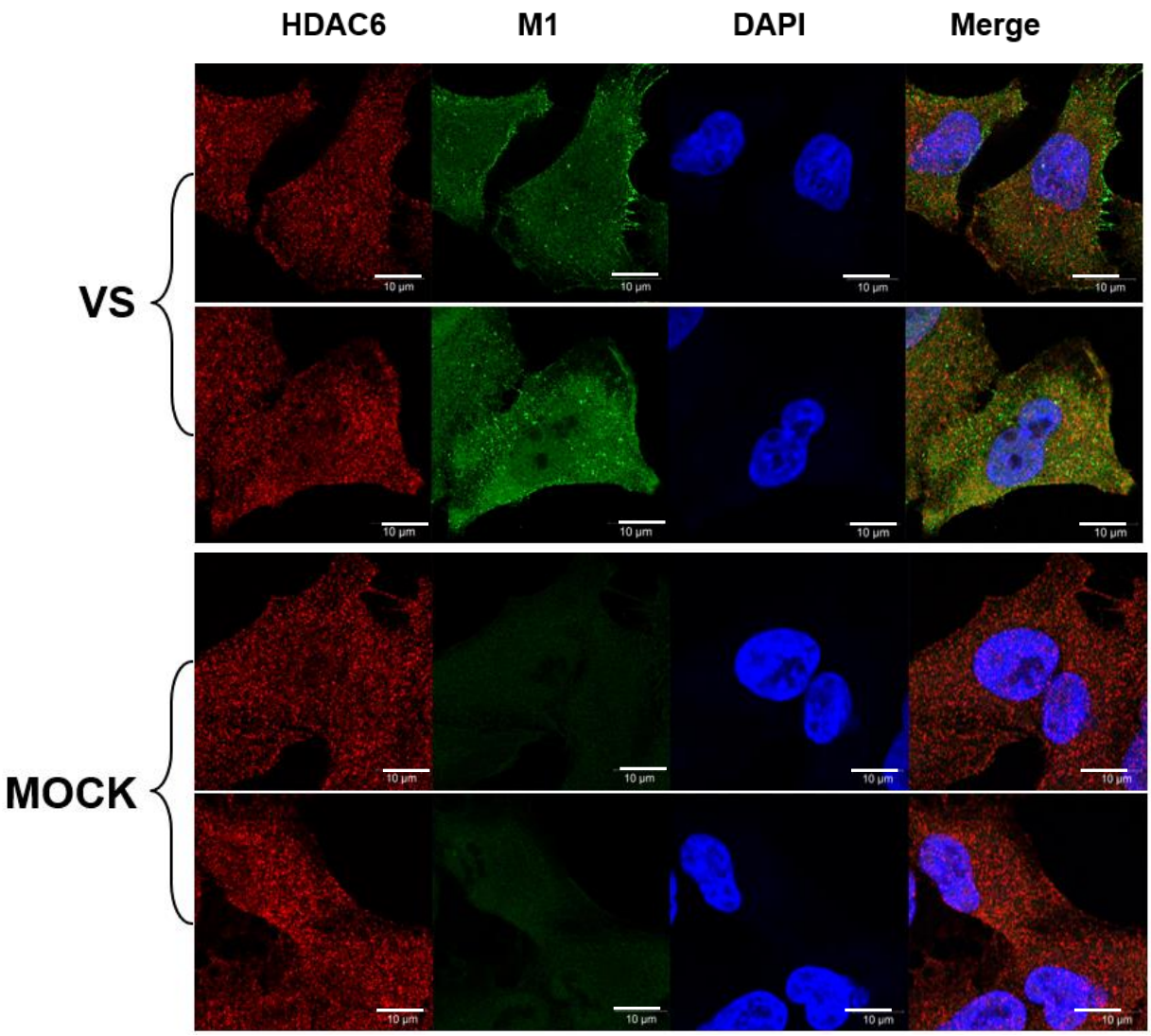

Figure 26 – **Confocal microscopy images showing HDAC6 distribution in infected cells 5 HPI.** A549 cells grown on glass coverslips were infected with 1 MOI of A/Udorn/72 H3N2 (wild type) or M2 mutants H90S, V92S or I94M or a Mock infection inoculum containing no virus, and infection was allowed to proceed for five hours. Image data is indicative of results seen in a triplicate repeat set. **Scale bar 10 µM.**

HDAC6 localisation appears to be unaffected in the mutant virus samples when compared to wild type virus (Figure 26). Small foci of HDAC6 are seen, and some colocalisation of M1 and HDAC6 is seen in the wild type, I94M and V92S mutant infections. In these viruses, some foci of M1 staining are present, indicating endocytosed virus, and some diffuse M1 staining is seen, indicating viral uncoating. However, the H90S mutant virus shows comparably little internalised virus as indicated by M1 staining, and aggregated 'spindle-like' presence of M1 on the cell surface. This may be an indication of a defect in viral entry for this mutant. For the V92S mutant, once again, the 'spindle-like' staining is visible on the cell surface, however there is far more virus internalised than with H90S. This suggests that the SIM mutants have a late stage vRNP trafficking defect and not an entry defect whereas protonation of the H90 residue may be involved in viral entry and uncoating.

3.17 Summary

The polysemy of the cytoplasmic tail of M2 has been shown through assays investigating its interaction with the key autophagy protein LC3; the small ubiquitin-like modifier SUMO; and mutations which may affect M2's interaction with other viral proteins. The highly conserved nature of the M2 CT points to the crucial role in both the entry, replication, and budding stages of the IAV lifecycle. The investigations herein demonstrating a still poorly understood role for the repeatable, but non-covalent, interaction of M2 with SUMO via a motif at the C terminal of the 97 amino acid protein, which is affected by point mutations targeting the LIR and the SIM. These point mutations are producible in whole virus through reverse genetics rescue, and show ability to replicate albeit with lower viral titres than the wild type A/Udorn/72 H3N2 virus. Studies with LIR mutant viruses and with WT and SIM mutants in HeLa cells deficient in autophagy demonstrate dysfunctional M2 and SUMO localisation. Analysis of viral budding through surface HA staining of cells infected with wild type or mutant viruses show altered viral morphology when the LIR or SIM domains are disrupted. Point mutations in the M2 CT also cause changes in viral protein packaging as seen in western blotting studies, and clearly influence the distribution of vRNPs within infected cells through an unknown mechanism. Furthermore, viral entry and uncoating is affected by M2 CT point mutations in a conserved protonatable histidine reside.

Subsequent work has looked at how viral filament formation is affected by: M2 interactions with the intermediate filament protein vimentin; the behaviour of an alternative splice variant of M2; and autophagy interactions of viruses used in seasonal intranasal vaccines.

3.2 M2, ALONG WITH OTHER M SEGMENT PROTEINS AND VIRAL SURFACE ANTIGENS, CAN INFLUENCE CELLULAR PROCESSES AND VIRAL MORPHOLOGY

Previously in this study, the effect of various mutations in the cytoplasmic tail region (positions 91 to 97) of the M2 ion channel protein of A/Udorn/72 H3N2 have been produced for analysis by transient expression in a plasmid vector, and in whole virus through generation by reverse genetics. Mutations were identified bioinformatically which would affect the ability of the M2 CT to bind to the autophagy protein, LC3, through the LIR at positions 91 – 94, and the SIM at positions 91 – 96. The data gathered demonstrated moderate colocalisation of M2 with LC3 specifically, with additional convincing data for the interaction of M2 with SUMO. Therefore, we attempted to investigate further factors which may modulate the overall interactions of the M2 CT and the regulation of viral filament formaton, through an alternative splicing variant of the M segment, the organisation of the intermediate cellular filament Vimentin (as demonstrated to interact with M2 in table 4 and figure 15), and the behaviour of virus strains used to produce seasonal influenza vaccines – the LAIV strains.

3.21 An alternative splice variant of M2 displays distinct colocalisation with LC3

All IAV subtypes have the capability to produce alternative splicing variants of segment seven, the 'M' segment of the viral genome. Though alternative splicing, some strains such as A/PR8/33(H1N1) can produce an 'M2-like' ion channel protein which can functionally compensate for M2 but contains a novel ectodomain of unknown function (Wise *et al.*, 2012). However, M42 is localised distinctly cytoplasmically, in contrast to the highly plasma membrane localisation of M2. M42 is largely retained within the Golgi apparatus during infection as seen in the original report by Wise *et al.*, 2012, and its localisation appears similar in this report in a plasmid based expression system. Newly investigated below is the propensity of M42 to highly colocalise with LC3, in a fashion surpassing that of M2. HEK 293T cells were transfected with plasmids encoding for LC3b-mCherry and either pEGFP-M42 or pEGFP-M2 from the PR8 strain of IAV. Cells were prepared for confocal microscopy after 24 hours incubation.

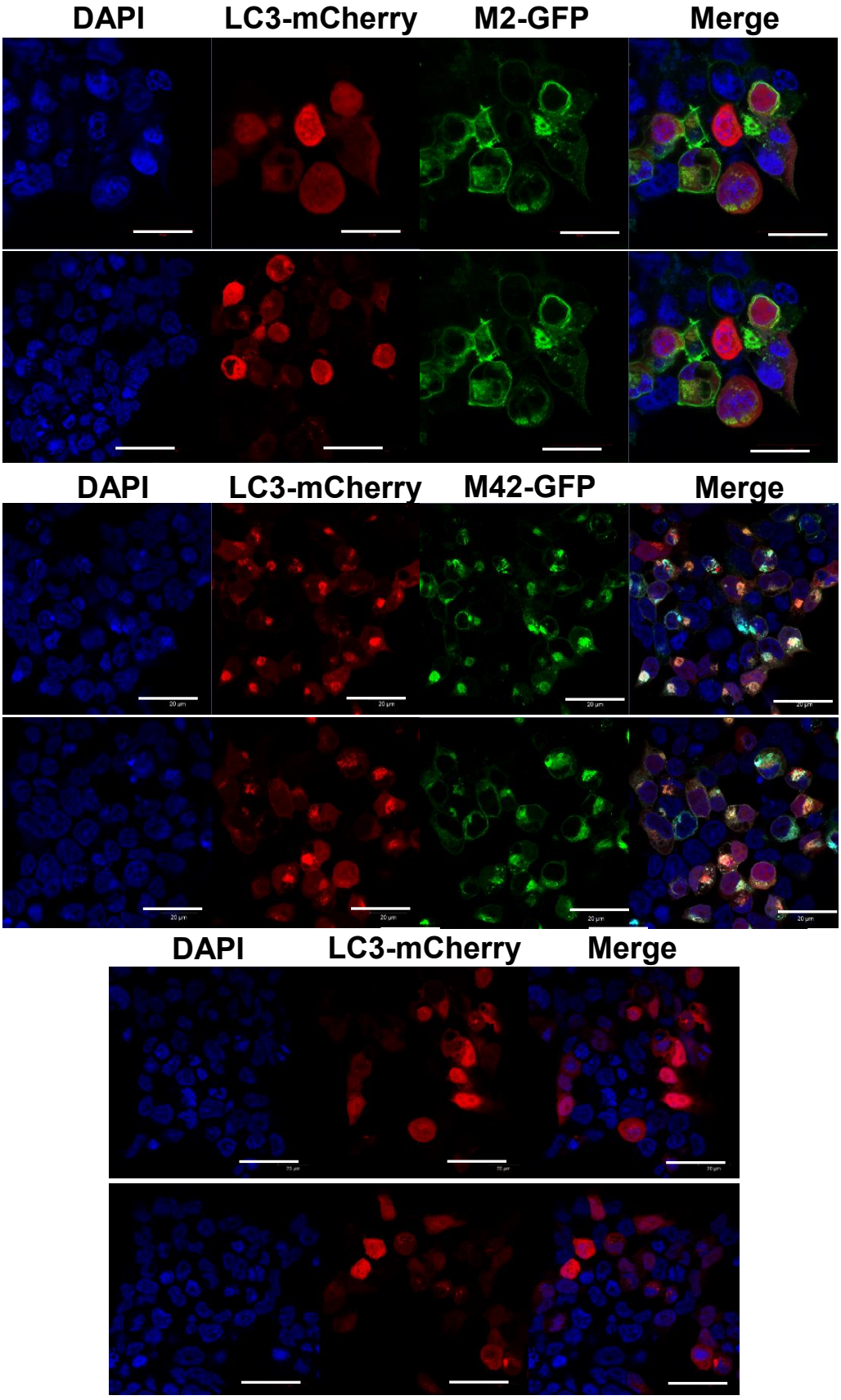

Figure 27 – **Colocalisation of M2/M42 with LC3.** HEK293T cells were grown on coverslips treated with poly-L-lysine before transfection. Cells were transfected using TransIT-LT1 with mCherry-LC3b and either GFP-M2 (top), GFP-M42 (middle) or empty vector (bottom). Image data is indicative of results seen in a triplicate repeat set. **Scale bar 20 µM.**

Figure 27 shows the difference in localisation between M42 and M2 of A/PR/8/34 H1N1 (‘PR8’) and LC3. LC3 in the negative control shows diffuse cytoplasmic localisation, and this appears similar in the M2 images, with only small foci observed. However, M42 localises distinctly with LC3, and is seen in significantly lower quantities at the plasma membrane in comparison to M2. This phenomenon is yet to be understood, as all previous literature and data point to, and confirm, that an LIR in the CT of M2 is responsible for binding to and sequestering LC3. M42 contains the same LIR-containing CT as M2 and thus, would be predicted to associate with comparably LC3, though the novel ectodomain may affect protein trafficking and thus localisation.

3.22 PR8 ΔM2 and ΔM42 viruses display altered budding patterns

The PR8 virus is a H1N1 strain which does not produce filamentous particles *in vitro*. Wild type A/Puerto Rico/8/34 (H1N1) produces both M2 and M42 in normal infection, and a number of other IAV strains have been identified as producing, or likely to produce, M42 from alternative splicing of segment 7 (Wise *et al.*, 2012). As demonstrated by Wise *et al.* and previously in this study (figure 27), M42 localises strongly intracellularly at the Golgi apparatus, with less plasma membrane distribution than M2. To investigate if the enhanced association between M42 and LC3 affects viral morphology we infected A549 cells with wild type A/Puerto Rico/8/34 (H1N1), or the PR8 splicing mutant viruses PR8ΔM2 (producing only M42) or PR8ΔM42 (producing only M2) and evaluated viral morphology. Samples were prepared 18 HPI, stained for HA and analysed using confocal microscopy.

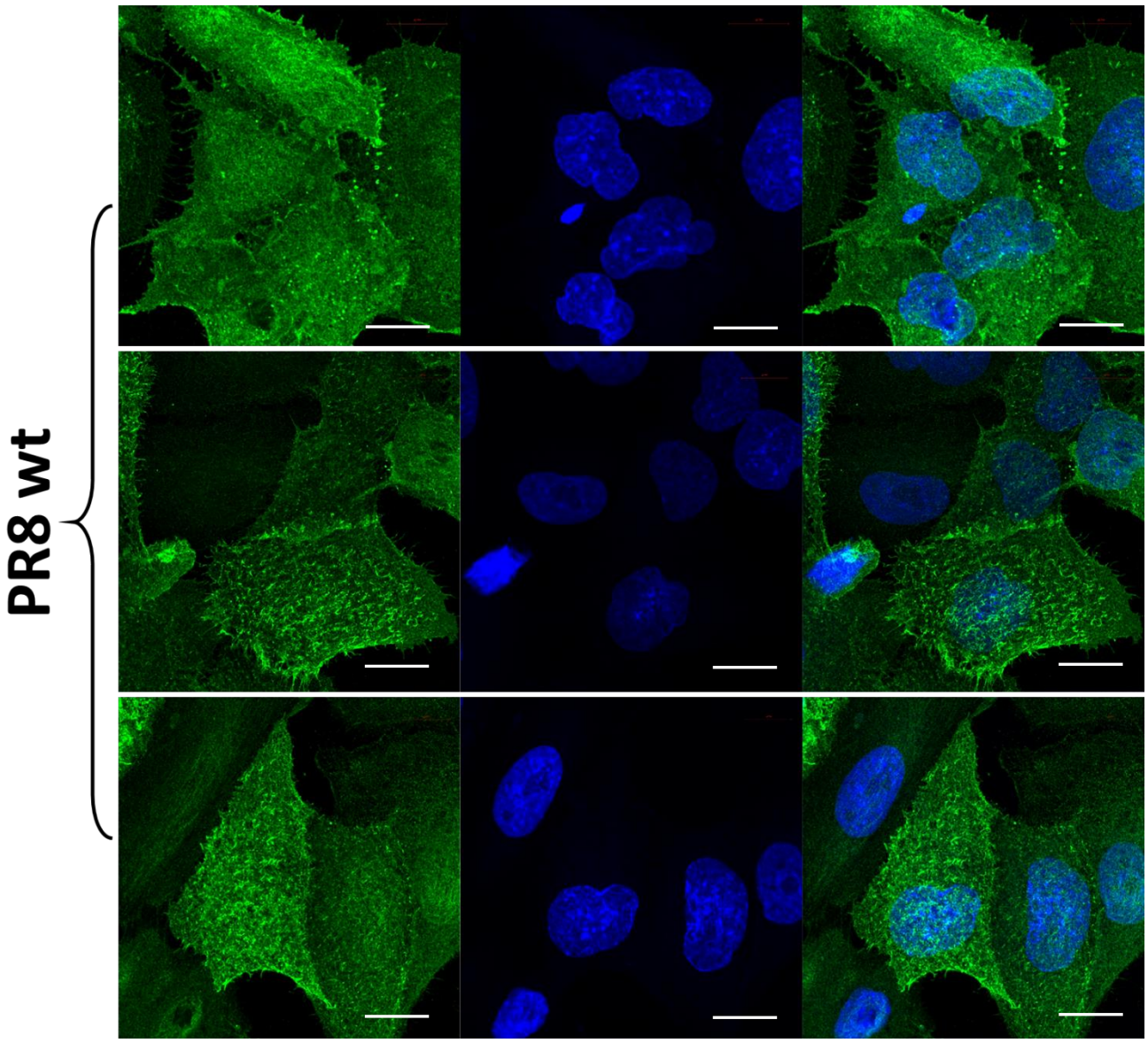
PR8 wt

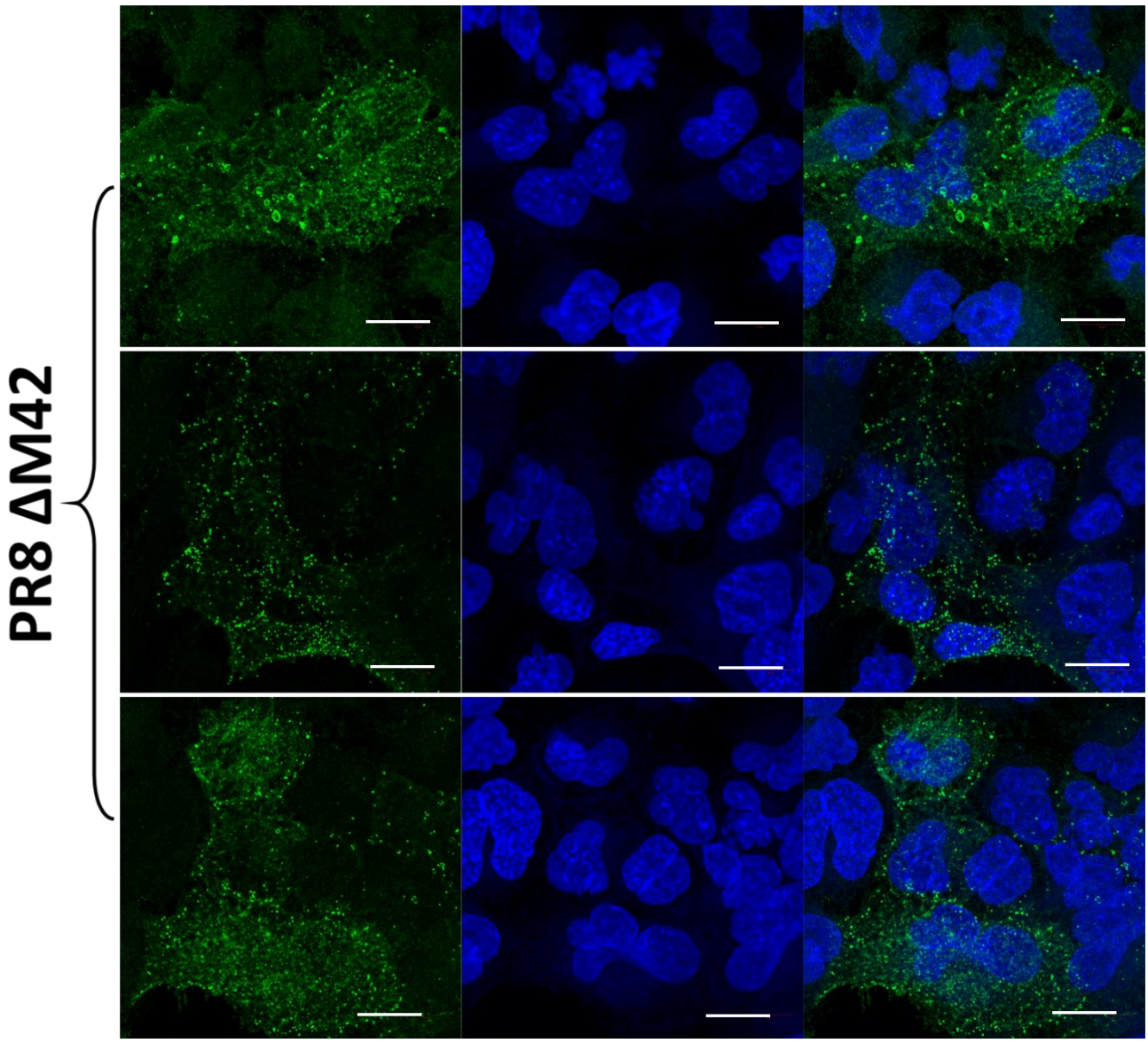
PR8 ΔM42

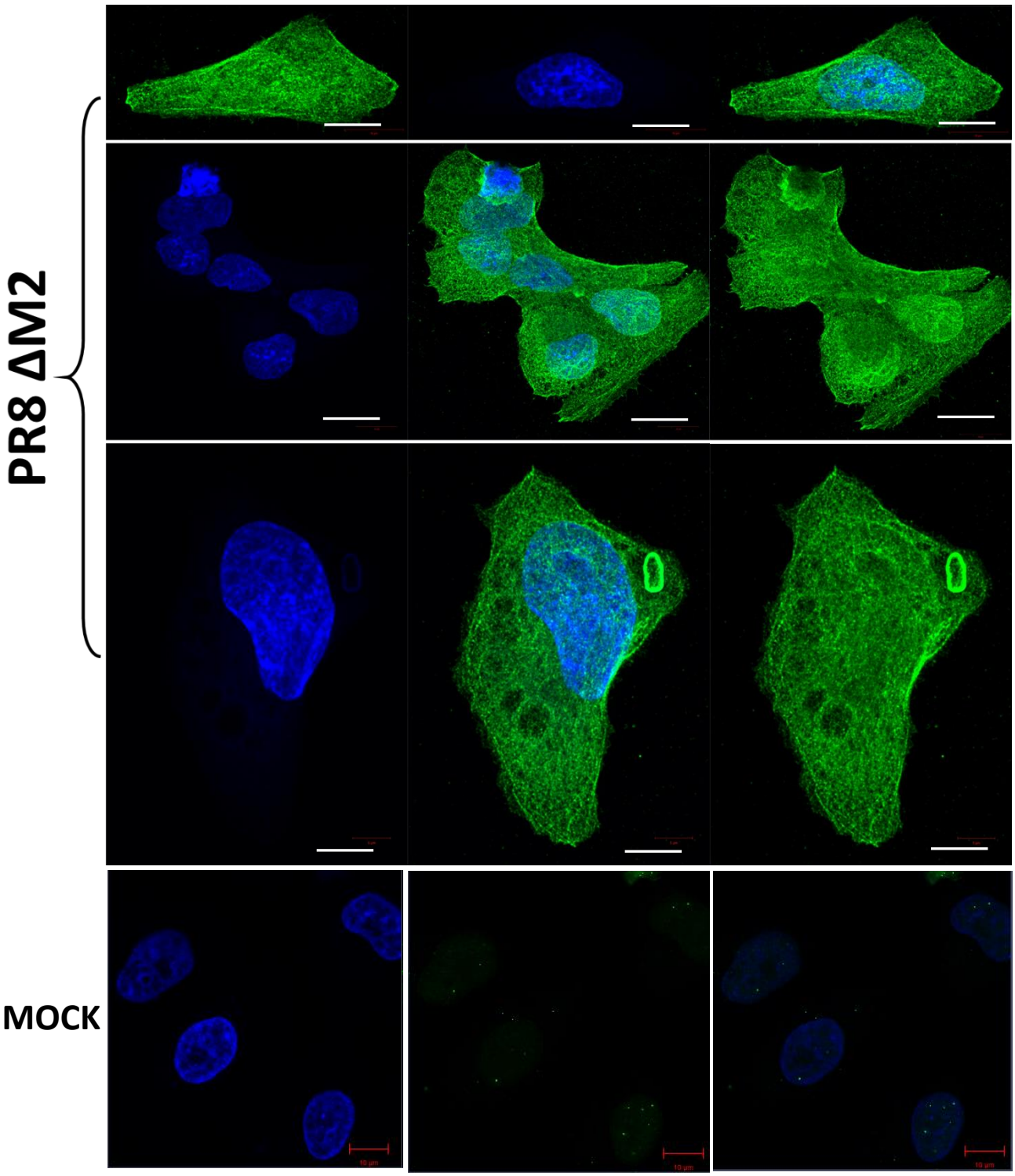

Figure 28 – **Viral morphology comparison between cells infected with wild type PR8, PR8ΔM42 or PR8ΔM2.** A549 cells grown on glass coverslips were infected with 1 MOI of A/Puerto Rico/8/34 (H1N1), PR8ΔM2 (producing only M42) or PR8ΔM42 (producing only M2), and infection was allowed to proceed for 18 hours. Image data is indicative of results seen in a triplicate repeat set. **Scale bar 10 µM.**

Wild type PR8 displays morphology consistent with previous publications – diffuse positive plasma membrane staining for HA, with some bacilliform budding present and few membrane aggregates (Figure 28). PR8ΔM42 shows distinct punctate staining of the plasma membrane, with few 'halo-like' structures on the cell surface, and no discernible bacilliform virus. PR8ΔM2 stains very evenly for HA, and shows more positive HA staining intra- and peri-nuclearly, with a further, large (~10 μm) circular structure. The perinuclear aggregration seen here and with M42 and LC3 (Figure 27) may indicate formation of viral induced aggresomes. This data suggests a differential and integral role for both M2 with M42 in the budding of A/Puerto Rico/8/34 (H1N1) which is not yet fully understood.

3.23 M2 within cells causes vimentin condensation, an indication of aggresome formation, and this is not affected by M2 CT mutations

Data has been presented in this study which points to the interaction of M2 with the intermediate cellular filament vimentin, through mass spectrometry analysis and co-immunoprecipitation assays. Vimentin is known to be involved in the formation of vimentin 'cages', which form as part of the aggresome complex during the process of unwanted protein degradation, such as during autophagy. M2 is known to contain an LC3 interacting region in its cytoplasmic tail, and through this it is able to interact with the process of autophagy. In addition, data in Figures 27-28 suggest that M2 splice variants may induce aggresome formation. To investigate whether M2, M42 and the generated M2 CT mutants can influence the arrangement of vimentin within the cell, HEK 293T cells were transfected with plasmids encoding for WT IAV A/Udorn/72 H3N2 M2, M42 or M2 CT mutants, and a pSmOrange-Vimentin vector. Cells were incubated for 24 HPI, and then prepared for confocal microscopy.

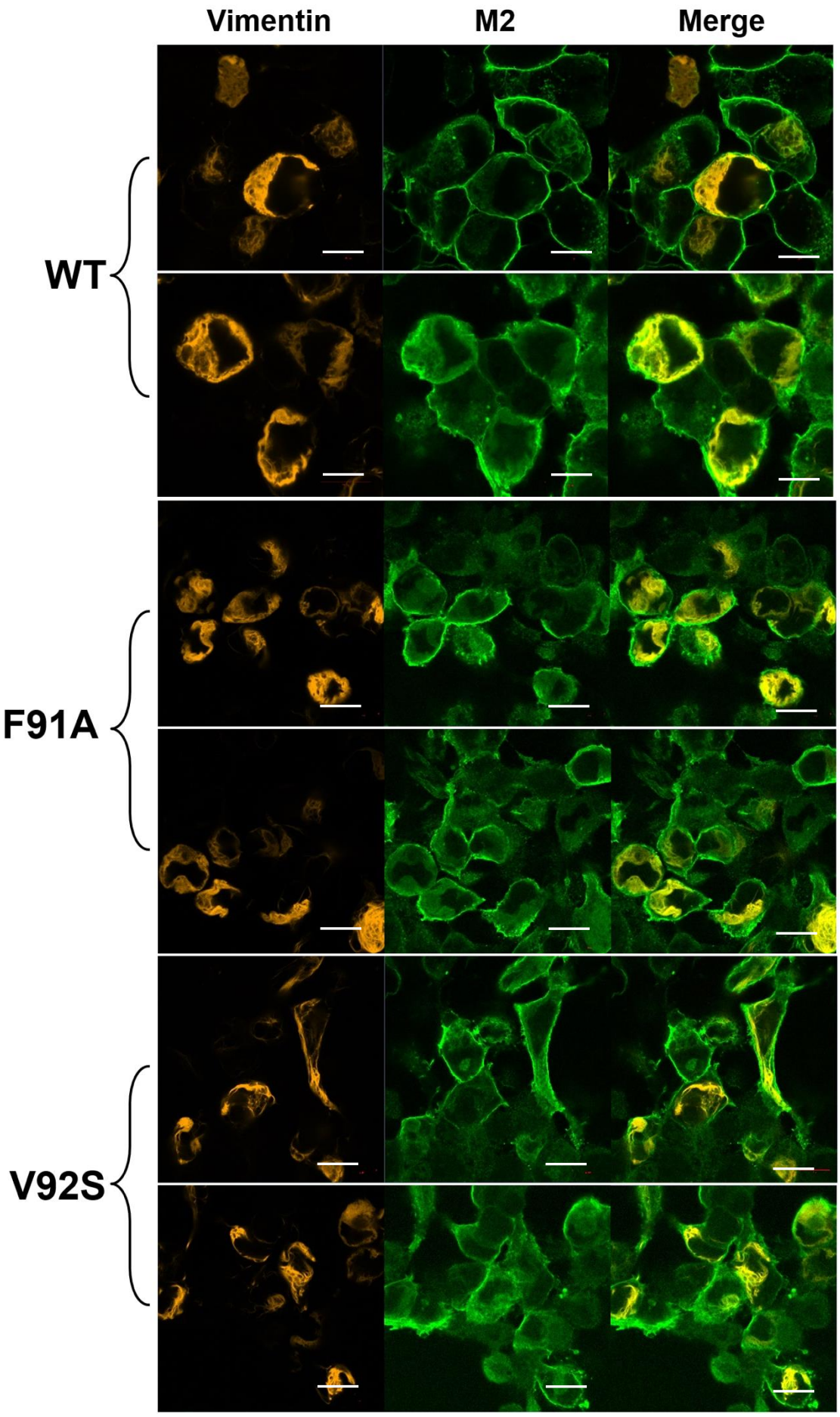
Vimentin
M2
Merge
WT
F91A
V92S

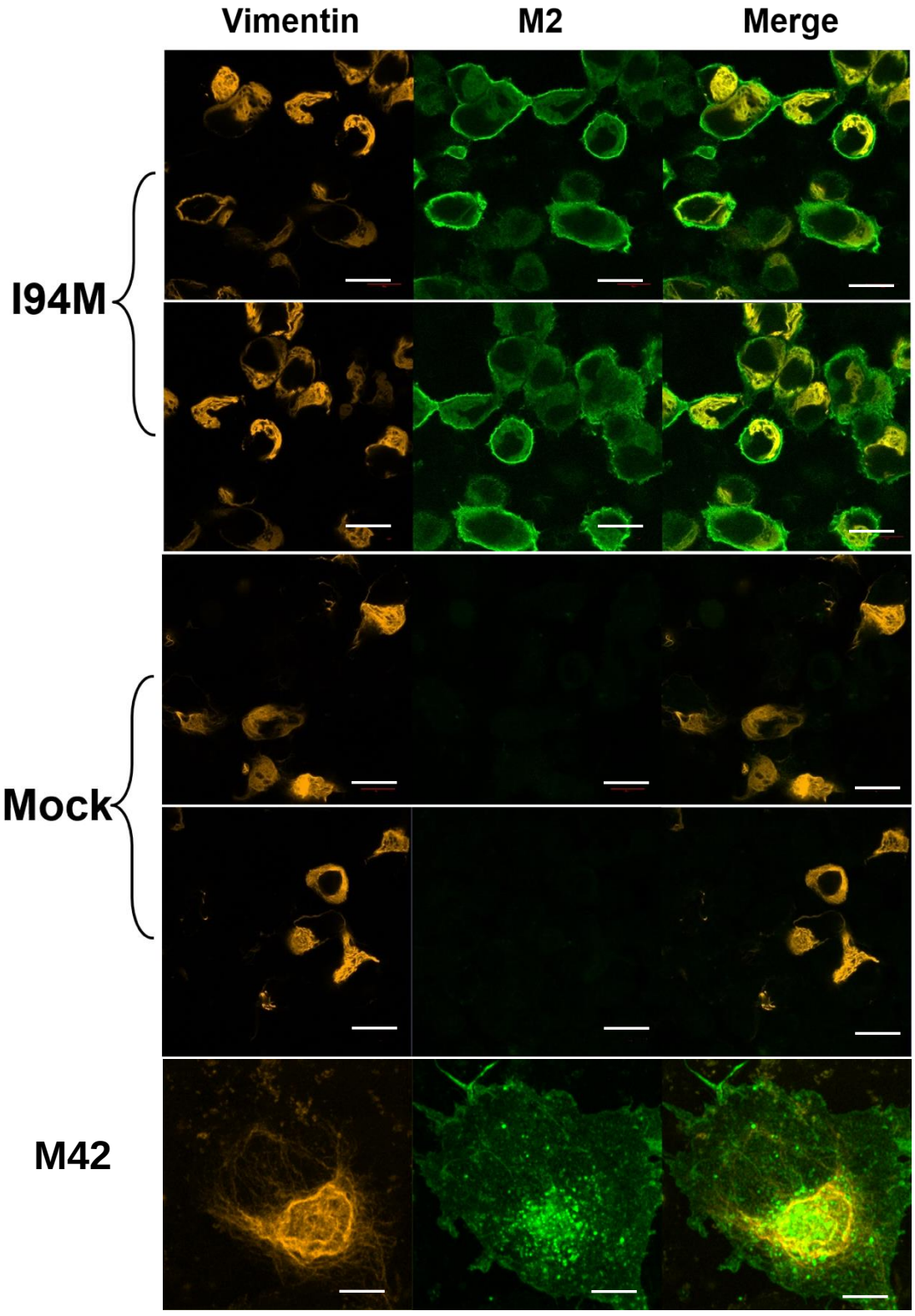

Figure 29 – **Confocal microscopy images of transiently expressed A/Udorn/72 H3N2 M2 CT mutants stained for M2 and Vimentin.** HEK293T cells were grown on coverslips treated with poly-L-lysine before transfection. Cells were transfected using TransIT-LT1 with pSmOrange-Vimentin and either 'wild type (WT)' M2 from A/Udorn/72 H3N2, M42 or indicated M2 CT mutant. Cells were allowed to grow and express for 24 hours. Image data is indicative of results seen in a triplicate repeat set. **Scale bar 15 µM.**

Reorganisation of vimentin superstructure within the cell is known to be one of the indicators of aggresome formation, as the proteins undergoing degradation and recycling are bound by interweaved strands of vimentin, known as a vimentin cage. Furthermore, vimentin is known to play a role in facilitating the early stages of IAV infection, influencing the acidification of late endosomes and their trafficking, both of which are necessary for efficient IAV replication (Wu and Panté, 2016). The organisation of vimentin was studied using a fluorescently tagged construct, vimentin-pSmOrange, and antibody labelling of transiently expressed M2, M42 or M2 CT mutants. Compared to the empty vector mock transfection, vimentin undergoes dramatic reorganisation in all of M2 conditions, even when the CT is mutated to remove LC3 or SUMO binding (Figure 29). Condensation of vimentin is hard to define at this resolution and with these assay parameters and so the interpretation of this reorganisation is difficult to define. However, in the presence of M42, vimentin forms a cage like structure circling aggregated M42 proteins. This strongly suggests that the aberrant trafficking and localisation of M42 results in the formation of aggresomes that contain M42, LC3 and are surrounded by a vimentin cage. This could explain the significant changes seen in virus assembly with M42 as compared to M2 (Figure 28).

3.24 HA sequences from LAIV strains

In addition to the M proteins, HA has also been shown to modulate viral morphology, possibly though manipulation of host cell autophagy (Jin, Leser and Lamb, 1994; Zhirnov and Klenk, 2013). We investigated the impact of subtle variations of HA on viral morphology and autophagy by using historic LAIV strains that all retain the same M1 and M2 proteins, but have subtle variations in HA. The donor IAV backbone is from A/Ann Arbor/6/60 (H2N2) which should produce spherical virions based on the M1 sequence. All the internal genes and the matrix proteins are identical in the LAIV strains, with only variations in HA and NA.

Figure 30 shows an amino acid sequence alignment produced using NCBI's BLAST alignment tool. Regions of conservation are red, regions of variance are in blue, and insertions are in green. Many of the strains have highly related HA sequences reflecting year to year antigenic drift.

```
A/Bolivia/1053/2010(H3N2)          1   MKTIIALSYILCLVFAQKLPGNDNSTATLCLGHHAVPNGTIVKTITNDQIEVTNATELVQNSSTGEICDS-PHQIIDGEN  79
A/Perth/16/2009(H3N2)              1   MKTIIALSYILCLVFAQKLPGNDNSTATLCLGHHAVPNGTIVKTITNDQIEVTNATELVQSSSTGEICDS-PHQILDGKN  79
A/South Dakota/06/2007(H1N1)       1   MK--VKLLVLLCTFTA-------TYADTICIGYHANNSTDTVDTVLEKNVTVTHSVNLLENSHNGRLCLLkGIAPLQLGN  71
A/Uruguay/716/2007(H3N2)           1   MKTIIALSYILCLVFAQKLPGNDNSTATLCLGHHAVPNGTIVKTITNDQIEVTNATELVQSSSTGEICDS-PHQILDGEN  79
A/Victoria/361/2011(H3N2)          1   MKTIIALSHILCLVFAQKLPGNDNSTATLCLGHHAVPNGTIVKTITNDQIEVTNATELVQNSSIGEICDS-PHQILDGEN  79

A/Bolivia/1053/2010(H3N2)         80   CTLIDALLGDPQCDGFQN-KKWDLFVERSKAY-SNCYPYDVPDYASLRSLVASSGTL---EFNNESFNWTGVTQNGTSSA  154
A/Perth/16/2009(H3N2)             80   CTLIDALLGDPQCDGFQN-KKWDLFVERSKAY-SNCYPYDVPDYASLRSLVASSGTL---EFNNESFNWTGVTQNGTSSA  154
A/South Dakota/06/2007(H1N1)      72   CSVAGWILGNPECELLISkESWSYIVEKPNPEnGTCYPGHFADYEELREQLSSVSSLerfEIFPKESSWPNHTVTGVSAS  151
A/Uruguay/716/2007(H3N2)          80   CTLIDALLGDPQCDGFQN-KKWDLFVERSKAY-SNCYPYDVPDYASLRSLVASSGTL---EFNNESFNWTGVTQNGTSSS  154
A/Victoria/361/2011(H3N2)         80   CTLIDALLGDPQCDGFQN-KKWDLFVERSKAY-SNCYPYDVPDYASLRSLVASSGTL---EFNNESFNWTGVTQNGTSSA  154

A/Bolivia/1053/2010(H3N2)        155   CIRRSNNSFFSRLNWLTHLNFKYPALNVTMPNNEQFDKLYIWGVHHPGTDKDQIFLYAQASGRITVSTKRSQQAVIPNIG  234
A/Perth/16/2009(H3N2)            155   CIRRSKNSFFSRLNWLTHLNFKYPALNVTMPNNEQFDKLYIWGVLHPGTDKDQIFLYAQASGRITVSTKRSQQTVSPNIG  234
A/South Dakota/06/2007(H1N1)     152   CSHNGESSFYRNLLWLTGKNGLYPNLSKSYANNKEKEVLVLWGVHHPPNIGNQKALYHTENAYVSVVSSHYSRKFTPEIA  231
A/Uruguay/716/2007(H3N2)         155   CIRRSNNSFFSRLNWLTHLKFKYPALNVTMPNNEKFDKLYIWGVHHPGTDNDQIFPYAQASGRITVSTKRSQQTVIPNIG  234
A/Victoria/361/2011(H3N2)        155   CIRRSNNSFFSRLNWLTHLNFKYPALNVTMPNNEQFDKLYIWGVHHPGTDKDQIFLYAQSSGRITVSTKRSQQAVIPNIG  234

A/Bolivia/1053/2010(H3N2)        235   SRPRVRNIPSRISIYWTIVKPGDILLINSTGNLIAPRGYFKIRSG-KSSIMRSDAPIGKCNSECITPNGSIPNDKPFQNV  313
A/Perth/16/2009(H3N2)            235   SRPRVRNIPSRISIYWTIVKPGDILLINSTGNLIAPRGYFKIRSG-KSSIMRSDAPIGKCNSECITPNGSIPNDKPFQNV  313
A/South Dakota/06/2007(H1N1)     232   KRPKVRDQEGRINYYWTLLEPGDTIIFEANGNLIAPRYAFALSRGfGSGIINSNAPMDKCDAKCQTPQGAINSSLPFQNV  311
A/Uruguay/716/2007(H3N2)         235   SRPRVRNIPSRISIYWTIVKPGDILLINSTGNLIAPRGYFKIRSG-KSSIMRSDAPIGKCNSECITPNGSIPNDKPFQNV  313
A/Victoria/361/2011(H3N2)        235   SRPRIRNIPSRISIYWTIVKPGDILLINSTGNLIAPRGYFKIRSG-KSSIMRSDAPIGKCNSECITPNGSIPNDKPFQNV  313
```

Figure 30 – **Amino acid sequence alignment of full-length HA from indicated LAIV strains.** Produced using the Basic Local Alignment Search Tool found at https://blast.ncbi.nlm.nih.gov/Blast.cgi. Regions of variance are in blue, conservation in red, and insertions in green.

3.25 HA variants affect M2 localization and viral filament formation

As demonstrated previously in this study, the M segment proteins and their interactions have a significant effect on M2 localisation, and therefore the morphology of budding virus. Subsequently, we have used a collection of LAIV strains to investigate the role of subtle variations in HA which may influence viral and cellular protein localisation and viral morphology. These viruses are all produced using the same MDV backbone, with alternative H and N genomic segments, producing a range of HA and NA surface antigens, eliciting different immune responses in vaccinated patients to respond effectively to seasonally circulating IAV.

With well reported and well characterised mutations of the matrix proteins, both in pre-existant literature and in this report, it is important to explore what other factors may influence filamentous IAV morphology. Seasonal LIAV immunisation strains were obtained from MedImmune and analysed through infection and immunofluorescent confocal microscopy.

The confocal images in figure 31 show interesting morphology between various candidate vaccine strains in A549 cells. A549 cells were infected with the LAIVs and probed for HA and M2, with or without cell permiabilisation to better understand surface distribution of HA and M2 (no data for Victoria permiabilised). Unlike previous images in this report of A/Udorn/72 H3N2, which produces both classical spherical virions, and mostly well formed, straight and undisrupted filaments, some of the vaccine strain viruses produce aberrant, tangled accumulations of HA-positive foci, though some, such as South Dakota, produced extensive filaments and others, such as Victoria, produced minimal filaments.

All LAIV strains, barring Victoria, display large positively HA straining aggregates on the cell surface, with differing localisation of M2 for all strains, with some strains, such as Uruguay, producing M2 perinuclear foci similar to that seen with M42. This suggests, that subtle variants in HA can indeed alter M2 localisation and viral morphology, despite possessing the same M1 and M2 proteins. Unfortunately, analysis of HA sequences did not identify any obvious variants that could explain this difference. In addition, some strains exhibited nuclear M2 staining, though the reason for this was not clear.

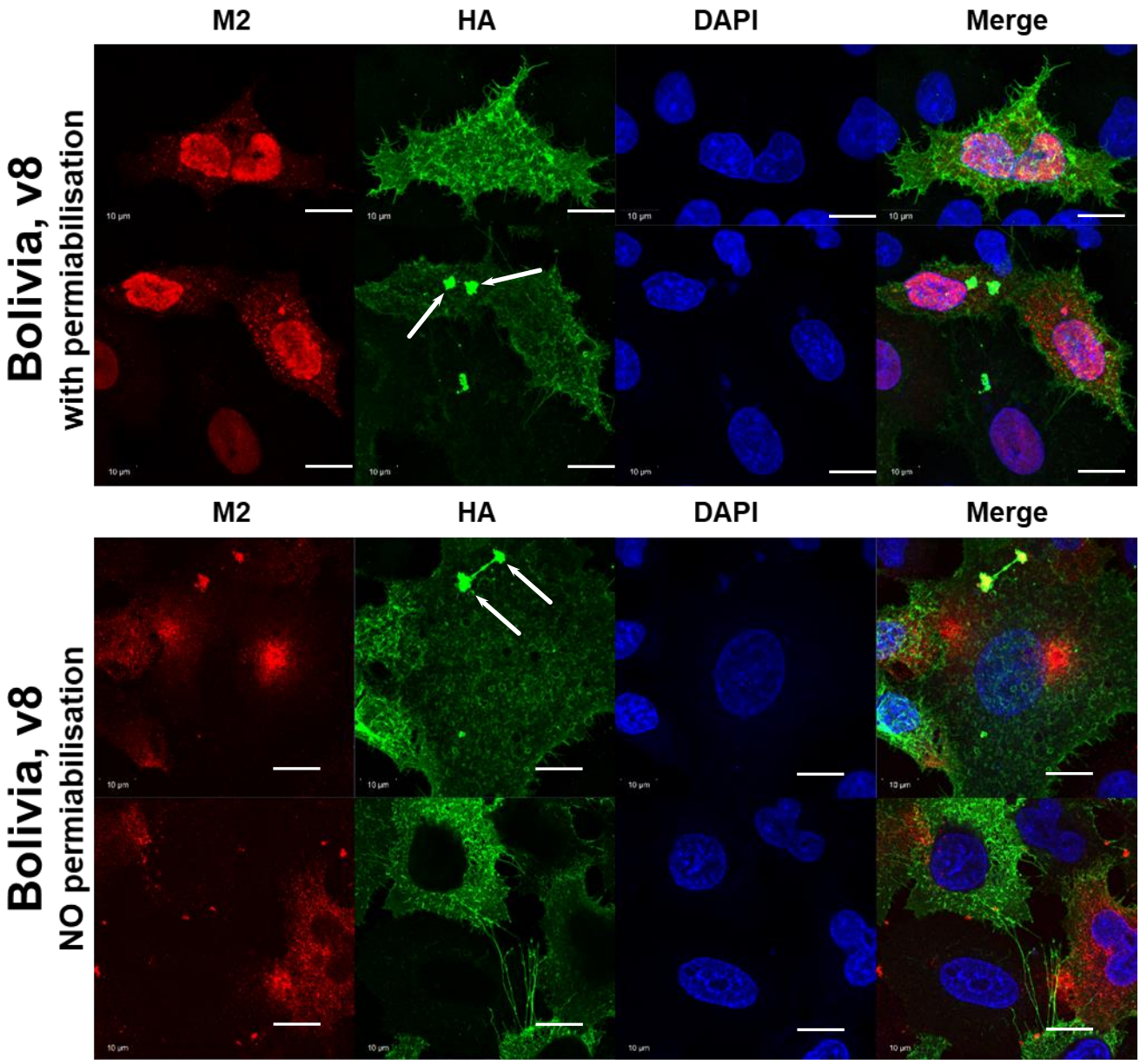
M2
HA
DAPI
Merge
Bolivia, v8
with permiabilisation
M2
HA
DAPI
Merge
Bolivia, v8
NO permiabilisation

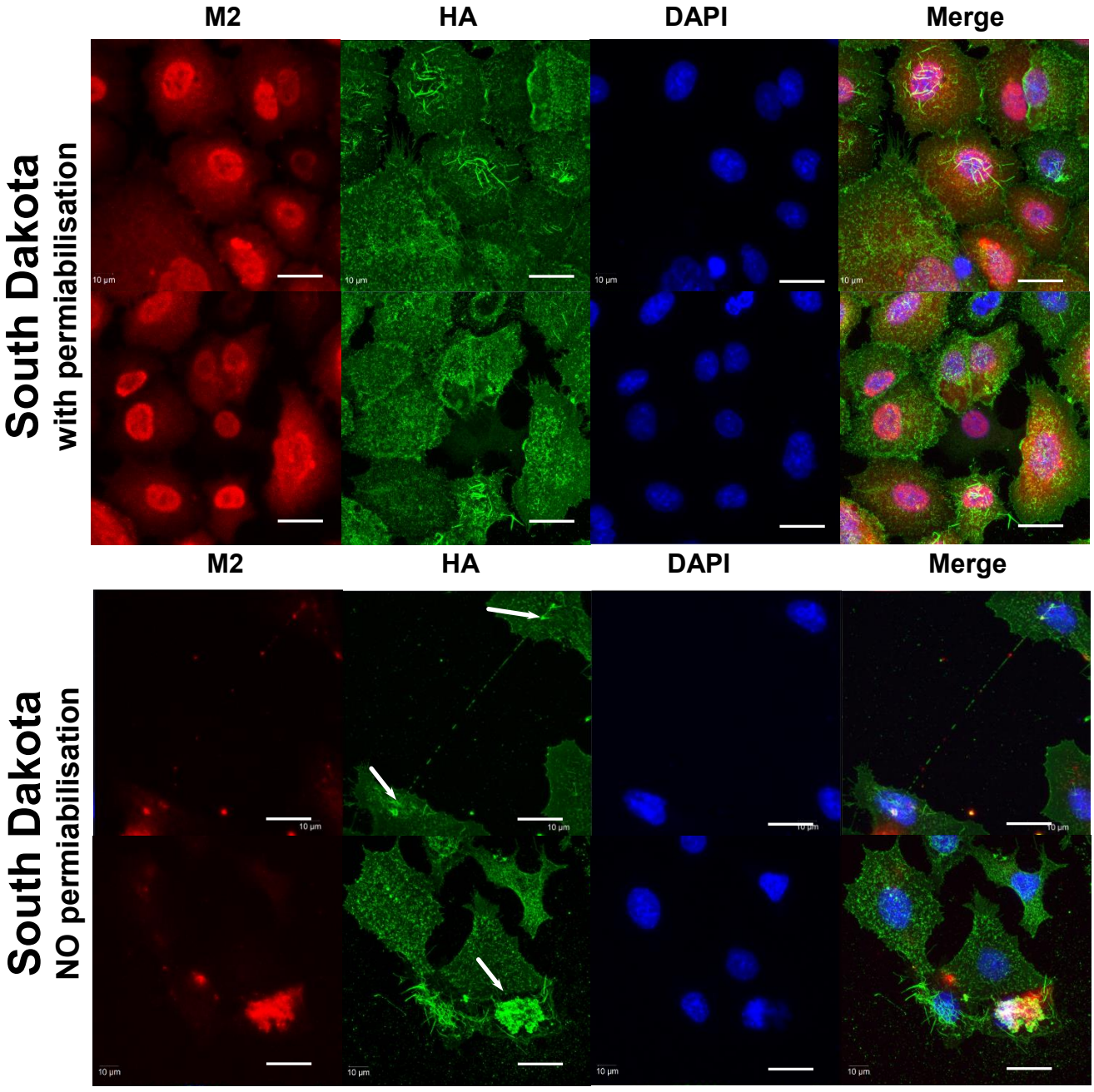
M2
HA
DAPI
Merge
South Dakota
with permiabilisation
M2
HA
DAPI
Merge
South Dakota
NO permiabilisation

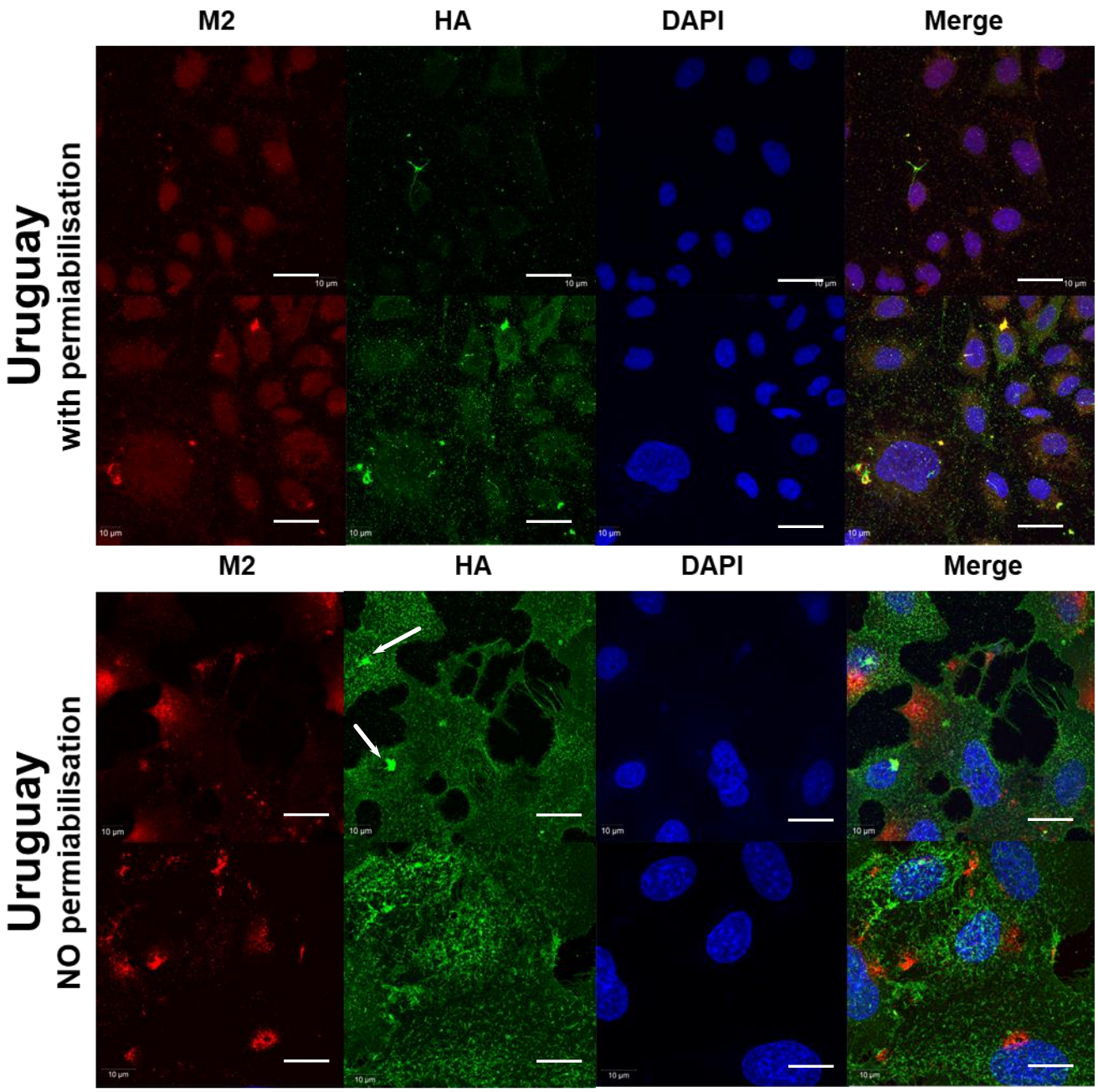
M2
HA
DAPI
Merge
Uruguay
with permiabilisation
M2
HA
DAPI
Merge
Uruguay
NO permiabilisation

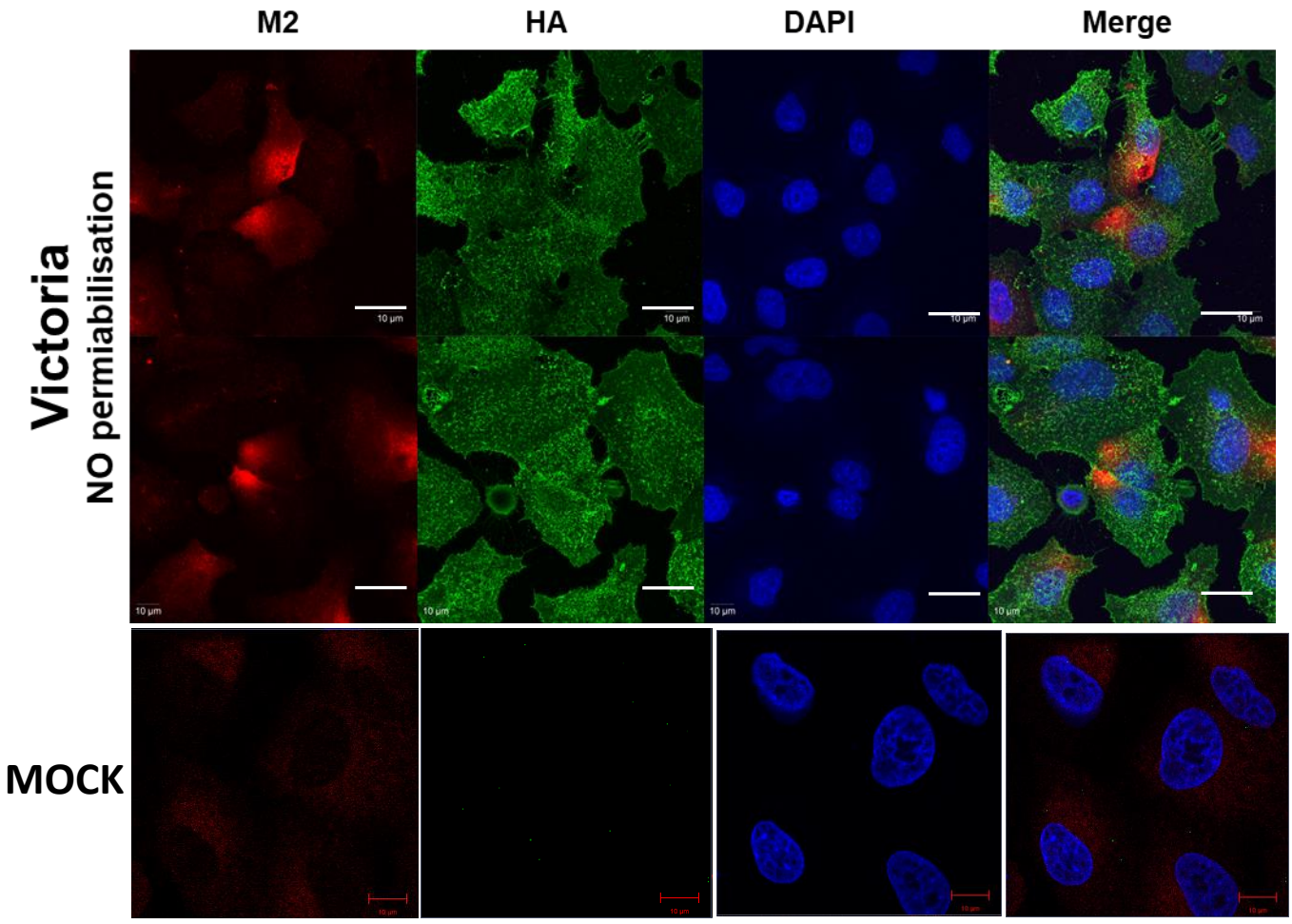

Figure 31 – **Confocal microscopy images of LAIV infected A549 cells.** A549 cells grown on glass coverslips were infected with 1 MOI of MedImmune vaccine strain viruses 'Bolivia v8', 'South Dakota', 'Uruguay' or 'Victoria', and infection was allowed to proceed for 18 hours. Image data is indicative of results seen in a triplicate repeat set. **Sca le bar 10 µM.**

3.26 LAIV strains induce LC3 puncta and M2 localises to the plasma membrane

M2 localises to the plasma membrane in the model strain A/Udorn/72 H3N2 used extensively in this study. As HA variations in the LAIVs affect M2 localisation we then investigated if alterations in autophagy induction may be responsible. LAIVs were used to infect A549 cells and after 18 hours the cells stained for LC3 and M2.

All the LAIV vaccine strains, produced using a donor virus backbone based on the A/Ann Arbor/6/60 IAV with HA and NA variations, still appears to induce autophagy through the formation of LC3 puncta (Figure 32). Strains Bolivia v8, Perth and South Dakota induce larger and more robust LC3 puncta, with Bolivia v8 displaying distinct colocalisation of M2 with LC3, interestingly these strains tended to produce more aggregated M2/HA foci and more robust filaments in Figure 31. Bolivia v4 induces smaller LC3 puncta, with less colocalisation with M2. Interestingly, Bolivia v4 shows less M2 overall at the plasma membrane than other strains, though the significance of this is not known.

As with A/Udorn/72 H3N2, the CT of M2 in the MDV strain also contains an LIR, and such the M2 expressed by all LAIV strains would predict to interact with LC3. Thus, the differences in autophagy activation, M2 localisation and colocalisation with LC3, and viral filament formation are likely due to subtle differences in different HA molecules, though the mechanism for this is unclear at present.

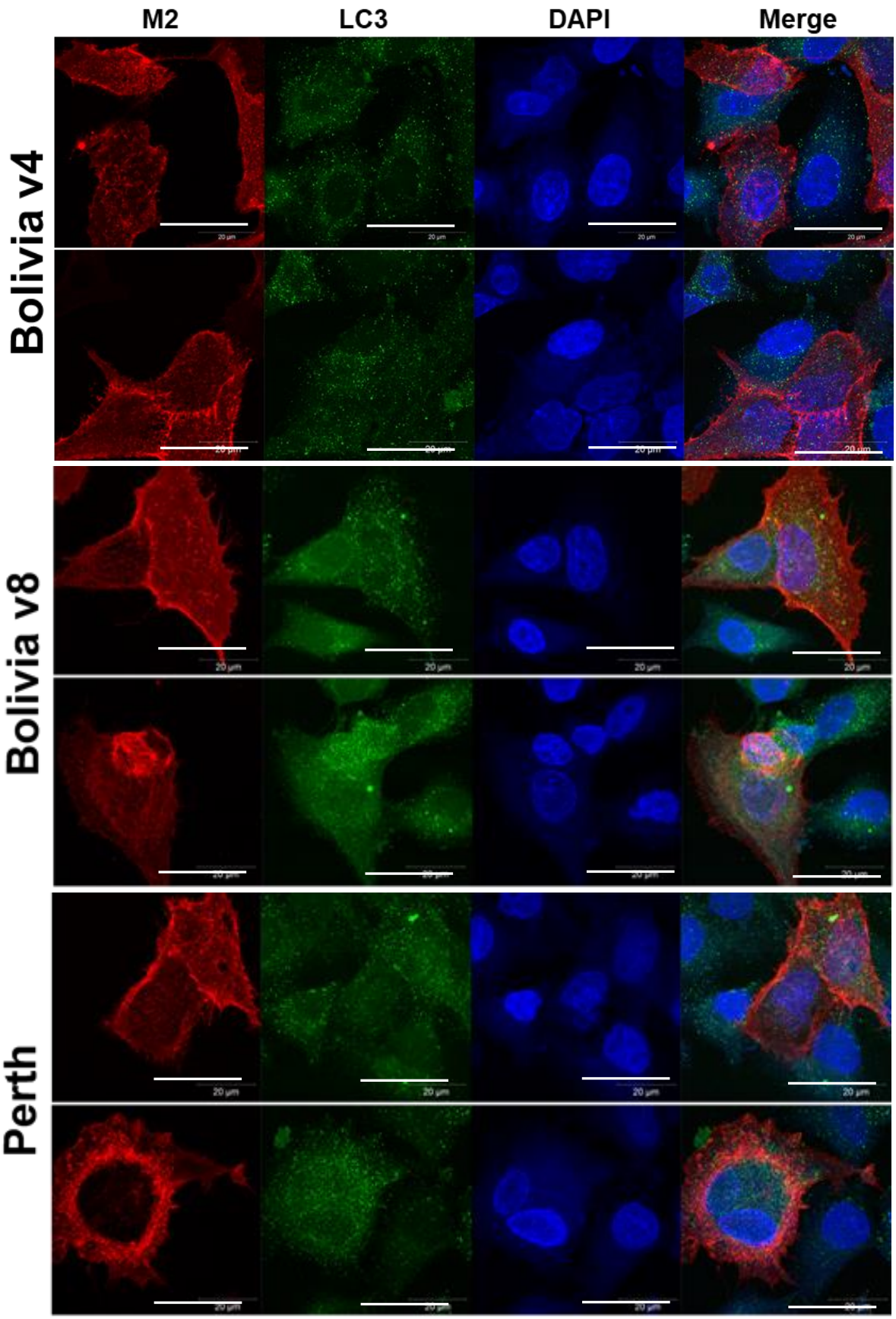
M2
LC3
DAPI
Merge
Bolivia v4
Bolivia v8
Perth

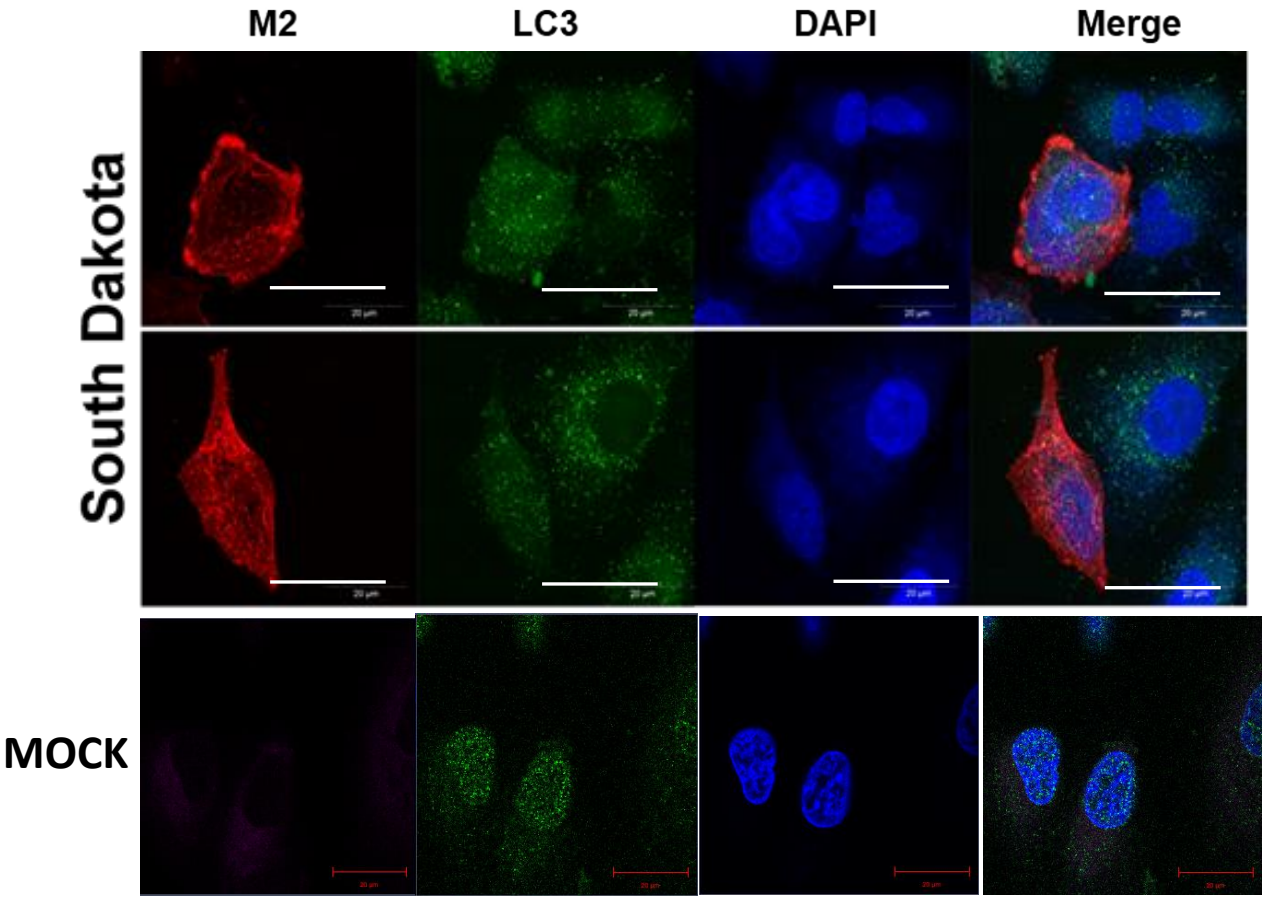

Figure 32 – **M2 and LC3 localisation in LAIV infected A549 cells.** A549 cells grown on glass coverslips were infected with 1 MOI of MedImmune vaccine strain viruses 'Bolivia v4', 'Bolivia v8', 'Perth' or 'South Dakota', and infection was allowed to proceed for 18 hours. Image data is indicative of results seen in a triplicate repeat set. **Scale bar 20 µM.**

3.27 Summary

We have demonstrated the ability of the alternative splice variant of M2, M42, to affect subcellular localisation and LC3 interaction whilst still retaining a genetically identical cytoplasmic tail to M2. M42's robust colocalisation with LC3 suggests that the ectodomain may affect trafficking of the protein throughout the cell and the ability to bind LC3, resulting in the formation of peri-nuclear aggresomes. This variation when studied in whole virus infection also causes both a change in the morphology of budding virus, and a distribution in positive surface HA staining in both A/PR8/34 H1N1 viruses which express either M2 alone or M42 alone. In PR8 at least, this suggests that differential expression of M2 and M42 significantly affects the budding of IAV from host cells.

In revisiting the A/Udorn/72 H3N2 M2 and M2 CT mutants in transient expression studies in relation to vimentin, a considerable reorganisation of this intermediate cellular filament is seen. This may be indicative of protein degradation pathways being altered in an M2 CT dependent manner, which would require further investigation, owing to vimentin reorganisation playing a role in the formation of 'vimentin cages' during aggresome formation, as was seen with the splice variant M42. Vimentin reorganisation also plays a role in the epithelial to mesenchyme transition (Mendez, Kojima and Goldman, 2010) and is known to have a role in the IAV lifecycle (Wu and Panté, 2016).

The LAIVs used to immunise against seasonal IAV strains keep the same viral backbone (A/Ann Arbor/6/60), with HA and NA proteins swapped in and out for immunogenicity. LAIV strains displaying varying HA surface proteins showed a wide and varied range of budding morphologies, notably with the formation of large tangled aggregates on the surface of infected cells. Localisation of M2 also appears altered as was the initiation of autophagy, seen through LC3 puncta, with Bolivia v8 and Perth strains particularly adept at inducing autophagy. This demonstrates that viral protein variations can have significant effects on protein localisation and viral morphology.

4 DISCUSSION

4.0 DISCUSSION

Through this investigation, the broad and promiscuous nature of the M2 ion channel has been investigated in regards to its influence on the morphology of budding IAV, its interaction with the autophagy protein LC3; its novel interaction with the small ubiquitin-like modifier, SUMO; further characterisation of the interaction of M42, an M segment splice variant, with LC3; the ability of M2 and M2 CT mutants to affect Vimentin reorganisation; and the effect of HA variability as used in LAIV strains to alter viral morphology.

Results presented in this body of work further characterise the nature of the cytoplasmic tail of the M2 protein of the influenza A virus. Further confirmation of the role of the M2 CT in binding to LC3 and the influence that various mutations have on this interaction have been studied. Furthermore, a novel interacting partner for the M2 CT has been proposed, SUMO. Data has shown that the M2 protein when expressed alone has the ability to interact with the Small Ubiquitin-Like Modifier, SUMO, expressed by the host cell, and that this interaction is not covalent (i.e. it is distinct from SUMOylation which occurs to cellular proteins and other IAV proteins, such as M1 (Wu, Jeng and Lai, 2011a)). The SUMO interaction is mediated by a proposed SUMO interaction motif, SIM, within the cytoplasmic tail of M2 and that this SIM overlaps with the LC3 interacting region, LIR. Initially, bioinformatics predictions identified this region, and through transient expression studies in HEK293T cells SUMO was shown to co-immunoprecipitate with M2 (figure 10, page 51). To further characterise this phenomenon, mutations were made using the residues indicated by the aforementioned bioinformatics. These mutations took in to account the already published data on the LIR, and not only set out to characterise the SIM, but also if this had any link to LC3 binding, M2 trafficking, uncoating and morphology of the virus.

4.01 The presence of a SIM in the cytoplasmic tail of the IAV ion channel M2

Not only was the interaction of SUMO confirmed with various mutant M2 proteins, and the wild type M2 protein, classically using co-immunoprecipitation, and PLA were also utilised to give an 'in-cell' understanding of interaction, and the localisation of this interaction. M2's interaction with SUMO was seen to be broadly perinuclear, concurring with previously published literature regarding the distribution of SUMO, as cellular SUMO is present in greatest quantities within the nucleus of mammalian cells (Johnson, 2007). Speculation is still to be made on what role the SIM in the M2 CT may have. Referring to M2's ability to bind and sequester LC3, enabling the subversion of autophagy (Beale, Wise, Stuart, Benjamin J. Ravenhill, *et al.*, 2014), it is possible that the SUMO interaction with the M2 CT could function in disrupting the interaction with LC3, affecting autophagy progression. In Figure 10 (page 51), F91A shows a good retention of SUMO interacting ability, comparable to that of the wild type, but a complete loss of LC3 binding. This is confirmed by the western blot in Figure 10 (page 51); however it is observed that for a slight drop in expression of F91A, an inverse increase in SUMO co-immunoprecipitaion is seen compared to the wild type. I94M and V92S also show correlating immunoprecipitation data, validating the prediction by GPS SUMO. However, when using the 'in-cell interaction assay', PLA, the foci/cell ratio for F91A interacting with SUMO was considerably lower than wild type M2. This finding suggests that, whilst transiently expressed F91A may retain normal interactions with SUMO, interactions in the setting of viral infection are affected by this point mutation. It is possible that, as the interaction of M2 is thought to be non-covalent (i.e. the M2 CT containing a SIM and not a SUMOylation site), interaction is through another viral protein which is SUMOylated, for example M1.

4.02 SUMO interaction in the context of viral infection

In order to understand how these mutations affect the viral lifecycle it was necessary to produce mutant virus using reverse genetics. When mutant viruses F91A, V92S and I94M were produced, the PLA displayed interesting results different to that of transiently expressed M2 constructs. F91A shared a foci/cell ratio of roughly equal

to that of wild type virus, V92S having around one and a half times the ratio, with I94M showing almost five times the number of foci per cell than wild type. This is in stark contrast to the bioinformatics predictions, and the western blots of co-immunoprecipitations with these transiently expressed mutants. What this does intriguingly suggest, however, is that whilst the existence of a SIM in the M2 CT can be demonstrated, SUMO interactions with the M2 CT proceed very differently in the context of a whole virus infection. One possibility to explain these phenomena is, as previously discussed with F91A, that M2 and M2 CT mutants are interacting with SUMO through a SUMOylated viral or cellular protein whose localisation and interactions with M2 are altered during virus infection. M2 is well publicised to interact with M1 (McCown and Pekosz, 2006; Benjamin J Chen *et al.*, 2008), and M1 is known to be covalently SUMOylated at K242 and this modification is important for viral budding (Wu, Jeng and Lai, 2011a). This may point to a necessity of M1 being present with M2 in the context of viral infection in order for an efficient and relevant M2-SUMO interaction to occur. In addition, the PLA is unable to distinguish between direct protein binding and close protein association in the form of a protein complex, thus increased M2 SUMO interactions seen by PLA in the SIM mutants V92S and I94M may not directly represent the retention of SUMO binding but M2's association in a tight protein complex with SUMOylated proteins.

M2 interacts and co-immunoprecipitates with SUMO in transient plasmid-based expression, and this is also the case with the with M2 CT mutant F91A (ΔLIR) as predicted bioinformatically and seen in the Western blot (Figure 10, page 51) and in PLA (Figure 11, page 53). However, when viruses containing CT mutations of M2 are generated and used to study the M2 SUMO interaction (Figure 12, page 53), an insignificant change in SUMO interaction is seen with the mutants V92S and F91A as compared to the wild type, with a dramatic increase in SUMO interaction with the I94M mutant (ΔSIM ΔLIR). What has not been investigated is the potential for the CT mutations to cause a conformational change in the M2 protein that may alter association with viral and cellular proteins, affecting the PLA results. One further possibility is that the CT mutations, specifically I94M in the context of viral infection, causes a conformational change in the whole M2 protein, exposing a different site to potential SUMO interaction or SUMOylation. Table 1 indicates other residues in the full length M2 which may be either SUMO interacting regions,

or lysine residues capable of covalent SUMOylation. However, this is less likely as activity of an alternate SIM motif would likely be noticeable in the plasmid-based co-immunoprecipitation assays. IAV infection is known to increase global SUMO expression by the host cell (Pal *et al.*, 2011; Domingues *et al.*, 2015), and this, together with changes in interactions with potentially SUMOylated viral proteins may provide the environment for a stronger SUMO positive signal as seen by PLA.

4.03 Mutations in the M2 CT can have a nuanced influence on viral morphology

Data specifically regarding the M2 CT mutant F91A is in agreement in reference to previous literature (Beale, Wise, Stuart, Benjamin J Ravenhill, *et al.*, 2014) that the inferring loss of the LIR in the F91A mutant, behaves as the F91S mutant generated by Beale et al in 2011. To further this, we used viruses containing not only the F91A mutation, but also other CT mutations shown bioinformatically and transiently to interact, or not interact, with SUMO and LC3. From the immunofluorescence microscopy in Figure 18 (page 64), we can see an indication of the behaviour of this mutant in regards to protein localisation and virus morphology. For all mutants except the previously reported spherical F91A mutant, budding of filamentous virus is seen clearly seen stained with anti-Udorn antibody, and with M2 aggregating at the plasma membrane and at cellular junctions. A considerable amount of SUMO is also present in the viral filaments and at sites of virus budding where the positive staining of Udorn proteins is most prominent. Notably, SUMO seems to co-localise weakly with M2. A likely explanation for the prevalence of SUMO at the sites of budding is not the M2-SUMO interaction but the SUMOylation of M1 (Wu, Jeng and Lai, 2011b), which being the most abundant viral protein, will incorporate a significant amount of SUMO protein in to budding virions. The nucleoprotein, NP, is also known to be SUMOylated (Han *et al.*, 2014), and as the anti-Udorn antibody used in Figure 18 (page 64) will detect both M1 and NP, it is not possible to discern which viral protein is carrying SUMO in to the budding virion. This may also explain the difference in resulting SUMO interactions in live virus infections versus transiently expressed M2 and M2 CT mutants, through the aforementioned possibility of an M1-M2 interaction mediated by SUMO, and the global SUMO expression increase upon IAV infection. However, in the F91A mutant, this is not the case – distinct M2-SUMO puncta are

clearly visible perinuclearly. This behaviour of SUMO is not visible in the other mutants or the wild type, and requires speculation on two fronts; firstly, the localisation of F91A being perinuclear and not at the plasma membrane, and secondly the nature of the seemingly significant interaction between F91A and SUMO. F91A is thought to lose the interaction with LC3 and prevent LC3 recruitment to the plasma membrane; however, here we see F91A directly affecting M2 localisation, suggesting that M2-LC3 interactions may also affect M2 trafficking and viral assembly. In regards to the F91A SUMO interaction, it is possible that the altered M2 localisation changes M1 association with M1 or NP and thus the visual colocalisation between M2 and SUMO may be more obvious.

4.04 Speculation on a role for the highly conserved residue H90

To further understand what may be influencing the M2 SUMO interaction, a further residue of note in the M2 CT was identified – H90. As seen in Figure 9 (page 49), H90 along with F91 is considerably well conserved, and such a synergistic reasoning behind this can be proposed, bringing together SUMO, LC3 and the interplay between the three – histidine protonation. Histidine has the ability to be protonated at low pHs (Mitchell and King, 2011), such as those found in the Golgi apparatus (Schapiro and Grinstein, 2000), and moreover, the protonation of histidine in the context of viral infection has been speculated as a determinant for fusion of IAV in the acidic endosome, albeit through histidine residues in HA (Mueller *et al.*, 2008). That being said, the distinction between a role for H90 protonation must be made between early and late infection. The barrier to the idea that H90 may be protonated in late infection, i.e during M2 trafficking post translation, is that M2 retains its ion channel ability during Golgi transition. M2 is able to equilibrate the pH over the Golgi with the cytoplasm, thereby neutralising intra-Golgi pH (Sakaguchi, Leser and Lamb, 1996). The raising of trans-Golgi pH slows down the trafficking of viral and cellular proteins through the Golgi (Henkel *et al.*, 2000)(Alconada, Bauer and Hoflack, 1996; Disbrow, Hanover and Schlegel, 2005; De Jong *et al.*, 2006), and is important for viral replication by preventing premature low pH triggering of HA (Skehel *et al.*, 1982; Robert W. DomsS, Ari Heleniuss, 1984). We tested the potential role for the protonation of H90 during virus assembly, and how this may affect M2-SUMO interactions, by using ammonium chloride to neutralise endosomal and Golgi pH. In both the presence and absence of ammonium chloride, no difference in PLA foci ratio was seen

between the H90S mutant (unprotonatable) and the wild type. This demonstrates that any effect of H90 on M2-SUMO interaction, at least, does not occur in the endosomal or budding stages of IAV infection, and that if H90 does play a role here, it is possible that this is during viral entry.

4.05 M2 CT mutations may affect viral entry

Recently, it has been reported that the ability of M2 to be ubiquitinylated plays a crucial role in the packaging of progeny virions, in order for efficient continuation of infection (Su *et al.*, 2018). The study notes how an M2-K78R mutation causes the virus to package inefficiently, with fewer vRNPs incorporated in to the newly forming virions, induced autophagy and apoptosis earlier than a wild type virus, and interacted less with M1, though the mechanism of this effect was not defined.

The ability of M2 to bind Ubiquitin is known to be key in the uncoating and subsequent release and trafficking of vRNPs. M2 and other viral components, through the ability to bind and carry ubiquitin in to budding virions, can exploit the aggresome machinery through HDAC6 to facilitate viral uncoating (Banerjee, Miyake, Philip Nobs, *et al.*, 2014; Su *et al.*, 2018). The ubiquitin chains carried by M2 and incorporated in to budding viruses may play a role in triggering a HDAC6-dependent pathway, which in turn recruits cellular machinery which is hijacked by IAV, facilitating viral uncoating and allowing the localisation of vRNPs to the nuclear membrane for import. It is not known if other ubiquitin-like molecules, such as SUMO and LC3, can also trigger HDAC6 and enhance viral uncoating. To study if this Ubiquitin – HDAC6 interaction may have been mediated by the ability of M2 CT to bind and interact with SUMO and / or LC3, immunofluorescence microscopy was employed to analyse viral uncoating, as seen in Figure 26 (page 89). The images appear to show no distinct relocalization of HDAC6 in relation to the mock infection, and this may point to inconsistencies in the assay itself; however some colocalisation of HDAC6 is seen with M1 in all samples suggesting that all the M2 CT mutants may retain the ability to recruit HDAC6 and uncoat, which is supported by the near normal level of virus replication seen with all the mutants.

To further investigate entry and uncoating, vRNP nuclear trafficking was then assessed following infection for one or five hours and visualisation of vRNPs in the cytoplasm and nucleus, as seen in Figures 24 (page 83) and 25 (page 86). At one HPI (Figure 25, page 86), vRNPs are present in the cytoplasm of all strains with a

minimal amount of vRNP in the nucleus. However, this is more dramatic when visualised at five HPI when new vRNPs have begun synthesis. Interestingly, V92S localises its vRNP to the nucleus far quicker than the other mutants (Figures 24, page 83 and 25, page 86), and in Figure 26 (page 89) it is also noted that the fluorescence signal in the M1 channel is brighter in comparison to the other mutants. This evidence suggests that the initial stages of infection (from entry to vRNP delivery to the nucleus) happen at a faster rate in V92S than in the wild type, with the other mutants falling in a range – with H90S being the slowest, though at five HPI V92S appears to have more vRNPs retained in the nucleus while the other mutants appear to have begun nuclear vRNP export. V92S causes a loss of SIM functionality, and a comparable interaction with LC3 compared to wild type M2, as predicted bioinformatically (Table 3, page 50) and confirmed via co-immunoprecipitation (Figure 10, page 51). Interestingly, V92S also displays a large amount of NP in budded virions, second only to I94M (Figure 22, page 76). One possible theory may be a relationship between vRNP expression levels, affected by entry and uncoating timing, and M2-M1-NP-SUMO trafficking and interactions in the late stages of infection during viral assembly and budding. As previously discussed, M1 is known to interact with M2 through its cytoplasmic tail (B. J. Chen *et al.*, 2008), and M1 is known to interact with NP through its middle domain (Noton *et al.*, 2007). NP is also believed to be SUMOylated (Pal *et al.*, 2011), along with M1 knowingly being SUMOylated at K242 (Wu, Jeng and Lai, 2011b). It is possible that the M2 CT can freely interact with SUMOylated M1 and NP during IAV assembly at the site of budding, and this would be affected by M1, NP and vRNP expression levels and could be necessary in order to efficiently incorporate these proteins in to the budding virion.

However, these results also raise the question of how mutations in the ability of the M2 CT to interact with SUMO are affecting viral entry and uncoating if not through HDAC6 interaction. Firstly, it is unlikely that initial infection of a host cell is affected by a mutation in the M2 CT. Viral attachment to a cell is mediated through HA binding sialic acid residues on the plasma membrane, after which an endocytosis event is triggered. M2 does not play a role here, and furthermore, the CT is sequestered within the core of the virus and does not become exposed until after the viral uncoating event in the acidified endosome. Potentially, the mutations within the CT of M2 may cause a conformational change within the full length of

M2 itself, either causing a disruption of tertiary protein structure, or the quaternary structure, affecting the ability of M2 to homotetramerise. This scenario is unlikely, as the probable outcome of a large-scale disruption of the tertiary or quaternary structures of M2 would likely result in an inability of IAV to propagate, through disruption of the ion channel activity, or the vital interactions with other viral proteins, or both. Therefore, it is likely that another process during the later stages of uncoating within the endosome – potentially the dissolution of the viral core and the release of vRNPs – is affected by these M2 CT mutations. This is supported by the observation that the unprotonatable M2 CT mutant H90S appears to be significantly delayed in vRNP kinetics. It is possible that H90 protonation facilitates the dissolution of M1-M2 association in the entering virion, facilitating uncoating and vRNP nuclear entry, though this was not investigated in the current study.

4.06 SUMO binding and vRNP trafficking

M2 is ubiquitinated at K78 and mutation of this site affects both autophagy and genome packing (Su *et al.*, 2017). Owing to the structural similarities of SUMO to ubiquitin, and the fact that this ubiquitin binding reported by Su *et al.* occurs in the cytoplasmic tail, close to the LIR/SIM motifs studied in this body of work, a role for SUMO and M2 during viral packaging, but not during initial infection is plausible. One theory is that SUMO interaction within the M2 CT may help stablise M2, possibly through SIM binding of ubiquitin at K78, within the same or neighbouring monomers of the M2 tetramer. Alternatively, the SUMO interaction may facilitate M2-M1 interaction and vRNP recruitment via binding of the M2 CT to SUMOylated M1.

M2 definitively interacts with the matrix protein, M1, through residues 71 to 97, and mutations within this region also affect the efficient incorporation of vRNPs in to progeny virions (B. J. Chen *et al.*, 2008). M1 is known to be covalently SUMOylated at K242, and mutations of this residue cause a drop in viral titre, and an accumulation of all viral proteins, and viral RNA, within the host cell (Wu, Jeng and Lai, 2011b). Having confidence that the interaction of the M2 CT with SUMO is not covalent in nature, a possible relationship between the accumulation of vRNPs in infection with M2 CT mutations could be that the M2 CT interacts with the covalently bound SUMO in M1 to stabilise the M2-M1-vRNP complex. In

studying the localisation of vRNP staining in Figure 24 (page 83), M2 CT mutant V92S (lacking SUMO interaction) and mutant I94M (lacking SUMO and LC3 binding) both cause an accumulation of vRNP within the cell nucleus, whereas the wild type virus does not. Furthermore, when M1 is stained in early infection, V92S displays far more positive cytoplasmic staining for M1 than other mutants. Thus, the M2-M1-vRNP interaction may be partly mediated though SUMO binding and affect vRNP trafficking and thus virus assembly and budding. Interestingly, in the case of I94M which causes a loss of both LC3 binding and SIM functionality, this mutation appears to induce a reversion of the virus to behaviour more akin to WT A/Udorn/72 H3N2. This is pertinent in the morphology of the budding virus (Figure 18) and the localisation of vRNPs (Figure 23, page 79), and could suggest that the functionality of IAV requires either both an intact LIR and SIM in the M2 CT, or neither, but never only one.

Results from this project propose a SUMO interaction motif (SIM) within the M2 cytoplasmic tail (residues 92-96) which overlaps with a known LC3 interacting region (LIR). Tables 2 and 3 (page 50) show that where mutations of the cytoplasmic tail of M2 enable an interaction with either LC3 or SUMO the interaction of the other is hindered or abolished. Preliminary mass spectroscopy has shown that in addition to the known binding partners of M2 there are many other proteins which can interact with the cytoplasmic tail of M2 which may provide IAV with ways of circumventing autophagy, enhancing replication, affecting viral budding and trafficking of the virus within the cell. The short cytoplasmic tail of M2 residues 82-97 seem to have a remarkable propensity to interact with many proteins which may be due to the lack of tertiary structure of these residues.

In the data presented here, a further attempt to elucidate and understand further the role of M2 in the viral lifecycle, and in the ability of this small protein to influence cellular activity, has been undertaken. Some further study in to the role of M2 and viral morphology may allow a link between the findings here of a SIM in the CT of M2, and the importance which M2 plays in viral genome packaging (Watanabe *et al.*, 2001; McCown and Pekosz, 2005). M2 is required for efficient NP and RNA packaging, and deletion of a portion of the CT causes a drop of four times in the ability of the virus to form competent particles, and of the particles successfully formed, a three log drop in infectivity. These phenomena show that the activity of

M2 in viral replication is far more than ion channel activity alone. M2 is characterised by ion channel activity, however we are only now, through this body of work and others relating to structural importance, uncovering essential roles for M2 beyond this.

4.07 Further speculations on modifications of the M2 CT

Low levels of phosphorylation of residues 82,89 and 93 has been reported by Holsinger et al (Holsinger, et al., 1995) to occur within the CT of M2. Holsinger et al have also proposed that M2 contains the phosphorylation motif for S82 Casein kinase I, S89 Glycogen synthase kinase-3 and Mammary gland casein kinase for S93. Phosphorylation of M2 residues 87-97 is of particular interest as mass spectroscopy has shown that Casein Kinase II interacts with M2 (Table 4, page 59), however the interaction was not observed through co-immunoprecipitation and not pursued further here, though it is possible there is an association that can regulate M2 phosphorylation to perform unknown functions.

The data presented in this work has failed to show interaction of wild type M2 with SUMO in the context of viral infection by co-immunoprecipitation, that being said there is a repeatable and significant M2 interaction with SUMO in transfected cells and when assessed by PLA during virus infection. The first explanation for these differing results is that the levels of M2 expression during transient plasmid-based expression may be considerably higher than the levels which would be observed in even a strong infection. IAV virions typically contain between two and five tetrameric M2 assemblies, roughly ten to 20 individual M2 molecules (Zebedee and Lamb, 1988). The greater abundance of M2 during transient expression, as the initial experiments herein were, may simply allow for a dose dependent interaction of M2 with SUMO through the SIM in the M2 CT. Secondly, viral-viral protein interactions must be considered. M2 has a wide and varied role during infection, packaging of the genome, uncoating and progeny virus release from host cells. M2 is known to bind to M1 through the cytoplasmic tail, and that disruptions of residues in the M2 CT which interfere with M1-M2 binding cause virion instability (Iwatsuki-Horimoto *et al.*, 2006). Furthermore, the M2 CT is known to bind vRNP, and is essential for recruitment of vRNP to the site of budding at the plasma

membrane, in order to facilitate viral packaging (B. J. Chen *et al.*, 2008). As opposed to covalent linkage of SUMO to the CT of M2, a weaker SUMO interaction is proposed here. SUMO is known to covalently bind or non-covalently interact with other IAV proteins, such as M1. M1 is known to be covalently SUMOylated at K242 (Wu, Jeng and Lai, 2011a), and mutation either of M1-K242 or siRNA knockdown of the SUMO conjugating enzyme UBC9 in target cells causes a wide range of viral budding and packaging discrepancies. For example, M1-K242E results in a 20-fold decrease in virion production compared to wild type, whilst also causing a considerable accumulation of vRNP within the cell. As an M1-vRNP complex is known to interact with M2 (McCown and Pekosz, 2006) a role for M2 interacting with the SUMO bound to M1 is presented. For example, in the context of viral infection the interaction of M2 with other viral proteins, namely M1 and vRNP, and the rate of turnover and trafficking of M2 within an infected cell, may simply not allow a free SUMO (i.e. not bound to M1) interaction with M1. In transient expression however, the SIM in the M2 CT, the far higher abundance of transiently expressed M2, and the lack of other viral protein influences may allow the interaction of sufficient M2 in a strong enough interaction to co-immunoprecipitate.

As previously mentioned, SUMOylation and SUMO interacting partners play a crucial role within the cell. Related closely structurally, but sharing only around 18% sequence homology with ubiquitin (Tatham *et al.*, 2003; van Wijk, Müller and Dikic, 2011), but not marking for degradation, SUMOylation is involved in packaging and transport of a multitude of cellular proteins. The first identified SUMO binding partner was the Ran GTPase-activating protein RanGAP1, which is a pivotal regulatory partner of the Ras-like GTPase Ran (Lee *et al.*, 1998). The latter is a controller of export from the nucleus to the cytoplasm, and importantly has shown only to interact with SUMOylated RanGAP1 and not free RanGAP1 (Mahajan *et al.*, 1998). This was the first reported requirement of SUMOylation for a native state cellular protein to perform its role. This had implications for the understanding of SUMO at a deeper level, and is pertinent to this body of work in understanding how SUMOylation and/or SUMO interactions may influence viral protein folding, trafficking or localisation through either direct conjugation (in the case of M1) or interaction (M2). What we speculate in regards to M2, is that SUMO

is acting as a bridging protein between SUMOylated proteins, and the SIM of the M2 CT.

The identification of a SIM within M2 may allow SUMOylated IAV proteins (M1, NS1, NS2, PB1 and NP) to interact with M2 through this novel interaction. M1 has been identified to interact with M2 most specifically through residues 71-76. H90 of M2 is a residue which is highly conserved and whose function has not been determined. Protonation of H90 could occur during endosomal/lysosomal acidification or within an autophagosome, which could change the conformation or accessibility of the cytoplasmic tail and influence SIM, phosphorylation, and the other interaction of the cytoplasmic tail. Chen *et al.*, (2008) performed triple alanine mutations of M2 residues 89 – 91 in order to study how this would affect M1 incorporation in to budding virions. This mutation showed a decreased amount of M1 incorporation in both virus and VLPs, and packaging of a vGFP pseudogene, though the mutation did not significantly affect virus growth and then effect on the M1-M2 interaction was not assessed. This study demonstrated that M1 and vRNP binding varies along the length of M2, and residues 86-91 may exert a subtler effect than residues 71-76 which are most important for the interaction between M1 and M2. This subtle effect may be a result of LIR and SIM. However, it is unknown as to whether the 88 – 91 triple alanine mutation would destroy the SIM, though it would interfere with LIR and with H90 protonation.

4.08 A novel M segment splice variant, M42

As studied in figures 27 and 29, the behaviour of the alternative M segment splice variant, M42, displays distinct localisation differences, as well as an effect on LC3 colocalisation and vimentin condensation. Retaining the same ion channel activity and CT as WT M2, M42 displays a different antigenic ectodomain, to which the 14C2 antibody does not react (Wise *et al.*, 2012). Whilst these phenomena require further investigation, we can speculate on the potential for the apparent slowing of M42 trafficking through the Golgi causing LC3 aggregation, and vimentin condensation and aggresome formation. It is possible that the formation of a clear vimentin cage in figure 29 (page 103) may be containing the stalled M42, and that the considerable LC3 aggregation with M42 may be forming part of the autophagy process.

4.09 Speculation on the role of the M2 CT SIM in IAV disease

The presence of a SIM within M2, would allow IAV to interact with SUMOylated proteins which could contribute towards disease and pathogenicity of the virus. Studies have suggested that IAV may have links to acute cardiac events such as myocardial infarction (Warren-Gash, Smeeth and Hayward, 2009). An interesting example of this could be an interaction between M2 and SR Ca^{2+}ATPase 2a (SERCA2a). SERCA2a is an ATPase which is critical for Ca^{2+} re-uptake during excitation-contraction coupling, as reduced activity of SERCA2a is a hallmark of heart failure. SERCA2a has been shown to be SUMOylated at lysine 480 and 585 which is essential for preserving its ATPase activity and stability (Kho *et al.*, 2011). Levels of both SUMO and SERCA2a have been shown to be greatly decreased during heart failure. Kho *et al* have also shown that SUMO restitution by adeno-associated virus-mediated gene delivery maintained the abundance of SERCA2a and improved cardiac function in mice. Preliminary mass spectroscopy in this body of work has shown a V-type proton ATPase subunits catalytic/B/C1/E1/D/G1/H and transcriptional endoplasmic reticulum ATPase (Table 4, page 59) to be interactors of M2 in HEK-293T cells. An interaction of SUMOylated SERCA2a with M2 though its SIM could prevent the function of SERCA2a or M2 could sequester SUMO upon infection of cardiac cells, so reducing levels of SUMO and inducing cardiac stress during viral infection.

SUMOylation has been shown to control the NF-KB pathway by modification of the inhibitory molecule IκBα (Mabb and Miyamoto, 2007), IKK subunit γ/NEMO (Ulrich, 2005) and the p52 precursor p100 (Vatsyayan *et al.*, 2008). IκBα is SUMOylated at K21, with ubiquitin also competing for binding at this residue. Polyubiquitination of IκBα depends on IKK-mediated phosphorylation of residues 32 and 36 for recognition by E3 ubiquitin ligase. In addition to independent SUMOylation and ubiquitination, ubiquitin forms hybrid chains on IκBα which increase the susceptibility of IκBα to be degraded by the 26s proteasome. IκBα serves as an example of the relationship between SUMO, ubiquitin and phosphorylation which can be applied to M2, as ubiquitin has been shown to bind the M2 CT by fluorescence polarisation. This interaction of ubiquitin could be through a UBD, or due to the sequence homology which SUMO and ubiquitin share. SUMO/ubiquitin chain formation within the context of IAV viral infection also requires investigation.

Finally, M2 through its SIM may be able to modulate apoptosis via an interaction with HSP90, which mass spectroscopy analysis conducted during this investigation has identified as interacting with M2 (data not shown). Hsp90 has been reported to be SUMOylated (Preuss *et al.*, 2015) and as such may be able to interact with M2 through its SIM. Hsp90 has a vast array of interacting partners which affect apoptosis, therefore speculation as to an M2 interaction with Hsp90 may be multi-faceted. Hsp90 is involved in forming a complex with IKKγ/IKKβ/CDC37 (Hinz *et al.*, 2007), interaction with kinases IKKβ/Akt/Src (Sato, Fujita and Tsuruo, 2000; Koga *et al.*, 2006), and inhibition of Apaf-1 and pro-apoptotic BID (Pandey, 2000). However a deficiency in autophagy (using ATG7 KO mouse embryonic fibroblasts) has been shown to impair Hsp90 induction and aberrant mTOR signalling in response to IAV infection (Liu *et al.*, 2016). ATG7 is the E1-like activating enzyme involved in ubiquitin-like systems (including SUMOylation) required for cytoplasm to vacuole transport and activates ATG8 for their conjugation with phosphatidylethanolamine (Schulman and Harper, 2009). ATG7 is required for autophagic cell death induced by caspase-8 inhibition (Yu *et al.*, 2004). Cleaved caspase-8 during conditions of cytoprotective autophagy co-localises with LC3-II and LAMP2 (Hou *et al.*, 2010). This suggests that there may be a relationship between SUMO, caspase-8, Hsp90, LC3 and the cytoplasmic tail of IAV M2 that could play a significant role in the regulation of IAV cell death.

4.1 USING LAIV STRAINS TO INVESTIGATE MORPHOLOGY

A further investigation in to the viral factors that regulate the morphology of budding influenza viruses was undertaken using viruses designated as vaccine strains provided by MedImmune. The LAIV used in to prepare the FluMist® nasal spray vaccine is prepared using a MDV backbone based on the A/Ann Arbor/6/60 strain of IAV (Buonagurio *et al.*, 2006), whereby only the surface antigens HA and NA are swapped seasonally, to invoke the desired immunogenicity relevant to yearly circulating influenza A virus strain. Strains are designated according to the original isolated virus (e.g. Bolivia, South Dakota, Uruguay and Victoria). Morphology of LAIVs can therefore only be influenced by the differing HA and NA proteins expressed. HA and NA have a clear effect on the appearance of viral filaments, producing elongated and robust filamentous budding in the Bolivia and South Dakota strains, with attenuated production in the Uruguay and Victoria

strains. Moreover, atypical organisation of viral filaments can be seen in some of the vaccine strains, such as accumulations of budding IAV, Archetti bodies, and positively staining cell-to-cell protrusions. The localisation of M2 (permiabilised samples) is distinctly nuclear in the Bolivia strain, more cytoplasmic in the South Dakota strain, and M2 is poorly expressed overall in the Uruguay strain. It is known that the HA and NA proteins alone from certain IAV strains can drive both spherical VLP budding (Chen *et al.*, 2007) and filamentous VLP budding (Chlanda, Schraidt, Kummer, Riches, Oberwinkler, Prinz, Kräusslich and John A. G. Briggs, 2015), with filamentous budding significantly enhanced through the addition of filamentous M segment proteins, M1 and M2. It is important to note the 'cold adapted' nature of the LAIV strains, as this may play an important role in morphology. The studies conducted herein were undertaken at 37°C, with the LAIV being cold adapted to 33°C, the temperature of the upper airway and site of replication of the LAIV (Harper *et al.*, 2003). Cold adaptation in vaccine strains is achieved through proprietary modification of the internal genes, and subsequent selection through passaging at lower temperatures (Maassab and Bryant, 2007). However, cold adaptations are also seen in the surface proteins, most notably HA (Lee *et al.*, 2016), and that HA units within LAIV strains as compared to wild type avian strains are less thermostable (Christopher D. O'Donnell, Leatrice Vogel, Yumiko Matsuoka, Hong Jin, 2014). The effect of changing temperature has been investigated in regards to its ability to alter its fusogenicity in certain strains (Schrauwen *et al.*, 2016), though was not further investigated here.

HA and NA have been known for some time to have significant effects on the morphology of budding IAV, and truncations of one or both cytoplasmic tail regions of these proteins cause a change in particle morphology (Jin *et al.*, 1997). Although the HA from the LAIV strains used in this study are full length, there are many differences in the CT region of HA, speculated by Jin *et al.* to be responsible for the alterations in morphology through M1 interactions. Further literature investigating the filamentous morphology of IAV postulated that M1 is the major driving force of filamentous budding (Elleman and Barclay, 2004), and it is well publicised that manipulations of the M segment between solely spherical IAVs and filamentous producing IAVs can also influence morphology (Noton *et al.*, 2007; Bruce, Digard and Stuart, 2010). Point mutations discussed and investigated in this body of work, as well as others, also describe mutations in the M2 CT as causing a

attenuation of filamentous virus production (McCown and Pekosz, 2006; Beale, Wise, Stuart, Benjamin J. Ravenhill, *et al.*, 2014). It is therefore a possibility that introducing HA to a mismatched backbone MDV can cause subtle disruptions in the HA CT interactions with M1 which may affect viral morphology. However, the different HAs also affect autophagy induction and M2 localisation, which may further affect the assembly and budding of filamentous virions. As already speculated, the M1 – M2 interaction may be mediated through a SIM in the M2 CT interacting with covalently SUMOylated M1 K242 to efficiently package and bud progeny virions. Whilst mutations in the antigenic ectodomain of HA are necessary for efficient vaccine production, even small changes in the sequence of HAs from various LAIV strains may have a significant effect on the efficiency and morphology of IAV budding and genome packaging, though modulation of autophagy and M2 trafficking.

4.2 IN CONCLUSION

Understanding the influenza A virus and its nuances of infectivity, replication, interactions and morphology continues and will continue to be both a source of frustration and great intrigue in equal measure. The reliability of annual resurgent disease, and its social, economic and personal impact must continue to serve as the main motivators in attempting to further understand the best ways to confront influenza virus disease. The eventual goal being a universal influenza vaccine, providing very high levels of protection from all IAV strains.

In this study, we have investigated the lifecycle of IAV, through the interactions of the cytoplasmic tail of the matrix protein 2. This has been studied through both expanding on previous literature relating to interaction of M2 with the autophagy protein LC3b, and demonstration of a novel ability of M2 to interact with the small ubiquitin-like modifier, SUMO. Experimentally, this has been achieved through the production of transiently expressible constructs of M2 CT mutants, and viruses produced using a reverse genetics approach which express these same M2 CT mutations. Using techniques such as co-immunoprecipitation, proximity ligation assay, and confocal microscopy, we have presented data alluding to these M2 CT mutations changing the morphology of the budding virus, altering the distribution of vRNPs, and changing the localisation of SUMO.

Furthermore, using LAIV strains, we have been able to analyse viral morphology in IAVs expressing different HA surface proteins used for producing seasonal influenza vaccines. Together these results suggest that the M2 CT broadly interacts with ubiquitin-like molecules. These interactions are affected by a variety of cellular and viral proteins and are important for proper M2 and vRNP trafficking, viral assembly and virion morphogenesis.

It is hoped that the investigations conducted for this thesis will provide the basis for a continuation of the study of M2 and other viral proteins in their contribution to viral morphology, and their interactions with cellular proteins and processes.

REFERENCES

Adamson, A. L. and Kenney, S. (2001) ‘Epstein-Barr Virus Immediate-Early Protein BZLF1 Is SUMO-1 Modified and Disrupts Promyelocytic Leukemia Bodies’, *Journal of Virology*, 75(5), pp. 2388–2399. doi: 10.1128/JVI.75.5.2388-2399.2001.

Alconada, A., Bauer, U. and Hoflack1 ’, B. (1996) ‘A tyrosine-based motif and a casein kinase 11 phosphorylation site regulate the intracellular trafficking of the varicella-zoster virus glycoprotein 1, a protein localized in the trans-Golgi network’, *The EMBO Journal*, 1522(22), pp. 6096–6110. doi: 10.1002/j.1460-2075.1996.tb00998.x.

Auewarakul, P. *et al.* (2007) ‘An Avian Influenza H5N1 Virus That Binds to a Human-Type Receptor’, *Journal of Virology*, 81(18), pp. 9950–9955. doi: 10.1128/JVI.00468-07.

Banerjee, I., Miyake, Y., Nobs, S. P., *et al.* (2014) ‘Influenza A virus uses the aggresome processing machinery for host cell entry.’, *Science (New York, N.Y.)*. American Association for the Advancement of Science, 346(6208), pp. 473–7. doi: 10.1126/science.1257037.

Banerjee, I., Miyake, Y., Philip Nobs, S., *et al.* (2014) ‘Influenza A virus uses the aggresome processing machinery for host cell entry’, *Science*, 346(6208), pp. 473–477. doi: 10.1126/science.1257037.

Barman, S. *et al.* (2004) ‘Role of Transmembrane Domain and Cytoplasmic Tail Amino Acid Sequences of Influenza A Virus Neuraminidase in Raft Association and Virus Budding’, 78(10), pp. 5258–5269. doi: 10.1128/JVI.78.10.5258.

Basu, A. *et al.* (2011) ‘Direct imaging of pH1N1 2009 influenza virus replication in alveolar pneumocytes in fatal cases by transmission electron microscopy’, *Journal of Electron Microscopy*, 60(1), pp. 89–93. doi: 10.1093/jmicro/dfq081.

Batishchev, O. V. *et al.* (2016) ‘pH-Dependent Formation and Disintegration of the Influenza A Virus Protein Scaffold To Provide Tension for Membrane Fusion’, *Journal of Virology*, 90(1), pp. 575–585. doi: 10.1128/JVI.01539-15.

Beale, R., Wise, H., Stuart, A., Ravenhill, B. J., *et al.* (2014) ‘A LC3-interacting motif in the influenza A virus M2 protein is required to subvert autophagy and maintain virion stability.’, *Cell host & microbe*. Elsevier, 15(2), pp. 239–47. doi:

10.1016/j.chom.2014.01.006.

Beale, R., Wise, H., Stuart, A., Ravenhill, B. J., *et al.* (2014) 'A LC3-interacting motif in the influenza A virus M2 protein is required to subvert autophagy and maintain virion stability', *Cell Host and Microbe*. Elsevier Inc., 15(2), pp. 239–247. doi: 10.1016/j.chom.2014.01.006.

Belshe, R. B. (2005) 'The Origins of Pandemic Influenza — Lessons from the 1918 Virus', *New England Journal of Medicine*, 353(21), pp. 2209–2211. doi: 10.1056/NEJMp058281.

Bies, J., Markus, J. and Wolff, L. (2002) 'Covalent attachment of the SUMO-1 protein to the negative regulatory domain of the c-Myb transcription factor modifies its stability and transactivation capacity', *Journal of Biological Chemistry*, 277(11), pp. 8999–9009. doi: 10.1074/jbc.M110453200.

Bos, T. J., Davis, A. R. and Nayak, D. P. (1984) 'NH2-Terminal Hydrophobic Region of Influenza Virus Neuraminidase Provides the Signal Function in Translocation', *Proceedings of the National Academy of Sciences*, 81(8), pp. 2327–2331. doi: 10.1073/pnas.81.8.2327.

Bosch, F. X. *et al.* (1981) 'Proteolytic cleavage of influenza virus hemagglutinins: primary structure of the connecting peptide between HA1and HA2determines proteolytic cleavability and pathogenicity of avian influenza viruses', *Virology*, 113(2), pp. 725–735. doi: 10.1016/0042-6822(81)90201-4.

Both, G. W. *et al.* (1983) 'Antigenic drift in influenza virus H3 hemagglutinin from 1968 to 1980: multiple evolutionary pathways and sequential amino acid changes at key antigenic sites.', *Journal of virology*. American Society for Microbiology Journals, 48(1), pp. 52–60. Available at: http://www.ncbi.nlm.nih.gov/pubmed/6193288 (Accessed: 22 October 2018).

Boulo, S. *et al.* (2007) 'Nuclear traffic of influenza virus proteins and ribonucleoprotein complexes', *Virus Research*, 124(1–2), pp. 12–21. doi: 10.1016/j.virusres.2006.09.013.

Bourmakina, S. V. and García-Sastre, A. (2003) 'Reverse genetics studies on the filamentous morphology of influenza A virus', *Journal of General Virology*, 84(3), pp. 517–527. doi: 10.1099/vir.0.18803-0.

Bouvier, N. M. and Palese, P. (2008) 'The biology of Influenza viruses', *Vaccine*, 12(26), pp. D49–D53. doi: 10.1002/ejoc.201701499.

Brown, I. H. (2000) 'The epidemiology and evolution of influenza viruses in pigs', *Veterinary Microbiology*, 74(1–2), pp. 29–46. doi: 10.1016/S0378-1135(00)00164-4.

Bruce, E. A. *et al.* (2009) 'Budding of filamentous and non-filamentous influenza A virus occurs via a VPS4 and VPS28-independent pathway', *Virology*. Elsevier

Inc., 390(2), pp. 268–278. doi: 10.1016/j.virol.2009.05.016.

Bruce, E. A., Digard, P. and Stuart, A. D. (2010) 'The Rab11 pathway is required for influenza A virus budding and filament formation.', *Journal of virology*, 84(12), pp. 5848–5859. doi: 10.1128/JVI.00307-10.

Buonagurio, D. A. *et al.* (2006) 'Genetic stability of live, cold-adapted influenza virus components of the FluMist®/CAIV-T vaccine throughout the manufacturing process', *Vaccine*, 24(12), pp. 2151–2160. doi: 10.1016/j.vaccine.2005.11.007.

Burleigh, L. M. *et al.* (2005) 'Influenza A Viruses with Mutations in the M1 Helix Six Domain Display a Wide Variety of Morphological Phenotypes', *Journal of Virology*, 79(2), pp. 1262–1270. doi: 10.1128/JVI.79.2.1262-1270.2005.

Burnet, B. Y. F. M. (1951) 'Genetic Approach to Variation in Influenza Viruses', *J. gen. Microbiol*, (1951), pp. 59–66. doi: 10.1021/ja9706514.

Burnet, F. M. and Lind, P. E. (1957) 'Studies on filamentary forms of influenza virus with special reference to the use of dark-ground-microscopy', *Archiv für die gesamte Virusforschung*, 7(5), pp. 413–428. doi: 10.1007/BF01241959.

Calder, L. J. *et al.* (2010) 'Structural organization of a filamentous influenza A virus.', *Proceedings of the National Academy of Sciences of the United States of America*, 107(23), pp. 10685–90. doi: 10.1073/pnas.1002123107.

Chakrabarti, S. R. *et al.* (2000) 'Posttranslational modification of TEL and TEL/AML1 by SUMO-1 and cell- cycle-dependent assembly into nuclear bodies', *Proc.Natl.Acad.Sci.U.S.A*, 97(24), pp. 13281–13285. doi: 10.1073/pnas.240315897.

Chang, T. H. *et al.* (2009) 'Ebola Zaire virus blocks type I interferon production by exploiting the host SUMO modification machinery', *PLoS Pathogens*, 5(6). doi: 10.1371/journal.ppat.1000493.

Chen, B. J. *et al.* (2007) 'Influenza virus hemagglutinin and neuraminidase, but not the matrix protein, are required for assembly and budding of plasmid-derived virus-like particles.', *Journal of virology*, 81(13), pp. 7111–7123. doi: 10.1128/JVI.00361-07.

Chen, B. J. *et al.* (2008) 'The influenza virus M2 protein cytoplasmic tail interacts with the M1 protein and influences virus assembly at the site of virus budding.', *Journal of virology*, 82(20), pp. 10059–10070. doi: 10.1128/JVI.01184-08.

Chen, B. J. *et al.* (2008) 'The Influenza Virus M2 Protein Cytoplasmic Tail Interacts with the M1 Protein and Influences Virus Assembly at the Site of Virus Budding', *Journal of Virology*, 82(20), pp. 10059–10070. doi: 10.1128/JVI.01184-08.

Chen, L. *et al.* (2017) 'Amino acid substitution K470R in the nucleoprotein increases the virulence of H5N1 influenza A virus in mammals', *Frontiers in Microbiology*, 8(JUL), pp. 1–12. doi: 10.3389/fmicb.2017.01308.

Cheong, W. C. *et al.* (2015) 'Influenza A virus NS1 protein inhibits the NLRP3 inflammasome', *PLoS ONE*, 10(5), pp. 1–16. doi: 10.1371/journal.pone.0126456.

Chlanda, P., Schraidt, O., Kummer, S., Riches, J., Oberwinkler, H., Prinz, S., Kräusslich, H.-G. and Briggs, J. A. G. (2015) 'Structural analysis of the roles of influenza A virus membrane-associated proteins in assembly and morphology.', *Journal of virology*, 89(17), pp. 8957–66. doi: 10.1128/JVI.00592-15.

Chlanda, P., Schraidt, O., Kummer, S., Riches, J., Oberwinkler, H., Prinz, S., Kräusslich, H.-G. and Briggs, J. A. G. (2015) 'Structural Analysis of the Roles of Influenza A Virus Membrane-Associated Proteins in Assembly and Morphology', *Journal of Virology*, 89(17), pp. 8957–8966. doi: 10.1128/JVI.00592-15.

Choi, Y. K. *et al.* (2005) 'Studies of H5N1 Influenza Virus Infection of Pigs by Using Viruses Isolated in Vietnam and Thailand in 2004', *Journal of Virology*, 79(16), pp. 10821–10825. doi: 10.1128/JVI.79.16.10821-10825.2005.

Choppin, P. W., Murphy, J. S. and Tamm, I. (1960) 'Studies of two kinds of virus particles which comprise influenza A2 virus strains. III. Morphological characteristics: independence to morphological and functional traits.', *The Journal of experimental medicine*, 112(18), pp. 945–952. doi: 10.1084/jem.112.5.945.

Christopher D. O'Donnell, Leatrice Vogel, Yumiko Matsuoka, Hong Jin, K. S. (2014) 'The Matrix Gene Segment Destabilizes the Acid and Thermal Stability of the Hemagglutinin of Pandemic Live Attenuated Influenza Virus Vaccines', *Journal of Virology*, 88(21), pp. 12374–12384. doi: 10.1128/JVI.01107-14.

Chu, C. M., Dawson, I. M. and Elford, W. J. (1949) 'Filamentous forms associated with newly isolated influenza virus.', *Lancet*, 1(6554), p. 602. doi: 10.1016/S0140-6736(49)91699-2.

Cohen, M. *et al.* (2013) 'Influenza A penetrates host mucus by cleaving sialic acids with neuraminidase.', *Virology journal*, 10, p. 321. doi: 10.1186/1743-422X-10-321.

Copeland, C. S. *et al.* (1988) 'Folding, trimerization, and transport are sequential events in the biogenesis of influenza virus hemagglutinin', *Cell*, 53(2), pp. 197–209. doi: 10.1016/0092-8674(88)90381-9.

Cowling, B. J. *et al.* (2013) 'Comparative epidemiology of human infections with avian influenza A H7N9 and H5N1 viruses in China: A population-based study of laboratory-confirmed cases', *The Lancet*, 382(9887), pp. 129–137. doi: 10.1016/S0140-6736(13)61171-X.

Cox, N. J. and Subbarao, K. (2000) 'Global Epidemiology of Influenza: Past and

Present', *Annual Review of Medicine*. Annual Reviews 4139 El Camino Way, P.O. Box 10139, Palo Alto, CA 94303-0139, USA , 51(1), pp. 407–421. doi: 10.1146/annurev.med.51.1.407.

Cyranoski, D. (2005) 'Bird flu spreads among Java's pigs', *Nature*, 435, pp. 390–390.

Daniel N. Hebert, Brigitte Foellmer, and A. H. (1995) 'Glucose Trimming and Reglucosylation Determine Glycoprotein Association with Calnexin in the Endoplasmic Reticulum', *Cell*, 81, pp. 425–433. doi: 10.1002/jms.3408.

Dias, A. *et al.* (2009) 'The cap-snatching endonuclease of influenza virus polymerase resides in the PA subunit', *Nature*, 458(7240), pp. 914–918. doi: 10.1038/nature07745.

Disbrow, G. L., Hanover, J. A. and Schlegel, R. (2005) 'Endoplasmic Reticulum-Localized Human Papillomavirus Type 16 E5 Protein Alters Endosomal pH but Not trans-Golgi pH', *Journal of Virology*, 79(9), pp. 5839–5846. doi: 10.1128/JVI.79.9.5839-5846.2005.

Domingues, P. *et al.* (2015) 'Global Reprogramming of Host SUMOylation during Influenza Virus Infection', *Cell Reports*, 13(7), pp. 1467–1480. doi: 10.1016/j.celrep.2015.10.001.

Durrer, P. *et al.* (1996) 'H+-induced membrane insertion of influenza virus hemagglutinin involves the HA2 amino-terminal fusion peptide but not the coiled coil region', *Journal of Biological Chemistry*, 271(23), pp. 13417–13421. doi: 10.1074/jbc.271.23.13417.

Edinger, T. O., Pohl, M. O. and Stertz, S. (2014) 'Entry of influenza A virus: Host factors and antiviral targets', *Journal of General Virology*, 95(PART 2), pp. 263–277. doi: 10.1099/vir.0.059477-0.

Elleman, C. J. and Barclay, W. S. (2004) 'The M1 matrix protein controls the filamentous phenotype of influenza A virus', *Virology*, 321(1), pp. 144–153. doi: 10.1016/j.virol.2003.12.009.

Elton, D. *et al.* (2013) 'The genetics of virus particle shape in equine influenza A virus', *Influenza and other Respiratory Viruses*, 7(SUPPL.4), pp. 81–89. doi: 10.1111/irv.12197.

Epstein, S. L. (2018) 'Epstein, S. L. (2018). Universal Influenza Vaccines: Progress in Achieving Broad Cross-Protection In Vivo', *American Journal of Epidemiology*, 0002. doi: 10.1093/aje/kwy145/5063616.

Fodor, E. *et al.* (2007) 'Rescue of Influenza A Virus from Recombinant DNA', *Journal of Virology*, 81(20), pp. 11282–11289. doi: 10.1128/JVI.00910-07.

Fujiyoshi, Y. *et al.* (1994) 'Fine structure of influenza A virus observed by electron cryo-microscopy.', *The EMBO journal*, 13(2), pp. 318–326. doi: 10.1093/embo-reports/kve234.

Gagnon, J. *et al.* (1997) 'Influenza virus M1 protein binds to RNA through its nuclear localization signal.', *Journal of General Virology*. Microbiology Society, 78(7), pp. 1589–1596. doi: 10.1099/0022-1317-78-7-1589.

Gamblin, S. J. and Skehel, J. J. (2010) 'Influenza hemagglutinin and neuraminidase membrane glycoproteins', *Journal of Biological Chemistry*, 285(37), pp. 28403–28409. doi: 10.1074/jbc.R110.129809.

Gannagé, M. *et al.* (2009) 'Matrix Protein 2 of Influenza A Virus Blocks Autophagosome Fusion with Lysosomes', *Cell Host & Microbe*. Cell Press, 6(4), pp. 367–380. doi: 10.1016/J.CHOM.2009.09.005.

Gao, H. *et al.* (2015) 'The contribution of PA-X to the virulence of pandemic 2009 H1N1 and highly pathogenic H5N1 avian influenza viruses', *Scientific Reports*. Nature Publishing Group, 5(1), p. 8262. doi: 10.1038/srep08262.

Garten, W. and Klenk, H. D. (1999) 'Understanding influenza virus pathogenicity', *Trends in Microbiology*, 7(3), pp. 99–100. doi: 10.1016/S0966-842X(99)01460-2.

Gerhard, W. and Webster, R. G. (1978) 'Antigenic drift in influenza A viruses. I. Selection and characterization of antigenic variants of A/PR/8/34 (HON1) influenza virus with monoclonal antibodies.', *The Journal of experimental medicine*. Rockefeller University Press, 148(2), pp. 383–92. doi: 10.1084/JEM.148.2.383.

Gething, M. J. *et al.* (1986) 'Studies on the mechanism of membrane fusion: Site-specific mutagenesis of the hemagglutinin of influenza virus', *Journal of Cell Biology*, 102(1), pp. 11–23. doi: 10.1083/jcb.102.1.11.

Ghioni, P. *et al.* (2005) 'The protein stability and transcriptional activity of p63α are regulated by SUMO-1 conjugation', *Cell Cycle*, 4(1), pp. 183–190. doi: 10.4161/cc.4.1.1359.

Girdwood, D. *et al.* (2003) 'p300 Transcriptional Repression Is Mediated by SUMO Modification allele knockouts of p300 and CBP display distinct tran- scriptional phenotypes indicate that DNA bound tran- scription factors are likely to be in competition for lim', *Molecular Cell*, 11, pp. 1043–1054. doi: 10.1016/S1097-2765(03)00141-2.

Gómez-Puertas, P. *et al.* (2000) 'Influenza virus matrix protein is the major driving force in virus budding.', *Journal of virology*, 74(24), pp. 11538–11547. doi: 10.1128/JVI.74.24.11538-11547.2000.

Gorai, T. *et al.* (2012) 'F1Fo-ATPase, F-type proton-translocating ATPase, at the plasma membrane is critical for efficient influenza virus budding', *Proceedings of the National Academy of Sciences*, 109(12), pp. 4615–4620. doi: 10.1073/pnas.1114728109.

Gostissa, M. *et al.* (1999) 'Activation of p53 by conjugation to the ubiquitin-like protein SUMO-1', *EMBO Journal*, 18(22), pp. 6462–6471. doi: 10.1093/emboj/18.22.6462.

Grantham, M. L. *et al.* (2010) 'Tyrosines in the influenza A virus M2 protein cytoplasmic tail are critical for production of infectious virus particles.', *Journal of virology*, 84(17), pp. 8765–8776. doi: 10.1128/JVI.00853-10.

Grohskopf, L. A. *et al.* (2016) 'Prevention and Control of Seasonal Influenza with Vaccines Recommendations of the Advisory Committee on Immunization Practices — United States, 2016–17 Influenza Season', *MMWR. Recommendations and Reports*, 65(5), pp. 1–54. doi: 10.15585/mmwr.rr6505a1.

Grohskopf, L. A. *et al.* (2017) 'Prevention and Control of Seasonal Influenza With Vaccines: Recommendations of the Advisory Committee on Immunization Practices—United States, 2017–18 Influenza Season', *American Journal of Transplantation*, 17(11), pp. 2970–2982. doi: 10.1111/ajt.14511.

Grohskopf, L., Sokolow, L. and Broder, K. (2018) 'Prevention and control of seasonal influenza with vaccines: recommendations of the advisory committee on immunization practices- United States, 2017-2017 influenza season', *Morbidity and Mortality Weekly Report*, 67(3), pp. 1–24. Available at: http://www.cdc.gov/mmwr/preview/mmwrhtml/rr5808a1.htm.

Guan, Z. *et al.* (2010) 'Interaction of Hsp40 with influenza virus M2 protein: implications for PKR signaling pathway.', *Protein & cell*. Springer, 1(10), pp. 944–55. doi: 10.1007/s13238-010-0115-x.

Gubareva, L. V. (2004) 'Molecular mechanisms of influenza virus resistance to neuraminidase inhibitors', *Virus Research*, 103(1–2), pp. 199–203. doi: 10.1016/j.virusres.2004.02.034.

Guilligay, D. *et al.* (2008) 'The structural basis for cap binding by influenza virus polymerase subunit PB2', *Nature Structural and Molecular Biology*, 15(5), pp. 500–506. doi: 10.1038/nsmb.1421.

Han, Q. *et al.* (2014) 'Sumoylation of influenza A virus nucleoprotein is essential for intracellular trafficking and virus growth.', *Journal of virology*. American Society for Microbiology Journals, 88(16), pp. 9379–90. doi: 10.1128/JVI.00509-14.

Hannoun, Z. *et al.* (2010) 'Post-translational modification by SUMO', *Toxicology*, 278, pp. 288–293. doi: 10.1016/j.tox.2010.07.013.

Hao, R. *et al.* (2013) 'Proteasomes activate aggresome disassembly and clearance by producing unanchored ubiquitin chains.', *Molecular cell*. NIH Public Access, 51(6), pp. 819–28. doi: 10.1016/j.molcel.2013.08.016.

Harper, S. A. *et al.* (2003) 'Using Live , Attenuated Influenza Vaccine for Prevention and Control of Influenza', 52(Cdc), pp. 1–8.

Harris, A. *et al.* (2001) 'The crystal structure of the influenza matrix protein M1 at neutral pH: M1-M1 protein: Interfaces can rotate in the oligomeric structures of M1', *Virology*, 289(1), pp. 34–44. doi: 10.1006/viro.2001.1119.

Harris, A. *et al.* (2006) 'Influenza virus pleiomorphy characterized by cryoelectron tomography', *Proceedings of the National Academy of Sciences*, 103(50), pp. 19123–19127. doi: 10.1073/pnas.0607614103.

Hayase, Y., Uno, F. & Nii, S. (1995) 'Ultrahigh-resolution scanning electron microscopy of MDCK cells infected with influenza viruses', *Journal of electron microscopy*, 44, pp. 281–288.

Hecker, C.-M. *et al.* (2006) 'Specification of SUMO1- and SUMO2-interacting motifs.', *The Journal of biological chemistry*. American Society for Biochemistry and Molecular Biology, 281(23), pp. 16117–27. doi: 10.1074/jbc.M512757200.

Henkel, J. R. *et al.* (2000) 'Influenza M2 proton channel activity selectively inhibits trans-Golgi network release of apical membrane and secreted proteins in polarized Madin-Darby canine kidney cells', *Journal of Cell Biology*, 148(3), pp. 495–504. doi: 10.1083/jcb.148.3.495.

Hilsch, M. *et al.* (2014) 'Influenza a matrix protein m1 multimerizes upon binding to lipid membranes', *Biophysical Journal*, 107(4), pp. 912–923. doi: 10.1016/j.bpj.2014.06.042.

Hinz, M. *et al.* (2007) 'Signal responsiveness of IκB kinases is determined by Cdc37-assisted transient interaction with Hsp90', *Journal of Biological Chemistry*, 282(44), pp. 32311–32319. doi: 10.1074/jbc.M705785200.

Hirst, G. K. and Gotlieb, T. (1953) 'The experimental production of combination forms of virus', *The Journal of experimental medicine*. Rockefeller University Press, 98(1), pp. 41–52. doi: 10.1084/JEM.98.1.41.

Holsinger, L. J. and Alams, R. (1991) 'Influenza virus M2integral membrane protein is a homotetramer stabilized by formation of disulfide bonds', *Virology*, 183(1), pp. 32–43. doi: 10.1016/0042-6822(91)90115-R.

Hou, W. *et al.* (2010) 'Autophagic degradation of active caspase-8: A crosstalk mechanism between autophagy and apoptosis', *Autophagy*, 6(7), pp. 891–900.

doi: 10.4161/auto.6.7.13038.

Hu, J. *et al.* (2015) 'PA-X Decreases the Pathogenicity of Highly Pathogenic H5N1 Influenza A Virus in Avian Species by Inhibiting Virus Replication and Host Response', *Journal of Virology*, 89(8), pp. 4126–4142. doi: 10.1128/JVI.02132-14.

Hughey, P. G. *et al.* (1995) 'Effects of antibody to the influenza A virus M2 protein on M2 surface expression and virus assembly.', *Virology*, pp. 411–21. doi: 10.1006/viro.1995.1498.

Hurt, A. C. (2014) 'The epidemiology and spread of drug resistant human influenza viruses', *Current Opinion in Virology*. Elsevier B.V., 8(November), pp. 22–29. doi: 10.1016/j.coviro.2014.04.009.

Huyghues-Despointes, B. M. P. *et al.* (2003) 'pK values of histidine residues in ribonuclease Sa: Effect of salt and net charge', *Journal of Molecular Biology*, 325(5), pp. 1093–1105. doi: 10.1016/S0022-2836(02)01274-3.

Ito, T. *et al.* (1997) 'Differences in sialic acid-galactose linkages in the chicken egg amnion and allantois influence human influenza virus receptor specificity and variant selection.', *Journal of virology*, 71(4), pp. 3357–62.

Itoh, Y. *et al.* (2009) 'In vitro and in vivo characterization of new swine-origin H1N1 influenza viruses.', *Nature*. Nature Publishing Group, 460(7258), pp. 1021–1025. doi: 10.1038/nature08260.

von Itzstein, M. (2007) 'The war against influenza: Discovery and development of sialidase inhibitors', *Nature Reviews Drug Discovery*, 6(12), pp. 967–974. doi: 10.1038/nrd2400.

Iwatsuki-Horimoto, K. *et al.* (2006) 'The cytoplasmic tail of the influenza A virus M2 protein plays a role in viral assembly.', *Journal of virology*. American Society for Microbiology Journals, 80(11), pp. 5233–40. doi: 10.1128/JVI.00049-06.

Jagger, B. W. *et al.* (2012) 'An overlapping protein-coding region in influenza A virus segment 3 modulates the host response', *Science*, 337(6091), pp. 199–204. doi: 10.1126/science.1222213.

Jin, H. *et al.* (1997) 'Influenza virus hemagglutinin and neuraminidase cytoplasmic tails control particle shape', *EMBO Journal*, 16(6), pp. 1236–1247. doi: 10.1093/emboj/16.6.1236.

Jin, H., Leser, G. P. and Lamb, R. A. (1994) 'The influenza virus hemagglutinin cytoplasmic tail is not essential for virus assembly or infectivity.', *The EMBO journal*, 13(22), pp. 5504–15. doi: 10.1007/978-3-540-77129-6_13.

Johnson, E. S. (2007) 'Protein modification by SUMO', *Seikagaku*, 79(12), pp. 1120–1130. doi: 10.1016/S0968-0004(01)01849-7.

Johnson, N. P. A. S. and Mueller, J. (2002) 'Updating the accounts: global mortality of the 1918-1920 "Spanish" Influenza Pandemic', *Bulletin of the History of Medicine*, 76(1), pp. 105–115. doi: 10.1353/bhm.2002.0022.

Johnston, J. A., Ward, C. L. and Kopito, R. R. (1998) 'Aggresomes: A cellular response to misfolded proteins', *Journal of Cell Biology*, 143(7), pp. 1883–1898. doi: 10.1083/jcb.143.7.1883.

De Jong, A. S. *et al.* (2006) 'The coxsackievirus 2B protein increases efflux of ions from the endoplasmic reticulum and Golgi, thereby inhibiting protein trafficking through the Golgi', *Journal of Biological Chemistry*, 281(20), pp. 14144–14150. doi: 10.1074/jbc.M511766200.

Joshua B. Plotkin, Jonathan Dushoff, and S. A. L. (2002) 'Hemagglutinin sequence clusters and the antigenic evolution of influenza A virus', *PNAS*, 99(9), pp. 6263–6268.

Kabeya, Y. *et al.* (2000) 'LC3, a mammalian homologue of yeast Apg8p, is localized in autophagosome membranes after processing.', *The EMBO journal*. European Molecular Biology Organization, 19(21), pp. 5720–8. doi: 10.1093/emboj/19.21.5720.

Kadam, R. U. and Wilson, I. A. (2017) 'Structural basis of influenza virus fusion inhibition by the antiviral drug Arbidol', *Proceedings of the National Academy of Sciences*, 114(2), pp. 206–214. doi: 10.1073/pnas.1617020114.

Kerscher, O. (2007) 'SUMO junction-what's your function? New insights through SUMO-interacting motifs.', *EMBO reports*. EMBO Press, 8(6), pp. 550–5. doi: 10.1038/sj.embor.7400980.

Kho, C. *et al.* (2011) 'SUMO1-dependent modulation of SERCA2a in heart failure', *Nature*. Nature Publishing Group, 477(7366), pp. 601–606. doi: 10.1038/nature10407.

Kilbourne, E. D. (1959) 'Studies on influenza in the pandemic of 1957-1958. III. Isolation of influenza A (Asian strain) viruses from influenza patients with pulmonary complications; details of virus isolation and characterization of isolates, with quantitative comparison of isol', *The Journal of clinical investigation*, 38(1 Part 2), pp. 266–274. doi: 10.1172/JCI103792.

Kilbourne, E. D. and Murphy, J. S. (1960) 'Genetic studies of Influenza Virus - Viral morphology and growth capacity as exchangable genetic traits. Rapid in ovo adaptation of early passage Asian strain isolates by combination with PR8', 9(7), pp. 151–160.

Kim, H., Webster, R. G. and Webby, R. J. (2018) 'Influenza Virus: Dealing with a Drifting and Shifting Pathogen', *Viral Immunology*, 31(2), p. vim.2017.0141. doi:

10.1089/vim.2017.0141.

Kishi, A. *et al.* (2003) 'Sumoylation of Pdx1 is associated with its nuclear localization and insulin gene activation', *American Journal of Physiology-Endocrinology and Metabolism*, 284(4), pp. E830–E840. doi: 10.1152/ajpendo.00390.2002.

Kobayashi, M. *et al.* (1996) 'Influenza virus PB1 protein is the minimal and essential subunit of RNA polymerase', *Archives of virology*, 141(3–4), pp. 525–39. Available at: http://www.ncbi.nlm.nih.gov/pubmed/8645093.

Koelle, K. *et al.* (2006) 'Epochal evolution shapes the phylodynamics of interpandemic influenza A (H3N2) in humans.', *Science (New York, N.Y.)*. American Association for the Advancement of Science, 314(5807), pp. 1898–903. doi: 10.1126/science.1132745.

Koga, F. *et al.* (2006) 'Hsp90 inhibition transiently activates Src kinase and promotes Src-dependent Akt and Erk activation', *Proceedings of the National Academy of Sciences*, 103(30), pp. 11318 –11322. doi: 10.1097/00005237-199409000-00006.

Kumlin, U. *et al.* (2008) 'Sialic acid tissue distribution and influenza virus tropism', *Influenza and other Respiratory Viruses*, 2(5), pp. 147–154. doi: 10.1111/j.1750-2659.2008.00051.x.

Kuo, R.-L. *et al.* (2016) 'Role of N Terminus-Truncated NS1 Proteins of Influenza A Virus in Inhibiting IRF3 Activation', *Journal of Virology*, 90(9), pp. 4696–4705. doi: 10.1128/JVI.02843-15.

Lamb, R. A. and Choppin, P. W. (1983) 'The Gene Structure and Replication of Influenza Virus', pp. 467–506.

Lang, G. *et al.* (1968) 'A new influenza A virus infection in turkeys II. A highly pathogenic variant, a/turkey/ontario 772/66', 9(7), pp. 151–160.

Lee, G. W. *et al.* (1998) 'Modification of Ran GTPpase-activating protein by the small ubiquitin- related modifier SUMO-1 requires Ubc9, an E2-type ubiquitin-conjugating enzyme homologue', *Journal of Biological Chemistry*, 273(11), pp. 6503–6507. doi: 10.1074/jbc.273.11.6503.

Lee, K. K. (2010) 'Architecture of a nascent viral fusion pore', *EMBO Journal*. Nature Publishing Group, 29(7), pp. 1299–1311. doi: 10.1038/emboj.2010.13.

Lee, Y. J. *et al.* (2016) 'Enhancement of the safety of live influenza vaccine by attenuating mutations from cold-adapted hemagglutinin', *Virology*. Elsevier, 491, pp. 1–9. doi: 10.1016/j.virol.2016.01.022.

Lin, X. *et al.* (2003) 'SUMO-1/Ubc9 promotes nuclear accumulation and metabolic stability of tumor suppressor Smad4', *Journal of Biological Chemistry*,

278(33), pp. 31043–31048. doi: 10.1074/jbc.C300112200.

Liu, G. *et al.* (2016) 'Autophagy is involved in regulating influenza A virus RNA and protein synthesis associated with both modulation of Hsp90 induction and mTOR/p70S6K signaling pathway', *International Journal of Biochemistry and Cell Biology*. Elsevier Ltd, 72, pp. 100–108. doi: 10.1016/j.biocel.2016.01.012.

Liu, Y.-C. (2004) 'Ubiquitin Ligases and the Immune Response', *Annual Review of Immunology*, 22(1), pp. 81–127. doi: 10.1146/annurev.immunol.22.012703.104813.

Ma, H. *et al.* (2012) 'Human annexin A6 interacts with influenza a virus protein M2 and negatively modulates infection.', *Journal of virology*. American Society for Microbiology Journals, 86(3), pp. 1789–801. doi: 10.1128/JVI.06003-11.

Maassab, H. F. and Bryant, M. L. (2007) 'The Development of Live Attenuated Cold-adapted Influenza Virus Vaccine for Humans', *American Journal of Obstetrics and Gynecology*, 196(1), pp. 237–244. doi: 10.1016/j.ajog.2006.06.055.

Mabb, A. M. and Miyamoto, S. (2007) 'SUMO and NF-κB ties', *Cellular and Molecular Life Sciences*, 64(15), pp. 1979–1996. doi: 10.1007/s00018-007-7005-2.

Mahajan, R. *et al.* (1998) 'Molecular characterization of the SUMO-1 modification of RanGAP1 and its role in nuclear envelope association. A small ubiquitin-related polypeptide involved in targeting RanGAP1 to nuclear pore complex protein RanBP2', *J Cell Biol*, 140(2), p. 259–70. doi: 10.1083/jcb.140.2.259.

Mänz, B. *et al.* (2012) 'Adaptive mutations in NEP compensate for defective H5N1 RNA replication in cultured human cells', *Nature Communications*, 3(May). doi: 10.1038/ncomms1804.

McCown, M. F. and Pekosz, A. (2005) 'The influenza A virus M2 cytoplasmic tail is required for infectious virus production and efficient genome packaging.', *Journal of virology*. American Society for Microbiology (ASM), 79(6), pp. 3595–605. doi: 10.1128/JVI.79.6.3595-3605.2005.

McCown, M. F. and Pekosz, A. (2006) 'Distinct domains of the influenza a virus M2 protein cytoplasmic tail mediate binding to the M1 protein and facilitate infectious virus production.', *Journal of virology*, 80(16), pp. 8178–89. doi: 10.1128/JVI.00627-06.

McEwan, D. G. *et al.* (2015) 'PLEKHM1 Regulates Autophagosome-Lysosome Fusion through HOPS Complex and LC3/GABARAP Proteins', *Molecular Cell*. Cell Press, 57(1), pp. 39–54. doi: 10.1016/J.MOLCEL.2014.11.006.

McGeoch, D., Fellner, P. and Newton, C. (1976) 'Influenza virus genome consists of eight distinct RNA species.', *Proceedings of the National Academy of Sciences of the United States of America*. National Academy of Sciences, 73(9), pp. 3045–9. doi: 10.1073/PNAS.73.9.3045.

Mendez, M. G., Kojima, S. I. and Goldman, R. D. (2010) 'Vimentin induces changes in cell shape, motility, and adhesion during the epithelial to mesenchymal transition', *The FASEB Journal*, 24(6), pp. 1838–1851. doi: 10.1096/fj.09-151639.

Mi, S. *et al.* (2010) 'Na+/K+-ATPase β1 subunit interacts with M2 proteins of influenza A and B viruses and affects the virus replication', *Science China Life Sciences*, 53(9), pp. 1098–1105. doi: 10.1007/s11427-010-4048-7.

Mi, Z. *et al.* (2010) 'SUMOylation of RIG-I positively regulates the type I interferon signaling', *Protein and Cell*, 1(3), pp. 275–283. doi: 10.1007/s13238-010-0030-1.

Minty, A. *et al.* (2000) 'Covalent modification of p73alpha by SUMO-1. Two-hybrid screening with p73 identifies novel SUMO-1-interacting proteins and a SUMO-1 interaction motif.', *The Journal of biological chemistry*. American Society for Biochemistry and Molecular Biology, 275(46), pp. 36316–23. doi: 10.1074/jbc.M004293200.

Mitchell, M. J. and King, M. R. (2011) 'Protonation, Tautomerization, and Rotameric Structure of Histidine: A Comprehensive Study by Magic-Angle-Spinning Solid-State NMR', *J Am Chem Soc.*, 133(5), pp. 1534–1544. doi: 10.1088/1367-2630/15/1/015008.Fluid.

Mitnaul, L. J. *et al.* (1996) 'The cytoplasmic tail of influenza A virus neuraminidase (NA) affects NA incorporation into virions, virion morphology, and virulence in mice but is not essential for virus replication.', *Journal of virology*, 70(2), pp. 873–9. doi: 10.1016/j.bmcl.2010.09.034.

Mizushima, N. and Yoshimori, T. (2007) 'How to Interpret LC3 Immunoblotting', *Autophagy*. Taylor & Francis, 3(6), pp. 542–545. doi: 10.4161/auto.4600.

Mizushima, N., Yoshimori, T. and Levine, B. (2010) 'Methods in Mammalian Autophagy Research', *Cell*. Cell Press, 140(3), pp. 313–326. doi: 10.1016/J.CELL.2010.01.028.

Molinari, N. A. M. *et al.* (2007) 'The annual impact of seasonal influenza in the US: Measuring disease burden and costs', *Vaccine*, 25(27), pp. 5086–5096. doi: 10.1016/j.vaccine.2007.03.046.

Mosley, V. M. and Wyckoff, R. W. G. (1946) 'Electron Micrography of the Virus of Influenza', *Nature*, pp. 263–263. doi: 10.1038/157263a0.

Mueller, D. S. *et al.* (2008) 'Histidine protonation and the activation of viral fusion proteins', *Biochemical Society Transactions*, 36(1), pp. 43–45. doi: 10.1042/BST0360043.

Müller, S. *et al.* (2000) 'c-Jun and p53 activity is modulated by SUMO-1 modification', *Journal of Biological Chemistry*, 275(18), pp. 13321–13329. doi: 10.1074/jbc.275.18.13321.

Naffakh, N. *et al.* (2000) 'Genetic analysis of the compatibility between polymerase proteins from human and avian strains of influenza A viruses', *Journal of General Virology*, 81(5), pp. 1283–1291. doi: 10.1099/0022-1317-81-5-1283.

Namanja, A. T. *et al.* (2012) 'Insights into high affinity small ubiquitin-like modifier (SUMO) recognition by SUMO-interacting motifs (SIMs) revealed by a combination of NMR and peptide array analysis.', *The Journal of biological chemistry*. American Society for Biochemistry and Molecular Biology, 287(5), pp. 3231–40. doi: 10.1074/jbc.M111.293118.

Nayak, D. P., Hui, E. K. W. and Barman, S. (2004) 'Assembly and budding of influenza virus', *Virus Research*, 106(2 SPEC.ISS.), pp. 147–165. doi: 10.1016/j.virusres.2004.08.012.

Ndoye, A. and Weeraratna, A. T. (2016) 'Autophagy- An emerging target for melanoma therapy', *F1000Research*, 5, p. 1888. doi: 10.12688/f1000research.8347.1.

Nelli, R. K. *et al.* (2010) 'Comparative distribution of human and avian type sialic acid influenza receptors in the pig', *BMC Veterinary Research*, 6. doi: 10.1186/1746-6148-6-4.

Neumann, G., Hughes, M. T. and Kawaoka, Y. (2000) 'Influenza A virus NS2 protein mediates vRNP nuclear export through NES-independent interaction with hCRM1', *EMBO Journal*, 19(24), pp. 6751–6758. doi: 10.1093/emboj/19.24.6751.

Noda, T. *et al.* (2006) 'Architecture of ribonucleoprotein complexes in influenza A virus particles.', *Nature*, 439(7075), pp. 490–492. doi: 10.1038/nature04378.

Nordholm, J. *et al.* (2013) 'Polar residues and their positional context dictate the transmembrane domain interactions of influenza a neuraminidases', *Journal of Biological Chemistry*, 288(15), pp. 10652–10660. doi: 10.1074/jbc.M112.440230.

Noton, S. L. *et al.* (2007) 'Identification of the domains of the influenza A virus M1 matrix protein required for NP binding, oligomerization and incorporation into virions', *Journal of General Virology*, 88(8), pp. 2280–2290. doi:

10.1099/vir.0.82809-0.

O'Neill, R. E., Talon, J. and Palese, P. (1998) 'The influenza virus NEP (NS2 protein) mediates the nuclear export of viral ribonucleoproteins', *EMBO Journal*, 17(1), pp. 288–296. doi: 10.1093/emboj/17.1.288.

Pal, S. *et al.* (2011) 'Influenza A virus interacts extensively with the cellular SUMOylation system during infection', *Virus Research*. Elsevier, 158(1–2), pp. 12–27. doi: 10.1016/J.VIRUSRES.2011.02.017.

Pal, S., Rosas, J. M. and Rosas-Acosta, G. (2010) 'Identification of the non-structural influenza A viral protein NS1A as a bona fide target of the Small Ubiquitin-like MOdifier by the use of dicistronic expression constructs', *Journal of Virological Methods*. Elsevier, 163(2), pp. 498–504. doi: 10.1016/J.JVIROMET.2009.11.010.

Palese, P. *et al.* (1974) 'Characterization of temperature sensitive influenza virus mutants defective in neuraminidase', *Virology*, 61(2), pp. 397–410. doi: 10.1016/0042-6822(74)90276-1.

Pandey, P. (2000) 'Negative regulation of cytochrome c-mediated oligomerization of Apaf-1 and activation of procaspase-9 by heat shock protein 90', *The EMBO Journal*, 19(16), pp. 4310–4322. doi: 10.1093/emboj/19.16.4310.

Pankiv, S. *et al.* (2007) 'p62/SQSTM1 Binds Directly to Atg8/LC3 to Facilitate Degradation of Ubiquitinated Protein Aggregates by Autophagy'. doi: 10.1074/jbc.M702824200.

Parrish, C. R., Murcia, P. R. and Holmes, E. C. (2015) 'Influenza virus reservoirs and intermediate hosts: dogs, horses, and new possibilities for influenza virus exposure of humans', *J Virol*, 89(6), pp. 2990–2994. doi: 10.1128/JVI.03146-14.

Pennington, T. H. (2008) 'Influenza.', *Scottish medical journal*, 53(1), pp. 2–3. doi: 10.1258/rsmsmj.53.1.2.

Pereira, C. F. *et al.* (2017) 'Influenza A Virus NS1 Protein Promotes Efficient Nuclear Export of Unspliced Viral M1 mRNA', *Journal of Virology*, 91(15), pp. e00528-17. doi: 10.1128/JVI.00528-17.

Pielak, R. M. and Chou, J. J. (2011) 'Influenza M2 proton channels', *Biochimica et Biophysica Acta (BBA) - Biomembranes*. Elsevier, 1808(2), pp. 522–529. doi: 10.1016/J.BBAMEM.2010.04.015.

Pinto, L. H., Holsinger, L. J. and Lamb, R. A. (1992) 'Influenza virus M2 protein has ion channel activity', *Cell*. Cell Press, 69(3), pp. 517–528. doi: 10.1016/0092-8674(92)90452-I.

Pleschka, S. *et al.* (1996) 'A plasmid-based reverse genetics system for influenza A virus.', *Journal of virology*, 70(6), pp. 4188–92. doi: 10.1111/1468-

2397.00218.

Poole, E. *et al.* (2004) ‘Functional domains of the influenza A virus PB2 protein: identification of NP- and PB1-binding sites’, *Virology*. Academic Press, 321(1), pp. 120–133. doi: 10.1016/J.VIROL.2003.12.022.

Preuss, K. D. *et al.* (2015) ‘Sumoylated HSP90 is a dominantly inherited plasma cell dyscrasias risk factor’, *Journal of Clinical Investigation*, 125(1), pp. 316–323. doi: 10.1172/JCI76802.

Robb, N. C. *et al.* (2009) ‘NS2/NEP protein regulates transcription and replication of the influenza virus RNA genome’, *Journal of General Virology*, 90(6), pp. 1398–1407. doi: 10.1099/vir.0.009639-0.

Robert W. DomsS, Ari Heleniuss, and J. W. (1984) ‘Membrane Fusion Activity of the Influenza Virus Hemagglutinin’, *Journal of Social and Personal Relationships*, 16(6), pp. 822–833. doi: 10.1177/0265407599166008.

Roberts, P. C. and Compans, R. W. (1998) ‘Host cell dependence of viral morphology.’, *Proceedings of the National Academy of Sciences of the United States of America*, 95(10), pp. 5746–5751. doi: 10.1073/pnas.95.10.5746.

Roberts, P. C., Lamb, R. A. and Compans, R. W. (1998) *The M1 and M2 Proteins of Influenza A Virus Are Important Determinants in Filamentous Particle Formation*. Available at: https://ac.els-cdn.com/S0042682297989169/1-s2.0-S0042682297989169-main.pdf?_tid=cca53a97-6e8e-4ac9-b384-6c9820fba11e&acdnat=1539528878_a6b5f4891fe38b808a7263227ecbfb83 (Accessed: 14 October 2018).

Rossman, J. S. *et al.* (2010) ‘Influenza Virus M2 Ion Channel Protein Is Necessary for Filamentous Virion Formation □’, 84(10), pp. 5078–5088. doi: 10.1128/JVI.00119-10.

Rossman, J. S. and Lamb, R. A. (2011) ‘Influenza virus assembly and budding’, *Virology*, 411(2), pp. 229–236. doi: 10.1016/j.virol.2010.12.003.

Rossman, J. S., Leser, G. P. and Lamb, R. a. (2012) ‘Filamentous Influenza Virus Enters Cells via Macropinocytosis’, *Journal of Virology*, 86(20), pp. 10950–10960. doi: 10.1128/JVI.05992-11.

Sakaguchi, T., Leser, G. P. and Lamb, R. A. (1996) ‘The ion channel activity of the influenza virus M2 protein affects transport through the Golgi apparatus.’, *The Journal of cell biology*. Rockefeller University Press, 133(4), pp. 733–47. doi: 10.1083/JCB.133.4.733.

Samson, M. *et al.* (2013) ‘Influenza virus resistance to neuraminidase inhibitors’, *Antiviral Research*, 98(2), pp. 174–185. doi: 10.1016/j.antiviral.2013.03.014.

Sandbulte, M. R. *et al.* (2011) 'Discordant antigenic drift of neuraminidase and hemagglutinin in H1N1 and H3N2 influenza viruses', *Proceedings of the National Academy of Sciences*, 108(51), pp. 20748–20753. doi: 10.1073/pnas.1113801108.

Sato, S., Fujita, N. and Tsuruo, T. (2000) 'Modulation of Akt kinase activity by binding to Hsp90', *Proceedings of the National Academy of Sciences*, 97(20), pp. 10832–10837. doi: 10.1073/pnas.170276797.

Schapiro, F. B. and Grinstein, S. (2000) 'Determinants of the pH of the Golgi complex', *Journal of Biological Chemistry*, 275(28), pp. 21025–21032. doi: 10.1074/jbc.M002386200.

Scheiffele, P. *et al.* (1999) 'Influenza Viruses Select Ordered Lipid Membrane Influenza Viruses Select Ordered Lipid Domains during Budding from the Plasma Membrane *', 274(4), pp. 2038–2044. doi: 10.1074/jbc.274.4.2038.

Schmidt, N. W., Mishra, A., Wang, J., Degrado, W. F., *et al.* (2013) 'Influenza virus A M2 protein generates negative gaussian membrane curvature necessary for budding and scission', *Journal of the American Chemical Society*, 135(37), pp. 13710–13719. doi: 10.1021/ja400146z.

Schmidt, N. W., Mishra, A., Wang, J., DeGrado, W. F., *et al.* (2013) 'Influenza Virus A M2 Protein Generates Negative Gaussian Membrane Curvature Necessary for Budding and Scission', *Journal of the American Chemical Society*. American Chemical Society, 135(37), pp. 13710–13719. doi: 10.1021/ja400146z.

Schnell, J. R. and Chou, J. J. (2008) 'Structure and mechanism of the M2 proton channel of influenza A virus', *Nature*, 451(7178), pp. 591–595. doi: 10.1038/nature06531.

Schrauwen, E. J. A. *et al.* (2016) 'Amino Acid Substitutions That Affect Receptor Binding and Stability of the Hemagglutinin of Influenza A/H7N9 Virus', *Journal of Virology*, 90(7), pp. 3794–3799. doi: 10.1128/JVI.03052-15.

Schulman, B. A. and Harper, J. W. (2009) 'Downstream Signalling Pathways', *Nature reviews. Molecular cell biology*, 10(5), pp. 319–331. doi: 10.1038/nrm2673.Ubiquitin-like.

Schweiger, B., Zadow, I. and Heckler, R. (2002) 'Antigenic drift and variability of influenza viruses', *Medical Microbiology and Immunology*, 191(3–4), pp. 133–138. doi: 10.1007/s00430-002-0132-3.

Seladi-Schulman, J. *et al.* (2014) 'Filament-producing mutants of influenza A/Puerto Rico/ 8/1934 (H1N1) virus have higher neuraminidase activities than the spherical wild-type', *PLoS ONE*, 9(11), pp. 1–10. doi: 10.1371/journal.pone.0112462.

Seladi-Schulman, J., Steel, J. and Lowen, A. C. (2013) 'Spherical influenza viruses have a fitness advantage in embryonated eggs, while filament-producing

strains are selected in vivo.', *Journal of virology*, 87(24), pp. 13343–53. doi: 10.1128/JVI.02004-13.

Sharp, G. B. *et al.* (1997) 'Coinfection of Wild Ducks by Influenza A Viruses : Distribution Patterns and Biological Significance', 71(8), pp. 6128–6135.

Shortridge, K. F. *et al.* (1998) 'Characterization of avian H5N1 influenza viruses from poultry in Hong Kong.', *Virology*, 252(2), pp. 331–342. doi: 10.1006/viro.1998.9488.

Shtykova, E. V. *et al.* (2017) 'Influenza virus Matrix Protein M1 preserves its conformation with pH, changing multimerization state at the priming stage due to electrostatics', *Scientific Reports*. Springer US, 7(1), pp. 1–16. doi: 10.1038/s41598-017-16986-y.

Shuai, K. and Liu, B. (2003) 'Regulation of JAK-STAT signalling in the immune system', *Nature Reviews Immunology*, 3(11), pp. 900–911. doi: 10.1038/nri1226.

Sieczkarski, S. B. and Whittaker, G. R. (2005) 'Characterization of the host cell entry of filamentous influenza virus', *Archives of Virology*. Springer-Verlag, 150(9), pp. 1783–1796. doi: 10.1007/s00705-005-0558-1.

da Silva, D. V. *et al.* (2015) 'The Influenza Virus Neuraminidase Protein Transmembrane and Head Domains Have Coevolved', *Journal of Virology*, 89(2), pp. 1094–1104. doi: 10.1128/JVI.02005-14.

Da Silva, D. V. *et al.* (2013) 'Assembly of subtype 1 influenza neuraminidase is driven by both the transmembrane and head domains', *Journal of Biological Chemistry*, 288(1), pp. 644–653. doi: 10.1074/jbc.M112.424150.

Skehel, J. J. *et al.* (1982) 'Changes in the conformation of influenza virus hemagglutinin at the pH optimum of virus-mediated membrane fusion.', *Proceedings of the National Academy of Sciences*, 79(4), pp. 968–972. doi: 10.1073/pnas.79.4.968.

Smith, D. J. *et al.* (2004) 'Mapping the antigenic and genetic evolution of influenza virus', *Science*, 305(5682), pp. 371–376. doi: 10.1126/science.1097211.

Squires, R. B. *et al.* (2012) 'Influenza Research Database: An integrated bioinformatics resource for influenza research and surveillance', *Influenza and other Respiratory Viruses*, 6(6), pp. 404–416. doi: 10.1111/j.1750-2659.2011.00331.x.

Steinhauer, D. A. (1999) 'Role of hemagglutinin cleavage for the pathogenicity of influenza virus', *Virology*, 258(1), pp. 1–20. doi: 10.1006/viro.1999.9716.

Sternsdorf, T., Jensen, K. and Will, H. (1997) 'Evidence for covalent modification of the nuclear dot-associated proteins PML and Sp100 by PIC1/SUMO-1', *Journal of Cell Biology*, 139(7), pp. 1621–1634. doi: 10.1083/jcb.139.7.1621.

Structure of influenza virus (no date). Available at: http://www.virology.ws/2009/04/30/structure-of-influenza-virus/ (Accessed: 29 October 2018).

Su, W.-C. *et al.* (2017) 'Ubiquitination of the Cytoplasmic Domain of Influenza A Virus M2 Protein is Crucial for Production of Infectious Virus Particles', *Journal of Virology*, 92(4), p. JVI.01972-17. doi: 10.1128/JVI.01972-17.

Su, W.-C. *et al.* (2018) 'Ubiquitination of the Cytoplasmic Domain of Influenza A Virus M2 Protein Is Crucial for Production of Infectious Virus Particles.', *Journal of virology*. American Society for Microbiology Journals, 92(4), p. JVI.01972-17. doi: 10.1128/JVI.01972-17.

Subbarao, E. K., London, W. and Murphy, B. R. (1993) 'A Single Amino Acid in the PB2 Gene of Influenza A Virus Is a Determinant of Host Range', *Journal of virology*. American Society for Microbiology Journals, 67(4), pp. 1761–1764. doi: 10.1118/1.597938.

Subbarao, K. *et al.* (1998) 'Characterization of an avian influenza A (H5N1) virus isolated from a child with a fatal respiratory illness', *Science*, 279(5349), pp. 393–396. doi: 10.1126/science.279.5349.393.

Tanida, I. *et al.* (2005) 'Lysosomal Turnover, but Not a Cellular Level, of Endogenous LC3 is a Marker for Autophagy', *Autophagy*. Taylor & Francis, 1(2), pp. 84–91. doi: 10.4161/auto.1.2.1697.

Tanida, I., Ueno, T. and Kominami, E. (2008) 'LC3 and Autophagy', in *Methods in molecular biology (Clifton, N.J.)*, pp. 77–88. doi: 10.1007/978-1-59745-157-4_4.

Tatham, M. H. *et al.* (2003) 'Role of an N-terminal site of Ubc9 in SUMO-1, -2, and -3 binding and conjugation', *Biochemistry*, 42(33), pp. 9959–9969. doi: 10.1021/bi0345283.

Taubenberger, J. K. *et al.* (2005) 'Characterization of the 1918 influenza virus polymerase genes', *International Congress Series*, 437(6), pp. 889–893. doi: 10.1016/S0531-5131(01)00629-X.

Tawaratsumida, K. *et al.* (2014) 'Quantitative Proteomic Analysis of the Influenza A Virus Nonstructural Proteins NS1 and NS2 during Natural Cell Infection Identifies PACT as an NS1 Target Protein and Antiviral Host Factor', *Journal of Virology*, 88(16), pp. 9038–9048. doi: 10.1128/JVI.00830-14.

Ulrich, H. D. (2005) 'Mutual interactions between the SUMO and ubiquitin systems: A plea of no contest', *Trends in Cell Biology*, 15(10), pp. 525–532. doi: 10.1016/j.tcb.2005.08.002.

Varghese, J. N. *et al.* (1992) 'The structure of the complex between influenza virus neuraminidase and sialic acid, the viral receptor', *Proteins: Structure,*

Function, and Bioinformatics, 14(3), pp. 327–332. doi: 10.1002/prot.340140302.

Varghese, J. N., Laver, W. G. and Colman, P. M. (1983) 'Structure of the influenza virus glycoprotein antigen neuraminidase at 2.9 Å resolution', *Nature*, 303(5912), pp. 35–40. doi: 10.1038/303035a0.

Varki, N. M. and Varki, A. (2007) 'Diversity in cell surface sialic acid presentations: Implications for biology and disease', *Laboratory Investigation*, 87(9), pp. 851–857. doi: 10.1038/labinvest.3700656.

Vatsyayan, J. *et al.* (2008) 'SUMO1 modification of NF-κB2/p100 is essential for stimuli-induced p100 phosphorylation and processing', *EMBO Reports*, 9(9), pp. 885–890. doi: 10.1038/embor.2008.122.

Vijayakrishnan, S. *et al.* (2013) 'Cryotomography of Budding Influenza A Virus Reveals Filaments with Diverse Morphologies that Mostly Do Not Bear a Genome at Their Distal End', *PLoS Pathogens*, 9(6). doi: 10.1371/journal.ppat.1003413.

de Vries, E. *et al.* (2011) 'Dissection of the influenza A virus endocytic routes reveals macropinocytosis as an alternative entry pathway.', *PLoS pathogens*. Public Library of Science, 7(3), p. e1001329. doi: 10.1371/journal.ppat.1001329.

Warren-Gash, C., Smeeth, L. and Hayward, A. C. (2009) 'Influenza as a trigger for acute myocardial infarction or death from cardiovascular disease: a systematic review', *The Lancet Infectious Diseases*. Elsevier Ltd, 9(10), pp. 601–610. doi: 10.1016/S1473-3099(09)70233-6.

Watanabe, T. *et al.* (2001) 'Influenza A Virus Can Undergo Multiple Cycles of Replication without M2 Ion Channel Activity Influenza A Virus Can Undergo Multiple Cycles of Replication without M2 Ion Channel Activity', *Society*, 75(12), pp. 5656–5662. doi: 10.1128/JVI.75.12.5656.

Webster, R. G. *et al.* (1982) 'Molecular mechanisms of variation in influenza viruses', *Nature*, 296(5853), pp. 115–121. doi: 10.1038/296115a0.

Webster, R. G. (1998) 'Influenza: An emerging disease', *Emerging Infectious Diseases*, 4(3), pp. 436–441. doi: 10.3201/eid0403.980325.

Weis, W. *et al.* (1988) 'Structure of the influenza virus haemagglutinin complexed with its receptor, sialic acid.', *Nature*, 333(6172), pp. 426–431. doi: 10.1038/333426a0.

Wenjun Ma, R. E. K. and J. A. R. (2009) 'The pig as a mixing vessel for influenza viruses: Human and veterinary implications', *J Mol Genet Med (2009)*, 3(1), pp. 158–166. Available at: http://www.nature.com/doifinder/10.1038/nchina.2008.185%5Cnpapers3://publication/doi/10.1038/nchina.2008.185.

Wharton, S. A. *et al.* (1994) 'Role of virion M2 protein in influenza virus uncoating: Specific reduction in the rate of membrane fusion between virus and liposomes by amantadine', *Journal of General Virology*, 75(4), pp. 945–948. doi: 10.1099/0022-1317-75-4-945.

WHO (2014) *Influenza Seasonal, Geneva: Media Center*. Available at: http://www.who.int/mediacentre/factsheets/fs211/en/.

WHO (no date) *Influenza Data and Statistics*. Available at: http://www.euro.who.int/en/health-topics/communicable-diseases/influenza/data-and-statistics.

van Wijk, S. J. L., Müller, S. and Dikic, I. (2011) 'Shared and unique properties of ubiquitin and SUMO interaction networks in DNA repair', *Genes and Development*, 25(17), pp. 1763–1769. doi: 10.1101/gad.17593511.

Wise, H. M. *et al.* (2012) 'Identification of a Novel Splice Variant Form of the Influenza A Virus M2 Ion Channel with an Antigenically Distinct Ectodomain', *PLoS Pathogens*, 8(11). doi: 10.1371/journal.ppat.1002998.

Wu, C.-Y., Jeng, K.-S. and Lai, M. M.-C. (2011a) 'The SUMOylation of matrix protein M1 modulates the assembly and morphogenesis of influenza A virus.', *Journal of virology*, 85(13), pp. 6618–28. doi: 10.1128/JVI.02401-10.

Wu, C.-Y., Jeng, K.-S. and Lai, M. M.-C. (2011b) 'The SUMOylation of matrix protein M1 modulates the assembly and morphogenesis of influenza A virus.', *Journal of virology*. American Society for Microbiology (ASM), 85(13), pp. 6618–28. doi: 10.1128/JVI.02401-10.

Wu, W. and Panté, N. (2016) 'Vimentin plays a role in the release of the influenza A viral genome from endosomes', *Virology*. Elsevier, 497, pp. 41–52. doi: 10.1016/j.virol.2016.06.021.

Yamada, S. *et al.* (2006) 'Haemagglutinin mutations responsible for the binding of H5N1 influenza A viruses to human-type receptors', *Nature*, 444(7117), pp. 378–382. doi: 10.1038/nature05264.

Yang, S. and Sharrocks, A. D. (2010) 'The SUMO E3 ligase activity of Pc2 is coordinated through a SUMO interaction motif.', *Molecular and cellular biology*. American Society for Microbiology Journals, 30(9), pp. 2193–205. doi: 10.1128/MCB.01510-09.

Yang, X. *et al.* (2014) 'A beneficiary role for neuraminidase in influenza virus penetration through the respiratory mucus', *PLoS ONE*, 9(10), pp. 1–11. doi: 10.1371/journal.pone.0110026.

Yu, L. *et al.* (2004) 'Regulation of an ATG7-beclin 1 program of autophaglic cell death by caspase-8', *Science*, 304(5676), pp. 1500–1502. doi: 10.1126/science.1096645.

Yuan, P. *et al.* (2009) 'Crystal structure of an avian influenza polymerase PA N reveals an endonuclease active site', *Nature*. Nature Publishing Group, 458(7240), pp. 909–913. doi: 10.1038/nature07720.

Zebedee, S. L. and Lamb, R. a (1988) 'Influenza A virus M2 protein: monoclonal antibody restriction of virus growth and detection of M2 in virions.', *Journal of virology*, 62(8), pp. 2762–2772.

Zebedee, S. L. and Lamb, R. a (1989) 'Growth restriction of influenza A virus by M2 protein antibody is genetically linked to the M1 protein.', *Proceedings of the National Academy of Sciences*, 86(3), pp. 1061–1065. doi: 10.1073/pnas.86.3.1061.

Zhang, J., Pekosz, a and Lamb, R. a (2000) 'Influenza virus assembly and lipid raft microdomains: a role for the cytoplasmic tails of the spike glycoproteins.', *Journal of virology*, 74(10), pp. 4634–4644. doi: 10.1128/JVI.74.10.4634-4644.2000.

Zhao, Q. *et al.* (2014) 'GPS-SUMO: a tool for the prediction of sumoylation sites and SUMO-interaction motifs', *Nucleic Acids Research*. Oxford University Press, 42(W1), pp. W325–W330. doi: 10.1093/nar/gku383.

Zhirnov, O. P. and Klenk, H.-D. (2009) 'Alterations in caspase cleavage motifs of NP and M2 proteins attenuate virulence of a highly pathogenic avian influenza virus', *Virology*. Academic Press, 394(1), pp. 57–63. doi: 10.1016/J.VIROL.2009.08.013.

Zhirnov, O. P. and Klenk, H. D. (2013) 'Influenza A Virus Proteins NS1 and Hemagglutinin Along with M2 Are Involved in Stimulation of Autophagy in Infected Cells', *Journal of Virology*, 87(24), pp. 13107–13114. doi: 10.1128/JVI.02148-13.

Zhirnov, O. P. and Syrtzev, V. V (2009) 'Influenza virus pathogenicity is determined by caspase cleavage motifs located in the viral proteins.', *Journal of molecular and genetic medicine : an international journal of biomedical research*. Library Publishing Media, 3(1), pp. 124–32. Available at: http://www.ncbi.nlm.nih.gov/pubmed/19565021 (Accessed: 11 October 2018).

Zhu, P. *et al.* (2017) 'Host Cellular Protein TRAPPC6AΔ Interacts with Influenza A Virus M2 Protein and Regulates Viral Propagation by Modulating M2 Trafficking.', *Journal of virology*. American Society for Microbiology Journals, 91(1), pp. e01757-16. doi: 10.1128/JVI.01757-16.

Zou, P. *et al.* (2009) 'The cytoplasmic domain of influenza M2 protein interacts with caveolin-1', *Archives of Biochemistry and Biophysics*. Academic Press, 486(2), pp. 150–154. doi: 10.1016/J.ABB.2009.02.001.